Distribution Category: Atomic, Molecular and Chemical Physics (UC-411)

ANL-88-8

ARGONNE NATIONAL LABORATORY
9700 South Cass Avenue
Argonne, Illinois 60439

A SYSTEMATIC ANALYSIS OF THE SPECTRA OF THE LANTHANIDES DOPED INTO SINGLE CRYSTAL LaF_3

by

W. T. Carnall, G. L. Goodman, K. Rajnak,* and R. S. Rana**

Chemistry Division

ANL--88-8

DE88 016317

February 1988

Work performed under the auspices of the Office of Basic Energy Sciences, Division of Chemical Sciences, U. S. Department of Energy, under Contract W-31-109-Eng-38.

*Physics Department, Kalamazoo College, Kalamazoo, MI 49007
**Physics Department, College of the Holy Cross, Worcester, MA 01610

TABLE OF CONTENTS

LIST OF FIGURES

LIST OF FIGURES

LIST OF FIGURES

LIST OF TABLES

LIST OF APPENDICES

A SYSTEMATIC ANALYSIS OF THE SPECTRA OF THE LANTHANIDES DOPED INTO SINGLE CRYSTAL LaF_3

W. T. Carnall, G. L. Goodman, K. Rajnak,
and R. S. Rana

ABSTRACT

The optical spectra of the lanthanides doped into single crystal LaF_3 have been interpreted in terms of transitions within $4f^N$ configurations. Energy-level calculations were based on a simultaneous diagonalization of the free-ion and crystal-field matrices using an approximate model with C_{2v} site symmetry instead of the actual C_2 symmetry. Excellent correlations between experimental transition energies and the computed level structures were obtained; predicted levels are given for Pm^{3+}. Previously unpublished experimental results for Nd^{3+} and Sm^{3+}:LaF_3 are included in the tabulations. The spectroscopic data for each ion were analyzed independently, then the parameters of the effective-operator model were intercompared and systematic trends were identified.

Since many of the $4f^N$ configurations extend well into the vacuum ultraviolet region, and thus beyond any presently available experimental observations, some of the free-ion (atomic) parameters were found to be only approximately defined by the accessible levels. However, the crystal-field parameters seem for the most part to be well established by fits to data at low energies.

A new chart of the lanthanide ion $4f^N$ configuration energy level structures is presented. It was generated by including all of the computed crystal-field levels in the 0-50000 cm^{-1} range. In most cases, experimental analyses of individual ions extended to ~ 40000 cm^{-1}.

1.0. INTRODUCTION

The low-temperature absorption and luminescence spectra of trivalent lanthanide ions, Ln^{3+}, doped into single crystal LaF_3, Ln^{3+}:LaF_3, in the range 0-50000 cm^{-1} reveal a narrow band structure characteristic of transi-

tions between states within the $4f^N$ configuration. These transitions are interpreted as connecting the ground state to upper-state energy levels, and their energies are used to define the parameters of an effective Hamiltonian which reproduces the complete structure of the crystal-field split $4f^N$ configuration. Parameters associated with the effective interactions, derived independently from the spectrum of each individual lanthanide ion, show a systematic variation across the lanthanide series. As expected, the effective free-ion interactions in LaF_3 are depressed relative to those derived from the atomic (free-ion) spectra, and this may be taken as evidence for ligand contributions to optically active orbitals.

Earlier experimental work with lanthanides doped into various crystal lattices, particularly the $LaCl_3$ lattice, as well as the basic theory of the atomic and crystal-field interactions was reviewed by Dieke.[1] Subsequent discussions of the theory have been given by Judd,[2] Wybourne,[3] and Hüfner.[4] A recent important addition to this literature, including the summary of a considerable volume of experimental data, was compiled by Morrison and Leavitt.[5]

Extensive spectroscopic data for $Ln^{3+}:LaF_3$ were published at a time when crystal-field calculations for low site-symmetries were rare. Since the site symmetry in LaF_3 was known to be low, C_{2v} or C_2, no attempt was made to address theoretical interpretation of the crystal-field structure itself. Typically, some average energy or center of gravity over a group of levels apparently belonging to a particular J state, was taken as the free-ion energy of the state. Crystal-host-dependent "free-ion" parameters were then derived via a process of least-squares fitting to the energy level structure established by these states. The theoretical models that were used varied considerably in their sophistication, and there was little evidence upon which to differentiate electronic from vibronic transitions in the assignment of crystal-field levels except relative intensity. There were, of course, limits, imposed by the J values, on the number of possible components. Polarization and Zeeman-effect data provided an independent means of assigning crystal-field states in $Ln^{3+}:LaCl_3$ spectra,[1] but in LaF_3 attempts to interpret polarization measurements have met with very limited success.[6,7]

The site symmetry of La^{3+} in LaF_3 is C_2,[8] but it can be approximated either as C_{2v} or as D_{3h}. This fact apparently led to some confusion in early crystallographic work, and it also influenced the first crystal-field analyses. Onopko[9] was the first to publish crystal-field parameters for Nd^{3+}:LaF_3 and Er^{3+}:LaF_3 in D_{3h} symmetry which we found could yield calculated sets of energy levels for any free-ion J state in those ions consistent with the observed splitting pattern of the state. Parameter fitting based on Onopko's results provided the basis for classification of a considerable amount of data for systems with odd N.[10,11] For all f^N configurations with odd N the maximum number of crystal-field components in a state with quantum number J is J + 1/2 in any symmetry lower than cubic. However, when N is even, a lower symmetry than D_{3h} must be used in crystal-field calculations to completely remove the symmetry-related degeneracy of each state.

Morrison and Leavitt[12] reported parametrized crystal-field calculations in the actual C_2 symmetry based on a limited number of states in each $4f^N$ configuration in LaF_3, but did not examine in detail the behavior of the free-ion operators. Initial (trial) crystal-field parameter values were computed from lattice sums. However, no attempt was made to re-examine the original data in the light of the calculated results.

We have used a C_{2v} crystal-field following the general approach outlined in Ref. 12, re-evaluating the original assignments in our own work and that of others. A C_{2v} symmetry removes all the symmetry-imposed degeneracy in even N systems, and is more tractable than C_2 symmetry for computational purposes. Thus the intent of the project reported here was to use a well-tested theoretical model to interpret a large body of experimental data, to highlight systematic trends, and to provide a basis for prediction of the energies of transitions not observed or beyond the normal optical range.

The approach used in our analysis of the spectra of Ln^{3+}:LaF_3 began with modeling the spectra of Nd^{3+}:LaF_3 and Er^{3+}:LaF_3 in D_{3h} site symmetry. Both spectra are characterized by numerous groups of absorption bands that are somewhat isolated in energy. In many groups the number of intense bands corresponded to the number expected for the predicted J-manifold, and

in each case the energy range of observation extended to ~50000 cm^{-1}, which encompassed nearly the entire configuration.[11] Excellent correlation of calculated energy levels with observed absorption bands was obtained for both Nd^{3+} and Er^{3+}. The fitting process was then repeated in the C_{2v} approximation. While, as expected, the overall degree of correlation between theory and experiment did not improve, the magnitude of each of the crystal-field parameters in the C_{2v} set was statistically determined even though there are 9 crystal-field parameters for C_{2v} symmetry as contrasted to only 4 for D_{3h}. We proceeded by using the C_{2v} parameter sets for Nd^{3+} and Er^{3+}:LaF_3 as models to begin the interpretation of the spectra of adjacent ions with even number of f electrons. Since crystal-field parameters in Ln^{3+}:$LaCl_3$ exhibit only moderate variation over the series,[1] the parameters for one ion serve as a reasonable approximation of those for nearest neighbor ions. Thus the crystal-field deduced for Er^{3+}:LaF_3 should serve as a reasonable approximation for that in both Ho^{3+}:LaF_3 and Tm^{3+}:LaF_3.

The use of the above principle has now led to consistent analyses of experimental f→f spectra for all Ln^{3+}:LaF_3 except Pm^{3+}:LaF_3. Progress reports in the analysis aspect of this investigation are given in Ref. 13-16. In each case, the experimental data were reexamined and corrections made where necessary. In some cases the complete experimental data included here have not previously been published.

As the host crystal used in this investigation, LaF_3 has several advantages. It is optically transparent over a wide spectral range extending well into the vacuum ultraviolet. Our experimental techniques only access the region 0-50000 cm^{-1}. It is chemically inert, so crystals, which are commercially available,[17] can be handled in air. The ionic character of the lattice appears to offer a good approximation to true free-ion interactions, and a useful basis for comparison with spectra in other crystalline environments.

Since intense photon light sources providing a wide range of energy in the vacuum ultraviolet are being planned, we can expect greater accessibility and interest in the energy level structure of the lanthanides in this range. Some results are already available.[18] At higher energies, it should be possible to examine in greater detail the influence of other configurations on the states of the f^N configuration. The present study

provides a set of predictions of the expected structure based entirely on information available in the optical range. Interest in both two-photon and multiphoton excitation is increasing, and such studies should also benefit from predictions that can be made using the present energy level systematics.

2.0. EXPERIMENTAL

Extensive spectra for most lanthanides doped into LaF_3 including both published and unpublished work from this laboratory were reanalyzed. Since the crystals were obtained from a commercial source,[17] the radioactivity associated with Pm unfortunately excluded it from study. The tendency of EuF_3 to reduce to EuF_2 at the high temperatures required for crystal growth, and the very strong broad band structure associated with Eu^{2+} in the visible and ultraviolet range due to $4f^7 \rightarrow 4f^6 5d$ transitions, has limited the extent of the data available for $Eu^{3+}:LaF_3$.[7,19]

In the course of the present investigation, measurements were made using several different (0.1-2%) concentrations of most of the lanthanides in LaF_3. Spectra in the range ~4000-15000 cm^{-1} were recorded using a Cary Model 14R (crystal-grating-0.5 meter monochromator) recording spectrophotometer. In the region 15000-50000 cm^{-1}, both a 1-meter Hilger-Engis Model 1000 spectrograph equipped with an EMI 9558 Q photomultiplier, and the Argonne 30-foot Paschen-Runge spectrograph (in second order) were used. Spectra were usually recorded at ~293, 77, and 4 K.

Early conflicting X-ray structure reports suggesting both C_{2v}[20] and D_{3h}[21] site symmetries of the La^{3+} ions in LaF_3, were resolved with subsequent studies[8,22,23] showing that the nine nearest-neighbor F^- ions present a sufficiently distorted environment so that the symmetry is D_{3d}^4 ($P\bar{3}c1$) with a C_2 site symmetry. A powder neutron-diffraction study of LaF_3 and CeF_3 provided additional confirmation of the latter structure.[24] Isostructural members of the series are LaF_3, CeF_3, PrF_3, and NdF_3; SmF_3 and the heavier trifluorides are dimorphic and also crystallize in the orthorhombic YF_3 lattice[25] where each Y^{3+} has 8-F^- at 2.3 Å and one at 2.6 Å.

The crystallographic evidence for a low site symmetry in LaF_3 was anticipated by the results of an early spectroscopic study of PrF_3 in which Sayre and Freed[26] pointed out that the number of lines observed at low temperature for electronic transitions associated with several excited states excluded a site symmetry higher than C_{2v}. The Raman spectrum of LaF_3 has been interpreted in terms of a C_2 site symmetry of the La^{3+}, but these results are also consistent with a small deviation from a higher symmetry.[27]

Many of the lines observed in the low temperature spectrum of Nd^{3+}:LaF_3 are polarized.[6] Such effects are not inconsistent with a C_2 (or C_{2v}) site symmetry, but no consistent set of selection rules could be discerned. It has been suggested that if there were strong enough coupling between the Nd^{3+} ions, that is if they were not statistically distributed in the host LaF_3, it could be appropriate to invoke the point group, D_{6h}, rather than the site group as the symmetry representation. However, a study of concentration quenching of the luminescence of Nd^{3+} and of Er^{3+} in LaF_3 indicates that in the doping concentrations usually employed these ions are statistically distributed.[28] The inability to use polarization as an independent check on assignment to a computed level structure is a considerable disadvantage, but is, in part, compensated by the model calculation approach already cited. It does mean that, particularly in groups where several levels are apparently not observed, there is no assurance that all of the correlations made are correct.

3.0. THE FREE-ION AND CRYSTAL FIELD HAMILTONIAN

The process of developing a complete Hamiltonian for $4f^N$ configurations relies on two important physical assumptions: first, we assume that these electronic states are well removed from other electronic states of the complex; and second, we assume that the influence of the non-spherically symmetric part of the electric field due to the solid state environment of the rare earth ion can be treated as a small perturbation of the f^N free-ion configuration. Thus, we approach the calculation of these electronic properties in two stages. The first deals with the energy-level structure of the gaseous free-ion, and the second with the additional

(crystal-field) interactions which arise when the ion is in a condensed phase. The free-ion or atomic Hamiltonian is assumed to be the same in both cases, and the centers of gravity of groups of crystal-field levels belonging to a particular state are interpreted as the counterparts of the degenerate levels of the gaseous free-ion. Because of the abundance of data in condensed media, and the paucity of true gaseous free-ion data, the free-ion Hamiltonian has been more extensively studied in condensed phases.

The effect of the crystalline environment on the electronic orbitals of the rare earth ion is appreciable, but, nevertheless, does turn out to be small compared with the "free-ion" interactions. Experience has shown that the energy-level structure for the trivalent lanthanides can be adequately treated in terms of a model whose basis states are the free-ion orbitals themselves, without need for specific structural detail of the interaction of the central ion with the ligands. Because the free-ion interactions are dominant, it is important to have an atomic Hamiltonian with enough terms to reproduce accurately the centers of gravity of the observed crystal level groupings.

The interactions primarily responsible for the free-ion structure in trivalent lanthanides are the electrostatic repulsion between electrons in the f^N configuration and the coupling of their spin and orbital angular momenta. There are two different approaches to modeling these interactions: the Hartree-Fock (HF) and the effective-operator methods. Both evolve from the Schrödinger equation for the steady state of a many-electron system.

The form of the Hamiltonian assumes that the nucleus can be treated as a point charge with infinite mass.[3,4] Since exact solutions are known only in the one-electron case, some method of approximation must be used. In both the HF and effective-operator approaches, the first step is to obtain approximate total wave-functions based on the central field approximation. Each electron is treated as if it moved independently in a spherically symmetric potential, $-U(r_i)$, and satisfied equations of the form:

$$\left[-\frac{h^2}{8\pi^2 m}\nabla^2 + U(r_i)\right]\phi(a^i) = E(a^i)\phi(a^i) \quad . \qquad (1)$$

The HF-approach seeks the evaluation of this potential using the variational principle.[29] Computed values of the desired integrals can be obtained to varying degrees of approximation depending upon the sophistication of the computer codes used.

In the effective operator or parametric approach, the Coulomb potential is replaced by an undefined central field potential U(r), eqn. (1). Variables are separated as for the hydrogen atom, and the angular parts of the interaction are evaluated explicitly. Since the radial equation contains the undefined function, U(r), it cannot be solved. The radial integrals are therefore treated as parameters to be evaluated from experimental data via an appropriate fitting procedure. The energy expression has the same form as that of the HF approach, but there is no radial function from which to evaluate the integrals. If we now add the spin variables, the atomic Hamiltonian, H, has the form:

$$H = H_0 + H_{EL} + H_{SO} \quad . \tag{2}$$

H_0 (involves the kinetic energy of the electrons and their interaction with the nucleus[3,4])

$$H_{EL} \text{ (electrostatic term)} \quad E_{EL} = \sum_{k=0}^{6} f_k F^k \text{ (k even)} \tag{3}$$

$$H_{SO} \text{ (spin-orbit interaction)} \quad E_{SO} = A_{SO}\zeta_f \quad . \tag{4}$$

The F^k and ζ_f are the electrostatic and spin-orbit integrals; f_k and A_{SO} represent the angular parts of the electrostatic and spin-orbit interactions, respectively. Although the same symbol is used, the F^k integrals as defined here are not to be identified as those of the HF model. As parameters, they absorb some of the effects of configuration interaction which are not part of the HF definition.

In eqn. 2 there is no explicit attempt to include the effects of configuration interaction, (CI). Rather, such effects are introduced into the Hamiltonian by the use of perturbation theory which allows one to represent some of the most important effects of CI by additional 2- and 3-body

(effective) operators operating wholly within the f^N configuration. The two-body (scalar) effective-operator terms are expressed here in the form given by Rajnak and Wybourne.[30] The Hamiltonian, eqn. (2), with the added two-body operators is written:

given by Rajnak and Wybourne.[30] The Hamiltonian, eqn. (2), with the added two-body operators is written:

$$H = H_o + \sum_{k=0}^{6} F^k(nf,nf)f_k + \zeta_f A_{SO} + \alpha L(L+1) + \beta G(G_2) + \gamma G(R_7) \quad (k \text{ even}) \qquad (5)$$

The parameters associated with the two-body correction terms are designated α, β, and γ; $G(G_2)$ and $G(R_7)$ are Casimir's operators for the groups G_2 and R_7, and L is the total orbital angular momentum.[3] The effects of configuration interaction that can be expressed in the same form as the f_k are of course automatically absorbed in the F^k radial integrals when they are treated as parameters. The additional terms, α, β, and γ represent effects that do not transform as the f_k.

The values of α, β, and γ arising from electrostatic configuration interaction calculated for Pr^{3+} by Morrison and Rajnak[31] using ab initio methods were in good agreement with those obtained by fitting experimental data, as shown in Table 1. One of the insights gained from this work was that higher energy processes such as excitation of one or two particles to the continuum made large contributions to the parameter values. The fact that the energies of the continuum states relative to the f^N configurations do not change significantly with atomic number may help to explain the near constancy of the fitted parameter values across the lanthanide series.[10,32] A subsequent perturbed-function approach to the calculation of the continuum interactions confirmed the earlier results.[33]

For configurations of three or more equivalent f electrons, three-particle configuration interaction terms have been added to the model in the form given by Judd.[34,35] Such terms arise from the perturbing effects of those configurations that differ from f^N in the quantum numbers of a single electron. They are expressed as $t_i T^i$ (i = 2, 3, 4, 6, 7, 8) where T^i are the parameters and t_i are three-particle operators, whose matrix elements are computed as shown in Ref. 34. As in the case of the two-body

Table 1. Elements of the Parametric Hamiltonian

		Sm^{3+} ($4f^5$) LaF_3 (cm^{-1})[a]	Sm^{3+} ($4f^5$) $LaCl_3$ (cm^{-1})[a,b]	Pu^{3+} ($5f^5$) $LaCl_3$ (cm^{-1})[a,c]	Ab Initio Calc. (cm^{-1})	
H_E (Electrostatic Term)	F^2	79805	78125	48670	110157[d]	
$\sum_{k=0}^{6} f_k F^k$ (k–even)	F^4	57175	56809	39188	69143	
	F^6	40250	40061	27493	49758	
H_{SO} (Spin–Orbit Interaction)	ζ_f	1176	1168	2241	1243[d]	
$A_{SO}\zeta_f$						
$H_{CI(2)}$ (Two–body Configuration Interaction)	α	20.2	21.6	29.7	28	Pr IV[e]
$\alpha L(L+1) + \beta G(G_2) + \gamma G(R_7)$	β	–567	–724	–671	–615	Pr IV[e]
	γ	[1500]	[1700]	1067	1611	Pr IV[e]
$H_{CI(3)}$ (Three Particle Configuration Interaction)	T^2	[300]	291	186	394	Pr III[f]
$\sum_i t_i T^i$ (i = 2,3,4,6,7,8)	T^3	[36]	13	48	–34	Pr III[f]
	T^4	[56]	34	38	89	Pr III[f]
	T^6	–347	–193	–364	–214	Pr III[f]
	T^7	373	288	364	314	Pr III[f]
	T^8	348	330	332	274	Pr III[f]
Electrostatically Correlated Spin–Orbit Interaction	P^2	357[g]	341[g]	822[g]	128[h]	
(Two–Body Pseudo–Magnetic Operators)	P^4	178	256	616	86	
	P^6	35.7	170	411	63	
Spin–Other–Orbit and Spin–Spin Effects: Marvin Integrals	M^0	2.60[i]	2.40[i]	0.95[i]	2.75[d]	
	M^2	1.45	1.34	0.53	1.54	
	M^4	0.99	0.91	0.36	1.04	
Crystal Field Interaction	$\sum_{k,q,i} B_q^{(k)} C_q^{(k)}(i)$ (terms appropriate to the crystal symmetry)					

[a] Fitted to experimental data; values in brackets were not varied.
[b] Reference 10
[c] Reference 32
[d] Values computed for $4f^5$ using a relativistic Hartree–Fock code.
[e] Reference 31
[f] Reference 36
[g] P^2 was freely varied, but P^4 and P^6 were constrained by the ratios $P^4/P^2 = 0.5$ and $P^6/P^2 = 0.1$ for Sm^{3+}:LaF_3 and the ratios 0.75 and 0.50, respectively, for Sm^{3+}:$LaCl_3$ and Pu^{3+}:$LaCl_3$.
[h] Reference 39
[i] M^0 was freely varied, but M^2 and M^4 were constrained by the ratios $M^2/M^0 = 0.56$, and $M^4/M^0 = 0.38$.

terms, values of the three-particle correction parameters have been calculated by ab initio methods[36] and found to agree with those defined by fitting experimental data.[35] In a similar manner four-particle and higher order terms could be defined for appropriate configurations. However, they do not appear to be necessary to a good representation of the experimental data.

Magnetically-correlated corrections to the working model have also been introduced using the form suggested by Judd et al.[37] Values of the Marvin integrals,[38] M^h (h = 0, 2, 4), which represent spin-spin and spin-other-orbit relativistic corrections, have been determined from parametric fits to some experimental data, and were found to be similar to those computed using HF-methods. Of the two-body magnetic corrections, the most important appears to be the electrostatically correlated spin-orbit perturbation which involves the excitation of an f electron into a higher-lying f-shell. The corresponding parameters P^f (f = 2, 4, 6) for lanthanides in crystals as evaluated by parametric fitting are consistent with values derived via HF methods.[39] To complete the correlations between parametric fit values and those computed via HF methods for the atomic Hamiltonian, results for the F^k using HF methods with a relativistic correction[40] have been computed, and are the subject of an extensive review.[41]

Although extensive corrections to the basic free-ion Hamiltonian, Eqn. (2), have been developed, practically all crystal-field calculations are carried out using a single-particle crystal-field theory[3,4] in which the parameters are appropriate to a given site symmetry:

$$H_{CF} = \sum_{k,q,i} B_q^{(k)} C_q^{(k)}(i) , \qquad (6)$$

where $C_q^{(k)}(i)$ is a spherical tensor of rank k depending on the coordinates of the i^{th} electron and the summation involving i is over all f electrons of the ion of interest; the values of k and q for which the parameters $B_q^{(k)}$ are nonzero depend on the site symmetry. To complete the interactions shown in Eqn. (5), the following terms are included in the Hamiltonian currently used in the parametric fitting of the experimental data:

$$\sum_{i=2,3,4,6,7,8} t_i T^i + \sum_{h=0,2,4} m_h M^h + \sum_{f=2,4,6} p_f P^f +$$

$$\sum_{k,q,i} B_q^{(k)} C_q^{(k)(i)}$$

Typical values of the free-ion parameters obtained for fits to experimental data for the f^5-configuration, $Sm^{3+}:LaF_3$, $Sm^{3+}:LaCl_3$ and the actinide ion, $Pu^{3+}:LaCl_3$, together with representative values computed by ab initio methods are shown in Table 1.

As has already been pointed out, the actual site symmetry in LaF_3 is C_2. However, the crystal-field calculation in C_2 symmetry requires determination of 14 independent parameters of which 5 have imaginary matrix elements.[3,4] This is a major computational problem when coupled with an extensive free-ion treatment. We reduced the number of crystal-field parameters to 9 by using an approximate C_{2v} symmetry, which is crystallographically appropriate in this case and is low enough to completely remove the symmetry-related degeneracy of crystal-field states. For configurations (f^4-f^{10}) in which the Hamiltonian matrices including the C_{2v} crystal-field are greater than 200 by 200 we have used a method of truncation to select managable portions of this matrix. The eigenstates of the free-ion Hamiltonian provide the basis states for these truncations.[41]

4.0. ANALYSIS OF EXPERIMENTAL DATA

Two different approaches to use of the C_{2v} approximation in treating spectra of $Ln^{3+}:LaF_3$ have been taken. One is to maintain the D_{3h} symmetry axis and add the additional parameters required in C_{2v} symmetry to simulate the distortion from D_{3h} symmetry. This was the course which we first explored. One of the problems encountered was that the D_{3h} approximation provides such a good correlation between experiment and theory for odd-electron systems that it is difficult to adequately determine the extra parameters arising in C_{2v} symmetry. Even the signs of some of these parameters can turn out to be indeterminate, depending upon the data being fit. This approach has also been discussed by Caro and coworkers.[42]

Another approach is to fit the crystal-field states of an odd-N system using as an initializing set the values of the real parameters computed for LaF_3 in C_2 symmetry.[12]

The values shown in Table 2 illustrate the relationship of the crystal-field parameters for $Nd^{3+}:LaF_3$ computed from a point-charge model assuming first D_{3h}, then C_2 point symmetry but with two different crystal axes. As noted in the table, the computed values in D_{3h} symmetry are similar to the results published by Onopko,[9] as well as to those determined in our fitting of experimental data.[11] When the real parts of the lattice sum calculation in C_2-symmetry with the z-axis of the A_{nm} parallel to the crystal axis, column 2 of Table 2, were used to initiate the least squares fitting of data (approximate C_{2v} symetry) the problem of certain parameters having indeterminate values was encountered. Comparing columns (1) D_{3h} and (2) C_2-symmetry, it is apparent why this might happen, since the large values of B_0^4, B_0^6, and B_6^6 in the initializing set can dominate the subsequent fitting process. In contrast, by using the real parts of the third set (C_2) in Table 2 to initialize the fitting process (z-axis of the A_{nm} perpendicular to the crystal axis), all 9 parameters were determined in several cases as in column (5) Table 2, and most of the parameters were typically determined. Since B_2^2 is small, it was frequently assigned a constant value.

The absorption spectrum of $Nd^{3+}:LaF_3$ played a critical role in the analysis of other light lanthanide spectra. The crystal-field parameters determined for $Nd^{3+}:LaF_3$ were used to model the energy level structures in Pr^{3+} and Pm^{3+}, as well as $Sm^{3+}:LaF_3$. Predicted splitting patterns were compared group by group with the experimental data as a means of discriminating against assignments to more intense vibrational modes.

For the heavy lanthanides, the model crystal-field parameters were derived for $Er^{3+}:LaF_3$. Starting with Onopko's insight into the structure of the ground state in D_{3h} site symmetry,[9] we obtained an excellent agreement between theory and experiment over the entire range of observation for $Er^{3+}:LaF_3$. Because of the very large number of assignments, we were subsequently able to determine the crystal-field parameters in C_{2v} symmetry. The $Nd^{3+}:LaF_3$ and $Er^{3+}:LaF_3$ systems are unique in the lanthanide series in

Table 2.

Crystal-Field Parameter Values (in terms of $B_q^{(k)}$ in cm^{-1}) for $Nd^{3+}:LaF_3$ Obtained from Lattice Sum Calculations Compared to Fit Values in C_2 and C_{2v}-Symmetries

	$B_q^{(k)}(D_{3h})^a$	$B_q^{(k)}(C_2)^b$		$B_q^{(k)}(C_2)^c$		$B_q^{(k)}(C_2)^d$		$B_q^{(k)}(C_{2v})^e$	
kq	Real	Real	Imag.	Real	Imag.	Real	Imag.	Real	Imag.
20	465	66	0	-145	0	-216	0	-256(22)	0
22		-46	79	5	0	-36	0	-48(12)	0
40	1849	994	0	652	0	700	0	496(73)	0
42		-103	178	422	118	197	71	521(39)	0
44		-56	-96	397	241	229	181	563(41)	0
60	949	844	0	523	0	490	0	641(54)	0
62		17	-30	-793	66	-928	-23	-839(39)	0
64		14	24	-113	-342	-131	-449	-408(35)	0
66	862	784	0	-442	-442	-427	-653	-831(41)	0

Table 2. (cont.)

[a]Lattice sum calculation[12] based on crystal structure data of K. Schylter,[21] similar to results of Onopko[9]. The c-axis and the D_{3h} axis are parallel.

[b]Lattice sum calculation[12] based on crystal structure of Cheetham et al.,[24] but with the z-axis of the A_{nm} parallel to the crystal axis.

[c]Lattice sum calculation[12] based on crystal structure of Cheetham et al.[24] with the z-axis of the A_{nm} perpendicular to the crystal axis.

[d]Fit to experimental data for $Nd^{3+}:LaF_3$,[12] z-axis as in (c).

[e]Fit to experimental data, complete diagonalization of free-ion and crystal-field matrices, z-axis as in (c). (Errors shown in parentheses).

the number of distinct free-ion states that are well separated in energy and in which the number of prominent crystal-field components corresponds to the expected number of crystal-field levels.

Use of the Er^{3+} crystal-field parameters in C_{2v} site symmetry with free-ion parameters for Ho^{3+} and Tm^{3+} resulted in numerous correlations with observed spectroscopic structure in the latter two ions. The initial "model" parameters for each ion were subsequently modified by a fit to level energies assigned to be consistent with the model calculations. The modified parameters in turn formed the detailed "model" for the next member of the series. Thus the initial parameters for Tb^{3+} were based on the analysis of $Dy^{3+}:LaF_3$.[15]

5.0. SUMMARY OF EXPERIMENTAL RESULTS AND THEIR INTERPRETATION

The following summary of experimental results for $Ln^{3+}:LaF_3$ does not attempt to be a complete review of the literature. Reference is limited to more extensive experimental investigations. The bulk of the tabulated experimental data taken in absorption was drawn from measurements made in the course of the present investigation. The fluorescence and far-infrared spectra are quoted from the literature. All data are reported in cm^{-1} (vacuum).

5.1. $Ce^{3+}:LaF_3$ ($4f^1$)

An examination of the infrared spectrum of $Ce^{3+}:LaF_3$,[43] revealed four bands that persisted at ~ 4 K identified as the components of the $^2F_{7/2}$ multiplet. Temperature dependent studies provided evidence for a component of the $^2F_{5/2}$ group at 150 cm^{-1}. Energy levels of the $^2F_{5/2}$ state deduced from Raman spectra were placed in the 140-170 cm^{-1} range and near 300 cm^{-1}.[44]

The crystal-field parameters obtained in the fit of data for $Pr^{3+}:LaF_3$ were used as a model for $Ce^{3+}:LaF_3$, and in the initial fitting procedure, only ζ was allowed to vary. While the resulting parameter set yielded a computed energy level scheme that was consistent with the observed structure, the correlation was significantly improved using the value $B_2^2 = -50$

cm^{-1} instead of -120 cm^{-1}. The lower value was also more consistent with trends in values for this parameter over the series as a whole. The fit to the observed energy levels and the final parameter values are shown in Tables 3 and 4, respectively.

An attempt was made to vary selected crystal-field parameters, since the whole set could not be varied simultaneously with such a limited number of observations. When B_0^4, B_0^6, and B_6^6 were varied in addition to ζ, the fit to experiment was improved but the parameter magnitudes increased relative to those for $Pr^{3+}:LaF_3$. Actually, an increase in the magnitude of the parameters is not unreasonable considering that the ionic radius of Ce^{3+} (1.034 Å) is considerably larger than that of the model Pr^{3+} (1.013 Å).[1] However in this case, since the number of parameters varied simultaneously must be severely limited, we only note that the trends in crystal-field parameter magnitudes extrapolated from analyses of other light lanthanide ions in LaF_3 are fully consistent with the experimental results.

5.2. $Pr^{3+}:LaF_3$ ($4f^2$)

Spectroscopic investigations of $Pr^{3+}:LaF_3$ at several laboratories at moderate to high resolution have identified crystal-field components of most of the states.[45-51] However, one of the weak points in the theoretical analysis has been the lack of rationale for unique assignments to components of the $^1I_6$ state. The intense components of $^3P_1$ are readily identified although they occur in the same region of the spectrum as that predicted for $^1I_6$. It has not been possible to distinguish apparent vibronic structure possibly in part associated with the $^3P_1$ levels from very low intensity electronic transitions to the $^1I_6$ state. As it turns out, the two-body operator parameterized by α is essentially defined by the energy of the $^1I_6$ state. Changes in α can shift the center of gravity of $^1I_6$ with respect to that of $^3P_1$ with little if any affect on the computed level energies for the rest of the configuration. Thus when we modelled the crystal-field splitting in $Pr^{3+}:LaF_3$ using the crystal-field parameters of $Nd^{3+}:LaF_3$ we were still only able to define an approximate value of α. The rationale for a possible definition is provided by the following discussion.

Table 3.
Experimental and Computed Energy Level Structure for $Ce^{3+}:LaF_3$

SLJ State	Obs.[a] (cm^{-1})	Calc.[b] (cm^{-1})	O-C
$^2F_{5/2}$	0	-3	3
	151	152	-1
	280[c]	284	-4
$^2F_{7/2}$	2160	2235	-75
	2240	2274	-34
	2635	2586	49
	2845	2783	62

[a]Ref. 43 (cm^{-1} vac).

[b]Parameter values are given in Table 4.

[c]Ref. 44.

Table 4. Energy Level Parameters for Ln^{3+}:LaF_3 (in cm^{-1}) [a]

	Ce	Pr	Nd	Pm	Sm	Eu	Gd	Tb	Dy	Ho	Er	Tm	Yb
F^2		68878(23)	73018(19)	76400	79805(16)	83125(31)	85669(17)	88995(58)	91903(69)	94564(38)	97483(32)	100134(23)	
F^4		50347(69)	52789(94)	54900	57175(45)	[59268 R]	[60825 R]	[62919 R]	64372(147)	66397(64)	67904(67)	69613(62)	
F^6		32901(37)	35757(42)	37700	40250(26)	[42560 R]	44776(24)	47252(72)	49386(139)	52022(63)	54010(60)	55975(104)	
ζ	647.3(11)	751.7(2)	885.3(1)	1025	1176(1)	1338(3)	1508(2)	1707(2)	1913(2)	2145(1)	2376(2)	2636(1)	2928(10)
α		16.23(.23)	21.34(.14)	20.50	20.16(.89)	[20.16]	18.92(.83)	18.40(.19)	18.02(.23)	17.15(.11)	17.79(.20)	17.26(.30)	
β		-566.6(15)	-593.0(8)	-560	-566.9(8)	[-566.9]	[-600]	-590.9(29)	-633.4(10)	-607.9(6)	-582.1(10)	-624.5(15)	
γ		1371(13)	1445(16)	1475	[1500]	[1500]	[1575]	[1650]	1790(47)	[1800]	[1800]	[1820]	
T^2			298(6)	300	[300]	[300]	[300]	[320]	329(9)	[400]	[400]	[400]	
T^3			35(3)	35	[36]	[40]	[42]	[40]	36(5)	37(2)	43(5)		
T^4			59(4)	58	[56]	[60]	[62]	[50]	127(22)	107(5)	73(5)		
T^6			-285(6)	-310	-347(7)	[-300]	[-295]	-395(28)	-314(16)	-264(16)	-271(11)		
T^7			332(8)	350	373(7)	[370]	[350]	303(17)	404(8)	316(20)	308(18)		
T^8			305(10)	320	348(5)	[320]	[310]	317(13)	315(7)	336(8)	299(17)		
M^0 [b]		2.08(.3)	2.11(.1)	2.4	2.60(.1)	[2.1]	3.22(.2)	2.39(.1)	3.39(.1)	2.54(.1)	3.86(.2)	3.81(0.3)	
P^2 [c]		-88.6(47)	192(31)	275	357(28)	[360]	676(75)	373(53)	719(30)	605(24)	594(63)	695(46)	
B^2_0	[-218]	-218(16)	-256(16)	-245	-224(19)	-217(56)	[-231]	-231(24)	-244(18)	[-240]	-238(17)	-249(14)	[-249]
B^4_0	[738]	738(40)	496(73)	470	452(47)	413(86)	[604]	604(49)	506(43)	560(27)	453(90)	457(29)	[457]
B^6_0	[679]	679(48)	641(54)	640	649(47)	558(92)	[280]	280(38)	367(40)	376(28)	373(83)	282(42)	[282]
B^2_2	[-50]	-120(13)	-48(12)	-50	[-50]	[-50]	[-99]	-99(16)	-65(12)	-107(10)	-91(14)	-105(9)	[-105]
B^4_2	[431]	431(27)	521(39)	525	597(29)	[597]	[340]	340(34)	305(33)	250(19)	308(60)	320(21)	[320]
B^4_4	[616]	616(27)	563(41)	490	408(28)	[408]	[452]	452(31)	523(25)	466(19)	417(56)	428(22)	[428]
B^6_2	[-921]	-921(32)	-839(39)	-750	-706(33)	[-706]	[-721]	-721(29)	-590(24)	-576(18)	-489(51)	-482(33)	[-482]
B^6_4	[-348]	-348(41)	-408(35)	-450	-508(34)	[-508]	[-204]	-204(29)	-236(27)	-227(20)	-240(51)	-234(36)	[-234]
B^6_6	[-788]	-788(38)	-831(41)	-760	-692(38)	[-692]	[-509]	-509(33)	-556(25)	-546(22)	-536(49)	-492(36)	[-492]
n [d]	7	75	146		232	29	70	146	198	204	127	56	5
σ [d]	51	16	14		13	16	10	12	12	10	19	10	38

[a] Values in parentheses are errors in the indicated parameters. Values in brackets were either not allowed to vary in the parameter fitting, or if followed by an R, were constrained: For Eu^{3+}, $F^4/F^2 = 0.713$, $F^6/F^2 = 0.512$; for Gd^{3+}, $F^4/F^2 = 0.710$; for Tb^{3+}, $F^4/F^2 = 0.707$. All parameters for Pm^{3+} are interpolated values.

[b] M^0 was varied freely, M^2 and M^4 were constrained by the ratios $M^2 = 0.56\,M^0$, $M^4 = 0.31\,M^0$.

[c] P^2 was varied freely, P^4 and P^6 were constrained by the ratios $P^4 = 0.5\,P^2$, $P^6 = 0.1\,P^2$.

[d] Deviation $(\sigma) = \sum[(\Delta i)^2/n-p]^{1/2}$, where Δi is the difference between observed and calculated energies, n is the number of levels fit, and p is the number of parameters freely varied.

The model crystal-field for Pr^{3+}:LaF_3 based on parameters for Nd^{3+}:LaF_3, with an earlier approximate set of free-ion parameters,[45] yielded an energy level scheme that was generally in very good agreement with the experimental data.[13] As anticipated, several modifications of the original assignments[45] were indicated. Correlations between computed and assigned energy levels appeared to be distorted by inclusion of levels at 508 and 4552 cm^{-1}. Typical experimental results are shown in Fig. 1 where the model calculation is indicated for comparison.

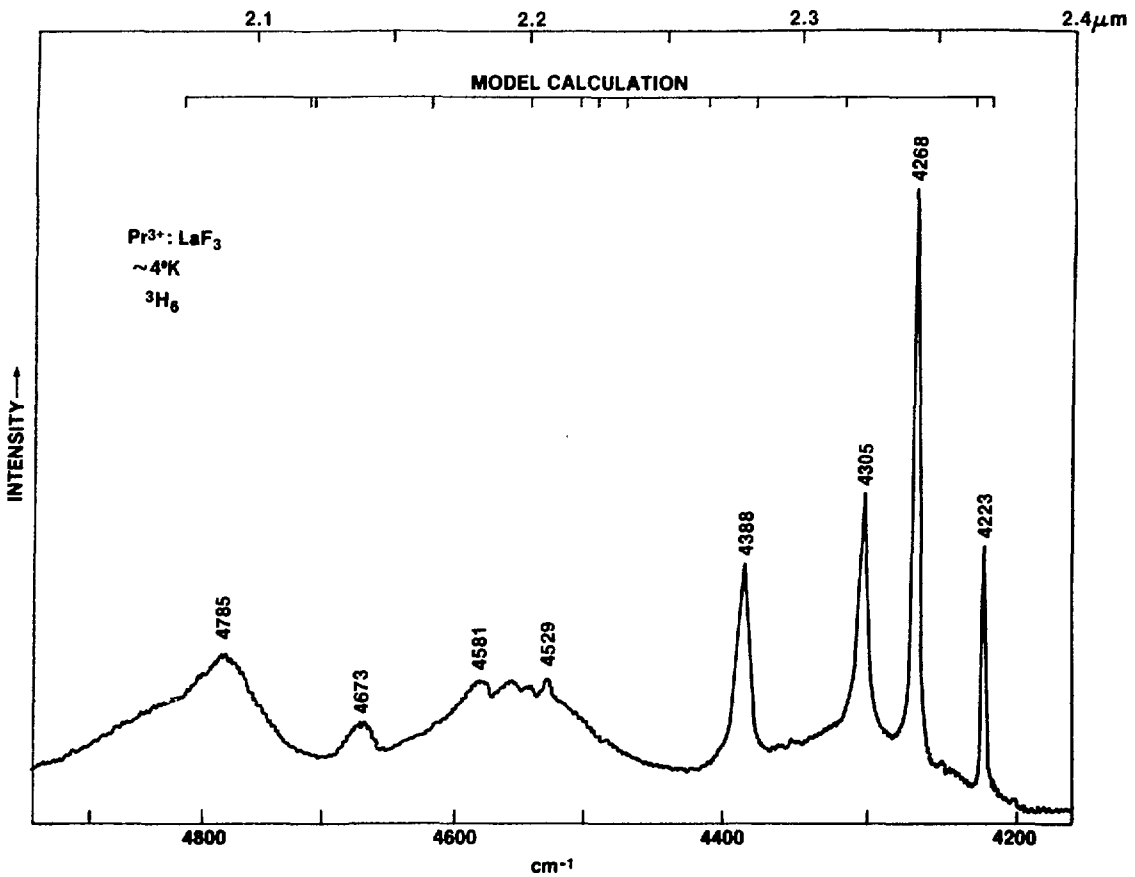

Fig. 1. Comparison of the Experimental Absorption Spectrum of Pr^{3+}:LaF_3 with the Model Energy Level Calculation in the Range 4200-4900 cm^{-1} (the $^3H_6$ State) at ~ 4 K.

The recent measurements of the energy of the $^1S_0$ level[50,51] are more accurate than, but within the limits of error of, the previous value.[45] If we take the new value together with the reported energies of transitions

from $^1S_0$ to levels of the $^3F_4$, $^1G_4$, and $^1I_6$ states,[49] and correct to cm^{-1} vac, several new assignments can be made, Table 5.

In the $^3F_4$ state, the 7025 cm^{-1} fluorescence line from $^1S_0$ agrees well with a transition observed in absorption, Appendix I, as does that at 7105 cm^{-1}, whereas the 7089 cm^{-1} line must, according to the model calculation, refer to another, possibly a perturbed site. We do see evidence of side-band structure at this energy in absorption.

Four of the five transitions connecting $^1S_0$ to the $^1G_4$ state, reported in fluorescence, are consistent with transitions predicted by the model calculation, and with structure observed in absorption in the present experimental study, Appendix I. As in the results for the $^3F_4$ state, there appear to be two lines, 10035 and 10057 cm^{-1}, which correspond to a single level observed in absorption.

While the $^1D_2$ state was not reported to be connected by fluorescence to the $^1S_0$ state, the model calculation suggests an interpretation of the transitions observed in absorption to the $^1D_2$ state that is inconsistent with previous proposed interpretations,[45,48] Figure 2.

A very interesting result of the reported fluorescence from $^1S_0$ is that attributed to terminal levels in the $^1I_6$ state. We noted earlier that the model predicts a very wide splitting of ~ 600 cm^{-1} for the $^1I_6$ state, Appendix I, but unique assignments were lacking. We noted previously[13] generally good correspondence between the model calculation and experiment with an assumed value of α. Examining the fluorescence results, Table 5, we see that they do span the predicted ~ 600 cm^{-1}. While levels at 21279 and 21331 cm^{-1} do not correspond to any structure observed in absorption, Fig. 3, there are weak bands near 21585 cm^{-1} and 21897 cm^{-1}. Thus we allowed these four transitions to define the energy of the $^1I_6$ state. This, together with assignment of the $^1S_0$ state, which defines the value of γ, specifies the free-ion parameters. Only a small adjustment in the crystal-field is required for an excellent correspondence between theory and experiment, Appendix I. Several additional assignments consistent with the new model and the results indicated in Fig. 3 were then made. The observed structure for $^3P_2$ is compared to the model calculation in Fig. 4. The final set of parameters values, Table 4, is consistent with

Table 5.

Emissions from the $^1S_0$ State of $Pr^{3+}:LaF_3$[a]

S'J'		λ (Å)	cm^{-1} (vac)	Terminal State (cm^{-1})[b]
$^1I_6$	A	3892	25686	21279
	B	3900	634	331
	C	3939	380	585
	D	3988	068	897
$^1G_4$	A	2686	37219	9746
	B	2697	067	9898
	C	2707	36930	10035
	D	2716	808	057
	E	2741	472	493
$^3F_4$	A	2503	39940	7025
	B	2507	876	7089
	C	2508	860	7105

[a]Ref. 49.

[b]Assume the initial state is in every case $^1S_0$ at 46965 cm^{-1} (vac).[51]

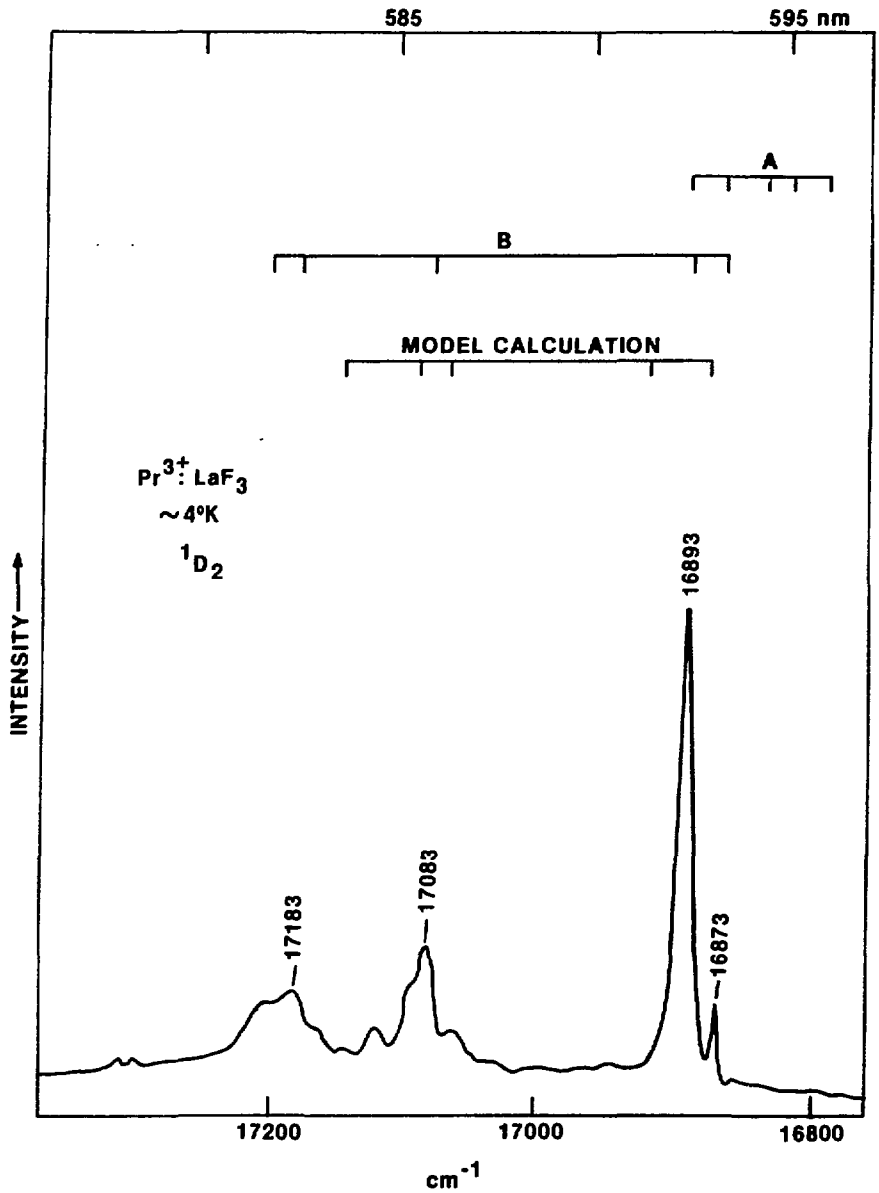

Fig. 2. Comparison of the Experimental Absorption Spectrum $Pr^{3+}:LaF_3$ with the Model Energy Level Calculation and with Previous Proposed Interpretations (A. Assignments of Ref. 48, B. Assignments of Ref. 45) of the Energy Level Structure in the Range 16800-17400 cm^{-1} (the $^1D_2$ State) at ~ 4 K.

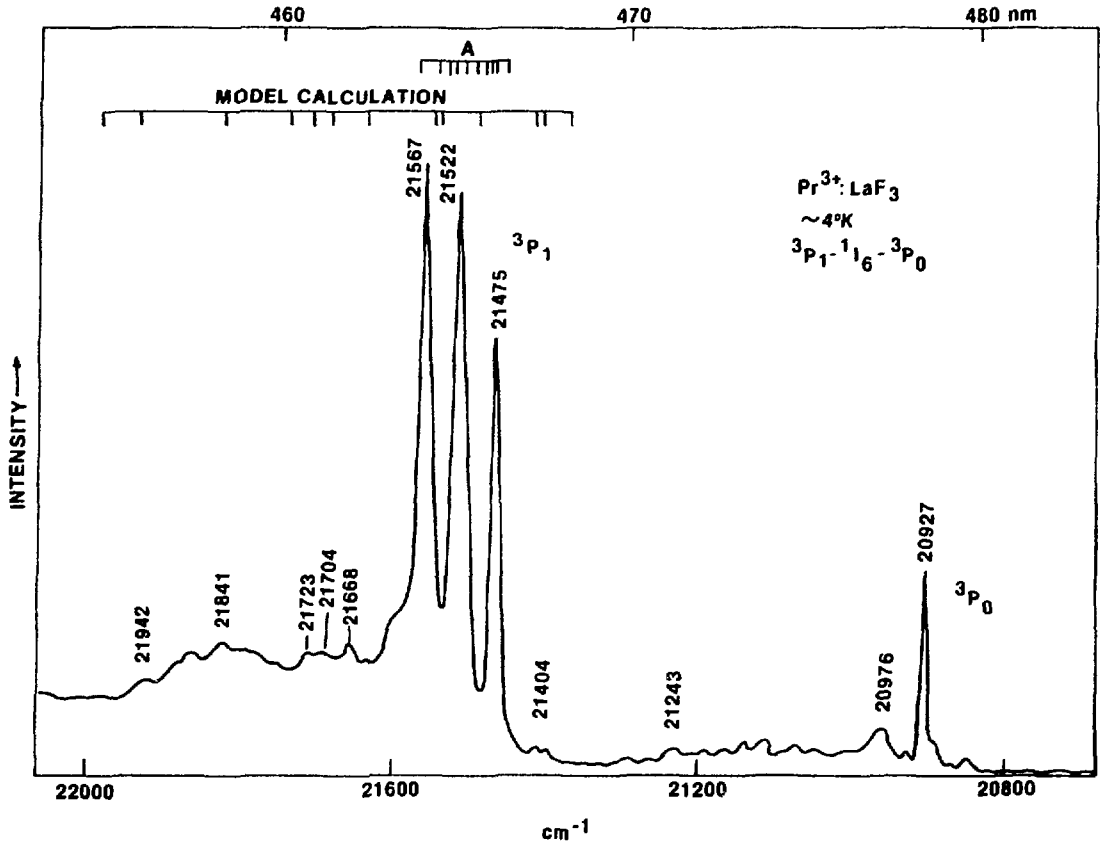

Fig. 3. Comparison of the Experimental Absorption Spectrum of $Pr^{3+}:LaF_3$ with the Model Energy Level Calculation and with a Previous Proposed Interpretation (A. Assignments of Ref. 45) of the Energy Level Structure in the Range 20800-22000 cm^{-1} (the $^3P_0$, $^1I_6$ and $^3P_1$ States) at ~ 4 K.

those originally assumed.[13] However, the interpretation remains speculative and will hopefully stimulate further experimental activity. In the last section of this report, it is noted that a larger value of α than that indicated here would be more consistent with apparent systematic trends, but a larger α shifts the $^1I_6$ states to higher energies relative to $^3P_1$.

5.3. $Nd^{3+}:LaF_3$ ($4f^3$)

There are extensive published reports of the structure observed in low-temperature absorption and fluorescence spectra of $Nd^{3+}:LaF_3$.[6,52-54] Wong, Stafsudd, and Johnston[6] reported a number of polarized absorption

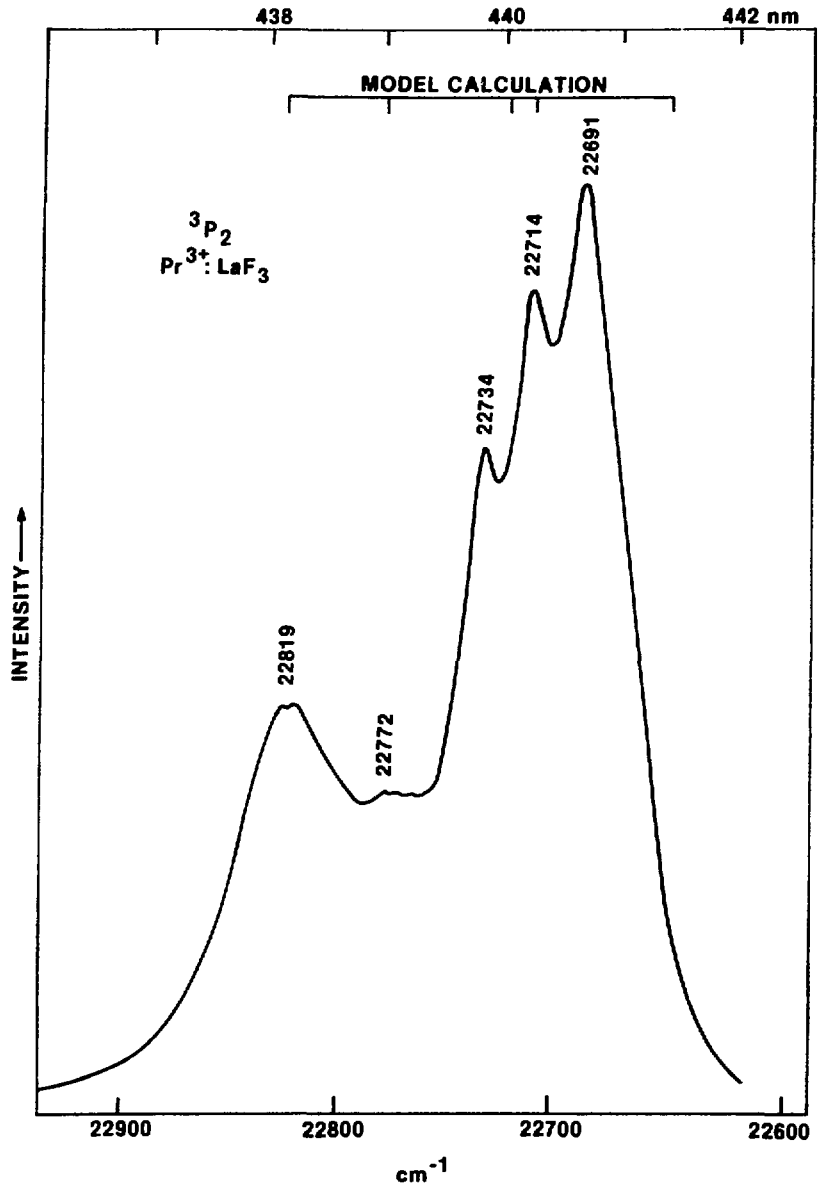

Fig. 4. Comparison of the Experimental Absorption Spectrum of $Pr^{3+}:LaF_3$ with the Model Energy Level Calculation in the Range 22600-22900 cm^{-1} (the $^3P_2$ State) at ~ 4 K.

lines in the range 11500-20000 cm^{-1}, while Caspers, Rast, and Buchanan[52] observed components of most of the atomic states to 24000 cm^{-1}. This group also established the energies of the ground and first excited states by fluorescence measurements. These data have been extended by previously unpublished work at ANL[11] to provide a relatively complete set of crystal-field components. Of the 182 levels in the f^3 configuration, 146 have been assigned, Appendix II. The data reported at >3000 cm^{-1} were obtained in the present investigation, and are in good agreement with previously published results. The free-ion structure is consistent with that established in the study of $Nd^{3+}:LaCl_3$.[55]

As indicated earlier, the observed spectrum of $Nd^{3+}:LaF_3$ is sufficiently extensive to provide an excellent basis for interpretation. Only one $^2F_{7/2}$ and one $^2F_{5/2}$ state lie beyond the present range of observation. Thus both the atomic and crystal-field parameters, Table 4, are considered well determined and they became the basis for extrapolation to neighboring ions. The experimental results reported here are based on a reexamination of earlier spectroscopic studies, and thus the line list differs marginally from that given in an earlier report.[11]

5.4. $Pm^{3+}:LaF_3$ ($4f^4$)

The absorption spectrum of $Pm^{3+}:LaF_3$ has not been reported, but an extensive interpretation of the absorption and fluorescence spectra of $Pm^{3+}:LaCl_3$ has been published.[56] We have used the regularities in the energy level parameters for $Ln^{3+}:LaF_3$ as the basis for interpolation of approximate parameter values for $Pm^{3+}:LaF_3$, Table 4. The corresponding computed crystal-field levels to ~25000 cm^{-1} are given in Appendix III.

5.5. $Sm^{3+}:LaF_3$ ($4f^5$)

The observation and analysis of the absorption and fluorescence spectra of $Sm^{3+}:LaF_3$ in the range 0-11000 cm^{-1} was reported by Rast, Fry, and Caspers,[57] while a line list extending to ~32000 cm^{-1} was given by Dieke.[1] The region of the spectrum measured was further extended in the present investigation and a composite tabulation with most of the energy assign-

ments based on work at ANL, is given in Appendix IV. Since the crystal-field structure of Sm^{3+} is very extensive, initial assignments were limited to the more isolated groups with the model calculation based on the crystal-field parameters for $Nd^{3+}:LaF_3$. Intercomparisons of our own and previously published data led to additional assignments consistent with the Nd^{3+} model. With Sm^{3+}, we are only able to observe ~50% of the total energy range covered by the $4f^5$-configuration. Thus the free-ion parameters, Table 4, are considered approximate for the total configuration even though they reproduce the available data quite well. Furthermore, the large number of states for $Sm^{3+}:LaF_3$ required truncation of the energy matrices[41] following a procedure cited in the analysis of the spectrum of $Pm^{3+}:LaCl_3$.[56] This introduces an error which is in general small, but may amount to several wavenumbers for some levels. Truncation procedures were used for f^5 (f^9), f^6 (f^8), and f^7 configuration analyses.

5.6. $Eu^{3+}:LaF_3$ ($4f^6$)

Crystals of LaF_3 doped with Eu^{3+} are found to contain some Eu^{2+}. The broad intense Eu^{2+} bands in the visible-near UV range conceal the Eu^{3+} transitions there. Weber[19] observed fluorescence in $Eu^{3+}:LaF_3$ from the excited states $^5D_0$, $^5D_1$, $^5D_2$, and $^5D_3$ using pulsed selective excitation, while more detailed measurements in absorption and fluorescence were subsequently reported by Kumar et al.[7] The energy-levels of the ^5D and ^7F states that can be deduced from the latter measurements are very similar to those reported for $Eu^{3+}:LaCl_3$.[1]

The experimental results of Kumar et al.[7] included polarization measurements, and the assigned energy levels in the ^7F and ^5D multiplets were identified by symmetry species assuming a C_{2v} site-symmetry. The present crystal-field calculations, using the crystal-field parameters for $Sm^{3+}:LaF_3$ as initial values, provide a direct comparison with these assignments. Two reported levels, those at 2847 and 2894 cm^{-1}, were clearly inconsistent with the initial parameter set. Only a very limited refinement of the parameters could be justified based on the small number of observations; however, variation of F^2, ζ, B_0^2, B_0^4, and B_0^6, with fixed ratios of F^4/F^2 and F^6/F^2 did result in a good fit to the data and param-

eter values consistent with series trends, Table 4 and Appendix V. The crystal-field parameters obtained in this way were, within the errors, the same as those for $Sm^{3+}:LaF_3$. While the ^7F and ^5D states are relatively pure, the eigenvectors of higher-lying states tend to be of mixed character.

The symmetry species associated with the various calculated energy levels for C_{2v} symmetry can be deduced from the eigenvectors and the character table for the symmetry group. Table 6 gives these characters for the two-fold rotation about the z direction (C_{2z}), and the xz reflection plane (σ_{xz}), for each of the four symmetry species of the C_{2v} point group, A_1, A_2, B_1 and B_2. The conventions used here agree with those used by Kumar et al.[7] The eigenfunctions in the crystal-field calculation are specified in terms of basis states of well-defined total angular momentum, J, and its projection in the z direction, M. The effect of C_{2z} is to multiply one of these basis states by $(-1)^M$ and the effect of reflection in the xz plane is to change the state $|J\ M\rangle$ into the state $|J\ -M\rangle$ and multiply it by $(-1)^{J+M+P}$, where P is the parity of the state determined by taking the sum of the orbital angular momentum for each electron in the ion of interest. For Eu^{3+} with six f electrons, J is an integer and P is even. Thus P can be ignored in this case.

Only for M=0 does M remain well defined for the eigenstates in C_{2v} symmetry. For other values of M, the eigenstates contain either the sum or the difference of the basis states corresponding to M and -M. If we use

$$|J\ |M|\ \text{plus}\rangle = [|J\ |M|\rangle + |J\ -|M|\rangle]/\ 2 \text{ and}$$
$$|J\ |M|\ \text{minus}\rangle = [|J\ |M|\rangle - |J\ |M|\rangle]/\ 2 \text{ for M nonzero,}$$

the remaining three columns of Table 6 allow us to classify the eigenvectors for Eu^{3+} according to whether $|M|$ is even or odd and whether J is even or odd. This table also gives the correct symmetry for M= 0 states by regarding these states as plus states for $|M|$ even.

Symmetry species for the eigenvectors are included in Appendix V. In all cases the A or B nature of the symmetry species from the experimental assignments and the calculation agrees. Since the eigenvalue calculation

Table 6.
Character Table for Each of the four Symmetry Species
of the C_{2v} Point Group

Species	C_{2z}	σ_{xz}	|M|	J even	J odd
A_1	1	1	even	plus	minus
A_2	1	-1	even	minus	plus
B_1	-1	1	odd	minus	plus
B_2	-1	-1	odd	plus	minus

is partitioned into one for |M| even and another for |M| odd, this part of the symmetry classification was simple to impose as a constraint on the fit of energy levels. For two levels in the $^7F_4$ state, the symmetry species A_1 and B_1 could not be distinguished experimentally.[7] Only one choice of assignment consistent with the energy level scheme could be made in each case.

The calculated symmetry species subscript, 1 or 2, is shown in parenthesis in Appendix V if it differs from the experimental assignment. Since the eigenvalue calculation was not partitioned into plus and minus states and thus experimental information about species subscripts was not introduced as a constraint on the fitting, it is not too surprising that half the calculated and experimental species subscripts disagree. This disagreement should be viewed as reminder that our understanding of the electronic structure for rare earth ions in the LaF_3 lattice is not yet complete with respect to the details of the eigenfunctions of these energy levels.

5.7. $Er^{3+}:LaF_3$ ($4f^{11}$)

Analyses of the heavy lanthanides in LaF_3 were developed starting with the analysis of the spectrum of $Er^{3+}:LaF_3$ and working back toward Gd^{3+} since the normal light lanthanide ion model for Gd^{3+} would have been Eu^{3+}--which is itself poorly established experimentally. $Er^{3+}:LaF_3$ was an excellent reference case because of the extensive spectral range over which measurements could be made. This range included ~ 80% of the free-ion states in the whole configuration.

The absorption and fluorescence spectra of $Er^{3+}:LaF_3$ measured at 77 K, which included levels up to ~ 39500 cm^{-1}, were reported by Krupke and Gruber.[58] Several higher-energy transitions were also tentatively identified. A subsequent investigation[59] included measurements at ~ 4 K in the range 6000-50000 cm^{-1}. We have made additional spectroscopic measurements at low temperature, so that the levels recorded in Appendix VI represent a composite of published results and in a number of cases a reevaluation of results originally given in Ref. 59. In reviewing our experimental data, a discrepency in the calibration standards applied to a number of absorption groups originally reported by Carnall, Fields, and Sarup[59] was discovered.[14] In addition, the initial crystal-field calculations, which reproduced the observed structure over the whole of the experimental range, were not consistent with several levels that had previously been identified as crystal-field components. These levels were excluded from further parameter fitting calculations in the present study and assumed to have a vibronic origin. We did not obtain fluorescence spectra; thus the energies of the crystal-field components of the ground term $^4I_{15/2}$ are those reported by Krupke and Gruber.[58] In general the results shown in Appendix VI are in good agreement with the somewhat less extensive data reported by others.[58,60] Several incomplete groups were not assigned in the first refinements of the parameters. For example the $^2K_{15/2}$ state calculated near 27800 cm^{-1} was included later because of the excellent agreement between calculated splitting pattern and the observed very weak absorption features in this energy range.

In the case of the $^2G_{7/2}$ group near 28250 cm^{-1}, an isolated band at 28338.1 cm^{-1} was earlier assigned as one of the crystal-field components,[59]

and we could identify a very weak absorption feature near this energy in our spectra. In contrast, the crystal-field calculations grouped all components of this level within a very narrow energy range (~ 25 cm^{-1}) consistent with a single strong absorption feature, and thus suggested that the weak feature arises from some other mechanism.

The character of the spectroscopic features observed in different groups varied considerably. In many instances the features were sharp and intense, but in others a relatively broad band corresponds to a single isolated crystal-field component. The broadening is ascribed to vibronic coupling.

One of the interesting aspects of the $Er^{3+}:LaF_3$ spectrum is the continuing string of isolated free-ion states extending from 0 to ~ 28000 cm^{-1} with major absorption features corresponding to each expected crystal-field component. The extent of the experimental data left little room for more than one interpretation within the systematic framework adopted here.

Examination of the fit to the data in Appendix VI reveals some defects in the energy level calculation. Although the crystal-field splitting of each J-state is well reproduced, a small constant adjustment for each of the lower energy free-ion groups would considerably improve the agreement with experiment. Thus it appears that the free-ion part of the model is inadequate. The need for corrections is not apparent at higher energies suggesting that the intrinsic purity of the lower-lying states may limit their adjustment by the fitting procedure. Fit values of some parameters that were inconsistent in magnitude with those predicted via extrapolation were amenable to change by the addition of constraints. By holding γ and T^2 constant, the values of F^k were forced to assume magnitudes consistent with systematic values. Thus the final fit to the data shown in Table 4 is not that recorded in Ref. 14, but one in which the F^k are more consistent with series trends; however, the energy levels computed with the new parameters were essentially identical to those obtained earlier without the constraints on γ and T^2.

5.8. $Tm^{3+}:LaF_3$ ($4f^{12}$)

Most of the crystal-field components of the various states which occur in the spectrum of $Tm^{3+}:LaF_3$[61] have been identified[13] and are given in Appendix VII. Although considerable structure has been observed, the number of assigned states in the $4f^{12}$-configuration is not sufficient to adequately determine all the parameters of the theoretical model. Thus trends in parameter values across the series were of importance in the initial calculations. Crystal-field parameters determined for $Er^{3+}:LaF_3$, together with free-ion parameters for Tm^{3+} established earlier,[61] were used to compute a model set of energy levels, Appendix VII.

Transitions between the ground state and excited multiplet states in the $4f^{12}$-configuration of Tm^{3+} all occur in the range 5000-40000 cm^{-1}, except for that to $^1S_0$. The energies of the $^1S_0$ state and the higher-lying crystal-field components of the ground state have not yet been estabished by experiment. Model calculations were particularly useful in identifying missing components of some groups and excluding from consideration some of the structure observed in other groups.

Examination of the model crystal-field for the $^3F_4$ state revealed a good correspondence with observed transitions with the exception that a level predicted to occur near 5600 cm^{-1} had not previously been reported. Additional spectroscopic measurements did reveal a relatively weak isolated band at 5615 cm^{-1} consistent with the prediction and obviously overlooked in our earlier work,[61] Fig. 5.

The structure observed in the energy range of the $^3H_5$ group was complex but the model calculation provided the basis for a tentative interpretation as indicated in Fig. 6. In this instance it was clear that much of the observed structure could not be attributed to f→f transitions. There is an apparent correlation between the splitting pattern of the three lowest energy transitions in the model calculation and that of the three most intense bands in the group. The complexity of the structure is typical of that observed in other $Ln^{3+}:LaF_3$ configurations and illustrates the value of the model calculation in developing the trial interpretation. The broad band structure observed in the $^3H_5$ group is also observed in the $^3H_4$ group,

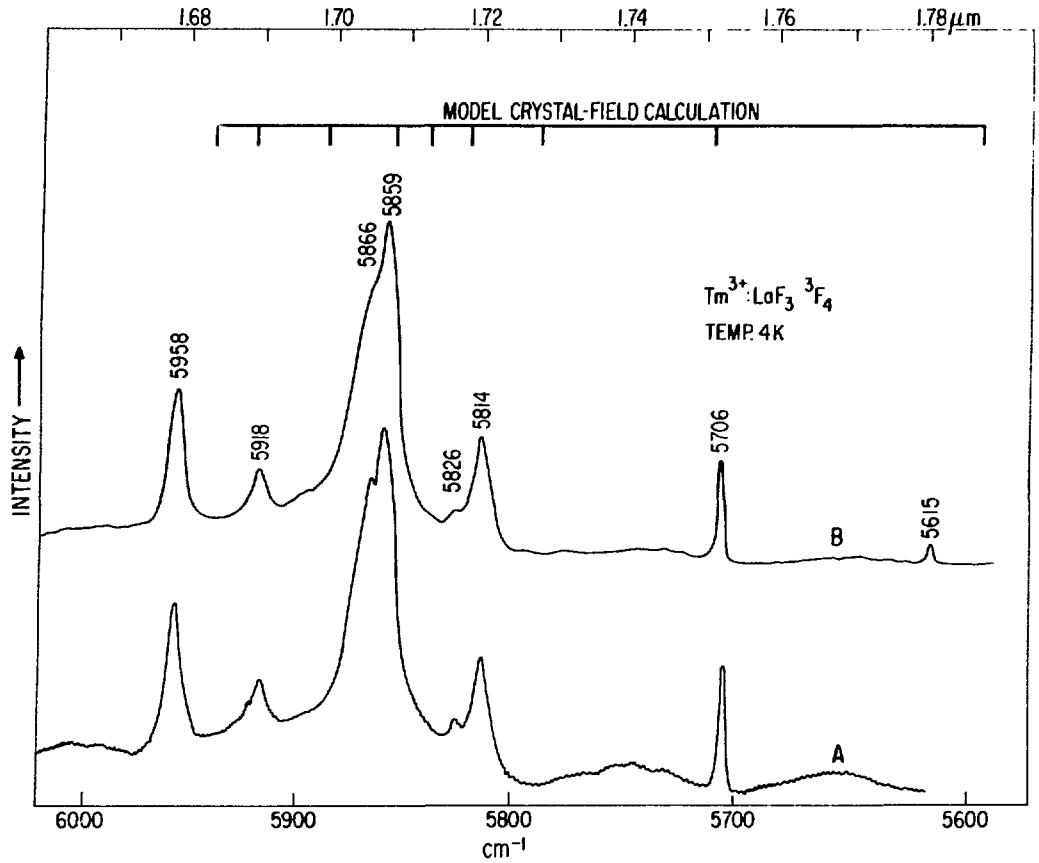

Fig. 5. Comparison of the Experimental Absorption Spectrum of Tm^{3+}:LaF_3 with the Model Energy Level Calculation in the Range 5600-6000 cm^{-1} (the $^3F_4$ State) at ~ 4 K.

Fig. 7, and similar considerations underlie the suggested interpretations in the two groups.

In the $^3F_3$ group near 14550 cm^{-1}, Fig. 8, the predicted narrow band splitting with two close doublets emphasizes the need for a higher resolution spectrum to resolve the structure in this case. The predicted total splitting of the $^3F_2$ group, Fig. 9, was essentially equal to that for the $^3F_3$ state, but the agreement of the predicted structure with the details of that observed was particularly good. The broad band character of the spectrum of the $^1D_2$ group, Fig. 10, is reminiscent of the $^3P_2$ group of Pr^{3+}:LaF_3, Fig. 4.

The $^1I_6$ and $^3P_1$ groups posed interesting interpretational problems in Tm^{3+}. As was found in the Pr^{3+} case, the $^1I_6$ state in Tm^{3+} was computed to

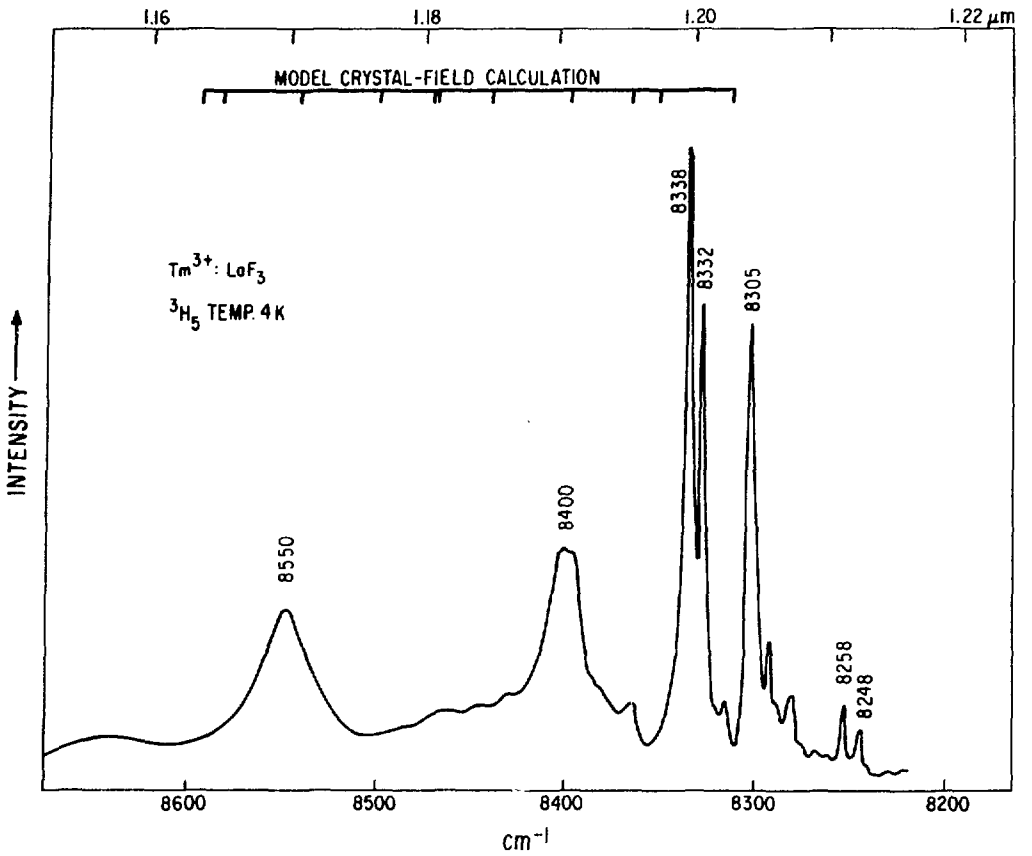

Fig. 6. Comparison of the Experimental Absorption Spectrum of Tm^{3+}:LaF_3 with the Model Energy Level Calculation in the Range 8200-8600 cm^{-1} (the $^3H_5$ State) at ~ 4 K.

have a large total splitting (about 500 cm^{-1}); however, in Tm^{3+} the group is isolated in energy from other free-ion groups, Fig. 11. This isolation draws attention to the fact that within an energy range characterized by a large amount of weak structure there are two bands, each with intensities approximately a factor of 10 greater than the average in that range. If we examine the eigenvectors of each component of $^1I_6$, only two components show a triplet character in excess of 1%; levels near 34769 cm^{-1} and 35107 cm^{-1} are identified with $^3P_1$ character of ~ 1.5 and 1.8%, respectively. Since the intensity is expected to be greatest in those components of $^1I_6$ containing the greatest triplet character, this correlation is a further

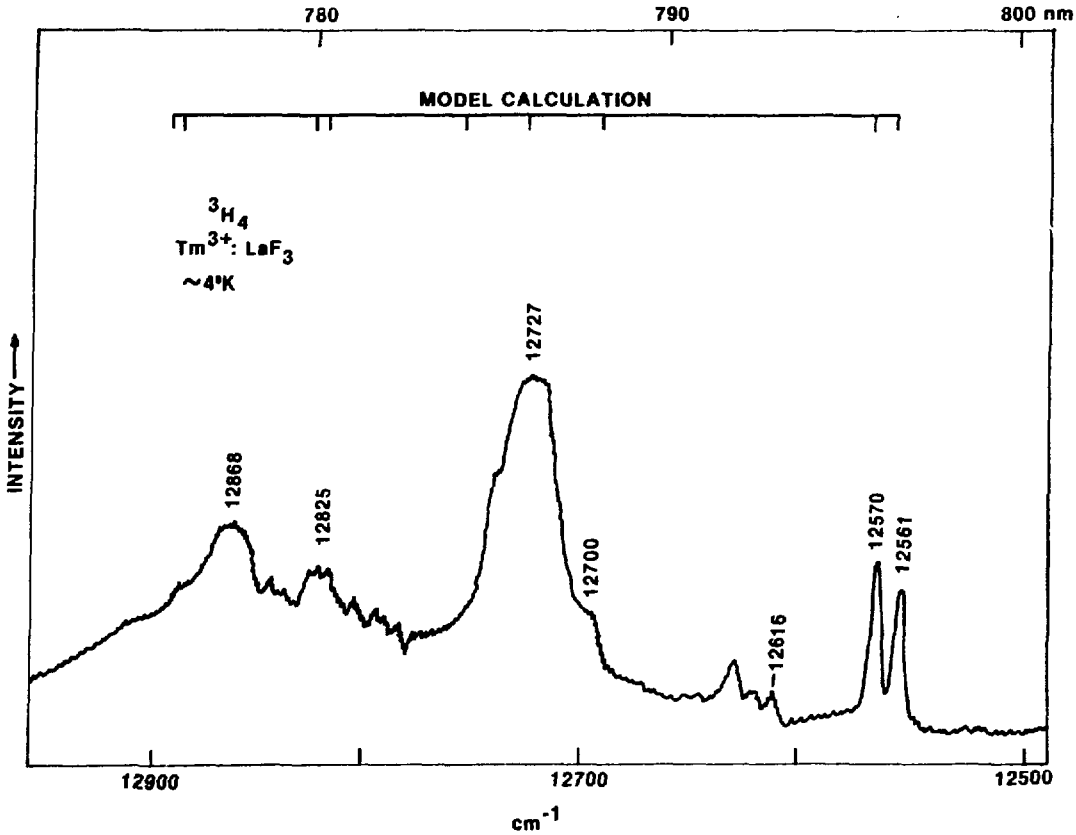

Fig. 7. Comparison of the Experimental Absorption Spectrum of Tm^{3+}:LaF_3 with the Model Energy Level Calculation in the Range 12500-12900 cm^{-1} (the $^3H_4$ State) at ~ 4 K.

confirmation of the model calculation. Assignments to two other absorption features can be made consistent with the model, but similar intensity arguments cannot be invoked.

The model predicted that two of the three components of $^3P_1$ would be separated by about 35 cm^{-1}. Since we observed only two relatively intense bands in this region of the spectrum, Fig. 11, in contrast with the three in Pr^{3+}, the model can be interpreted as suggesting a close doublet in Tm^{3+} which was not resolved in the experimental study. Model calculations also identify the electronic transtions in the $^3P_2$ group as distinct from other weaker structure, Fig. 12. We could conclude for Tm^{3+}:LaF_3 that all of the

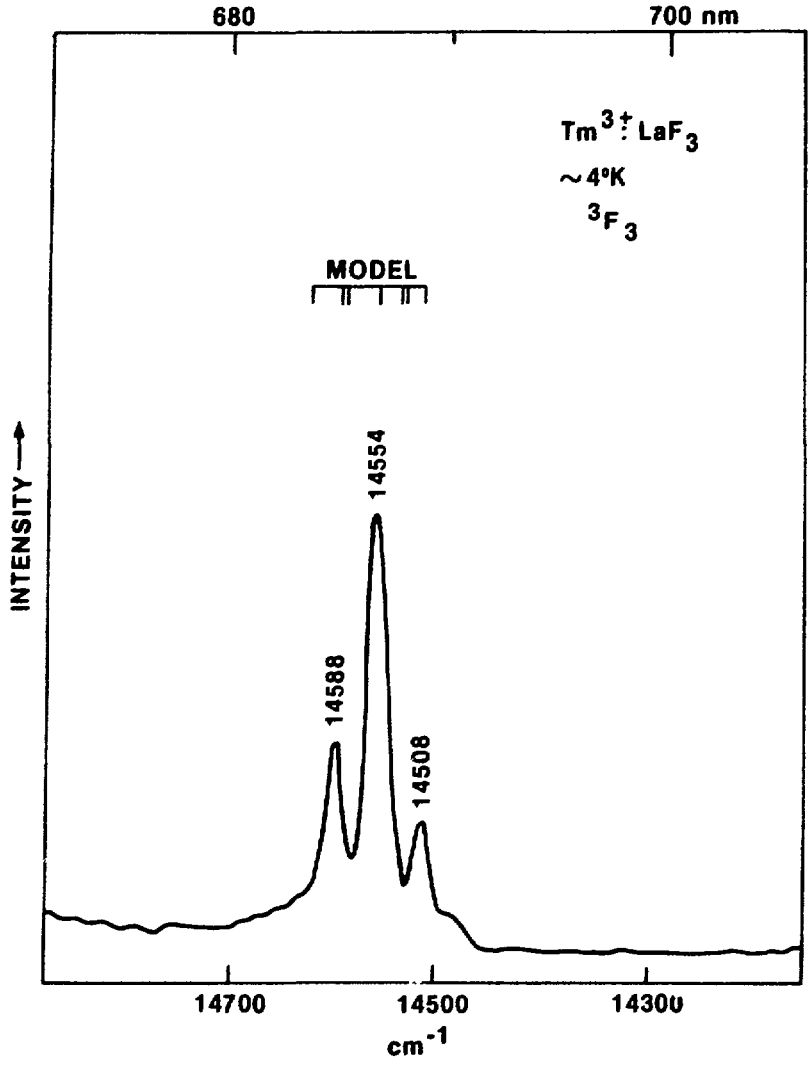

Fig. 8. Comparison of the Experimental Absorption Spectrum of $Tm^{3+}:LaF_3$ with the Model Energy Level Calculation in the Range 14300-14700 cm^{-1} (the $^3F_3$ State) at ~ 4 K.

experimental results were consistent with the $Er^{3+}:LaF_3$ model crystal-field.

In the final determination of the parameters, the value of T^2 was not well determined and thus was assigned consistent with observed parameter trends. Since the $^1S_0$ state was not observed, a similar lack of sensitivity was found for γ, and it was also assigned a fixed value. The parameter values are given in Table 4.

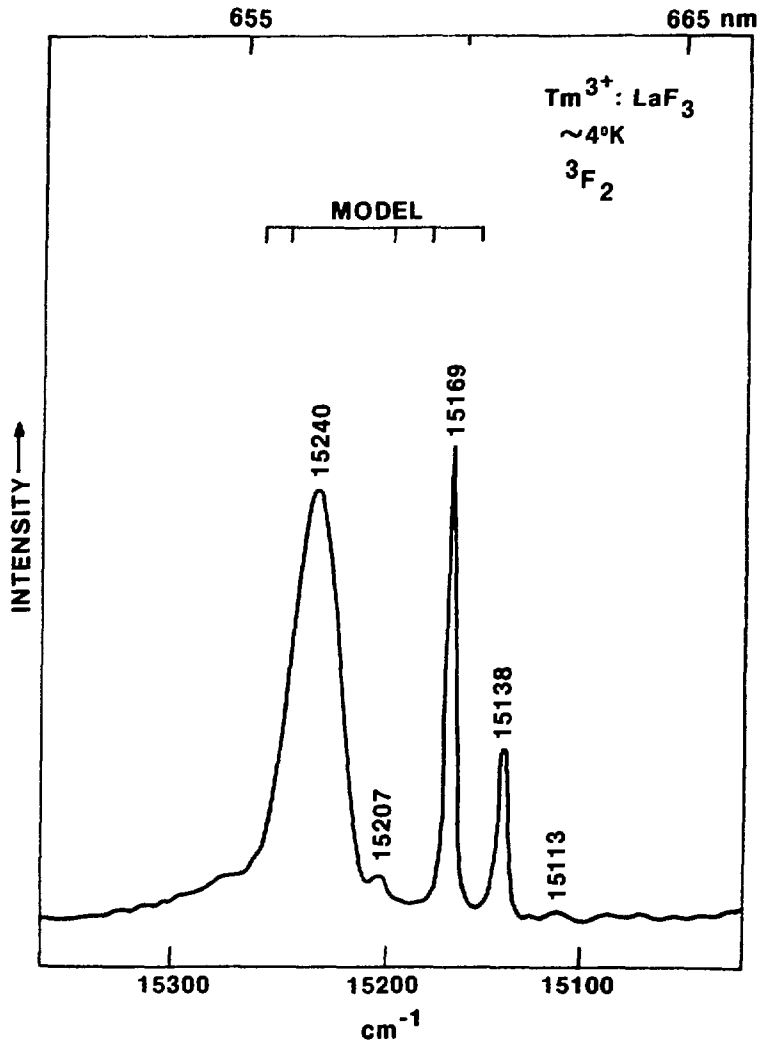

Fig. 9. Comparison of the Experimental Absorption Spectrum of Tm^{3+}:LaF_3 with the Model Energy Level Calculation in the Range 15100-15300 cm^{-1} (the $^3F_2$ State) at ~ 4 K.

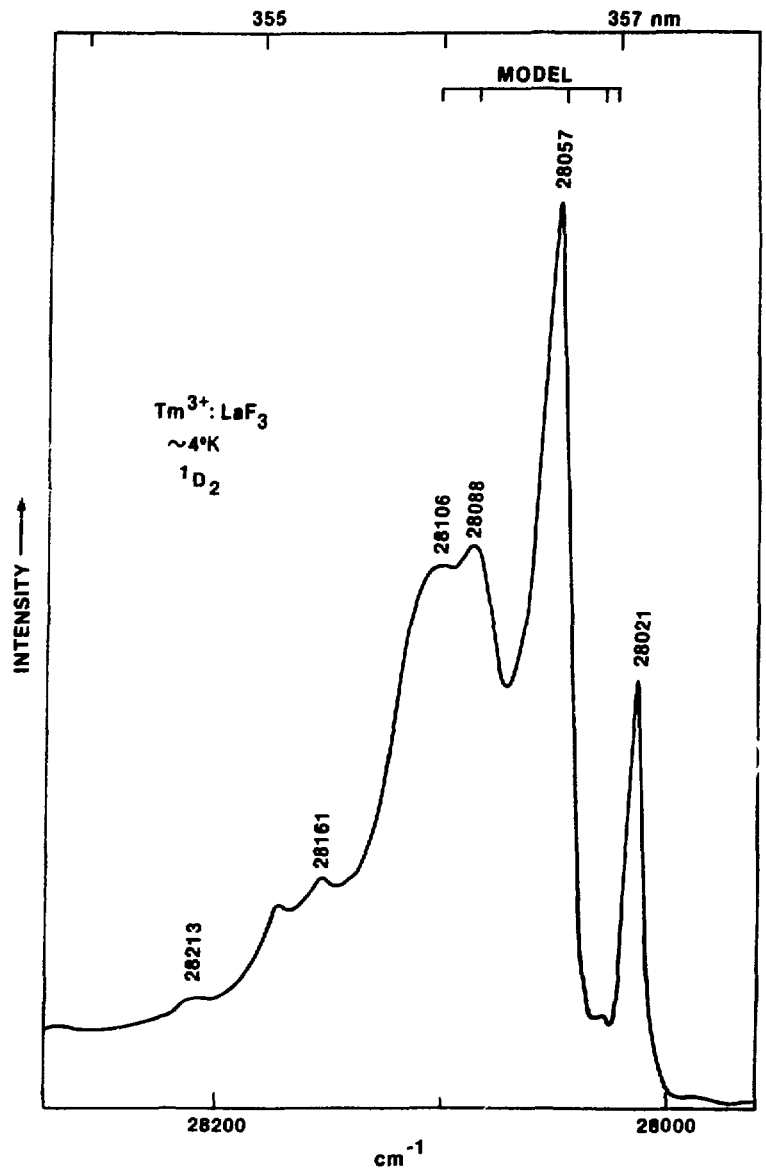

Fig. 10. Comparison of the Experimental Absorption Spectrum of $Tm^{3+}:LaF_3$ with the Model Energy Level Calculation in the Range 28000-28200 cm^{-1} (the $^1D_2$ State) at ~ 4 K.

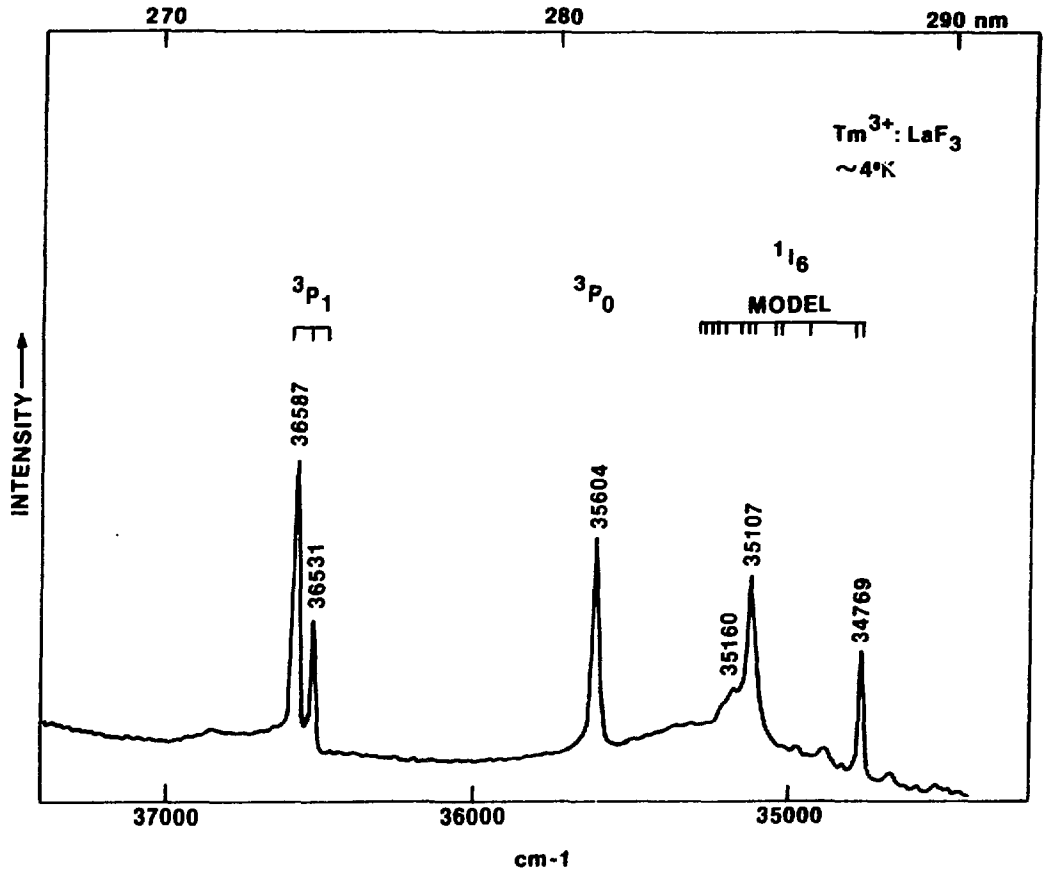

Fig. 11. Comparison of the Experimental Absorption Spectrum of $Tm^{3+}:LaF_3$ with the Model Energy Level Calculation in the Range 34500-37000 cm^{-1} (the $^1I_6$, $^3P_6$, and $^3P_1$ States) at ~ 4 K.

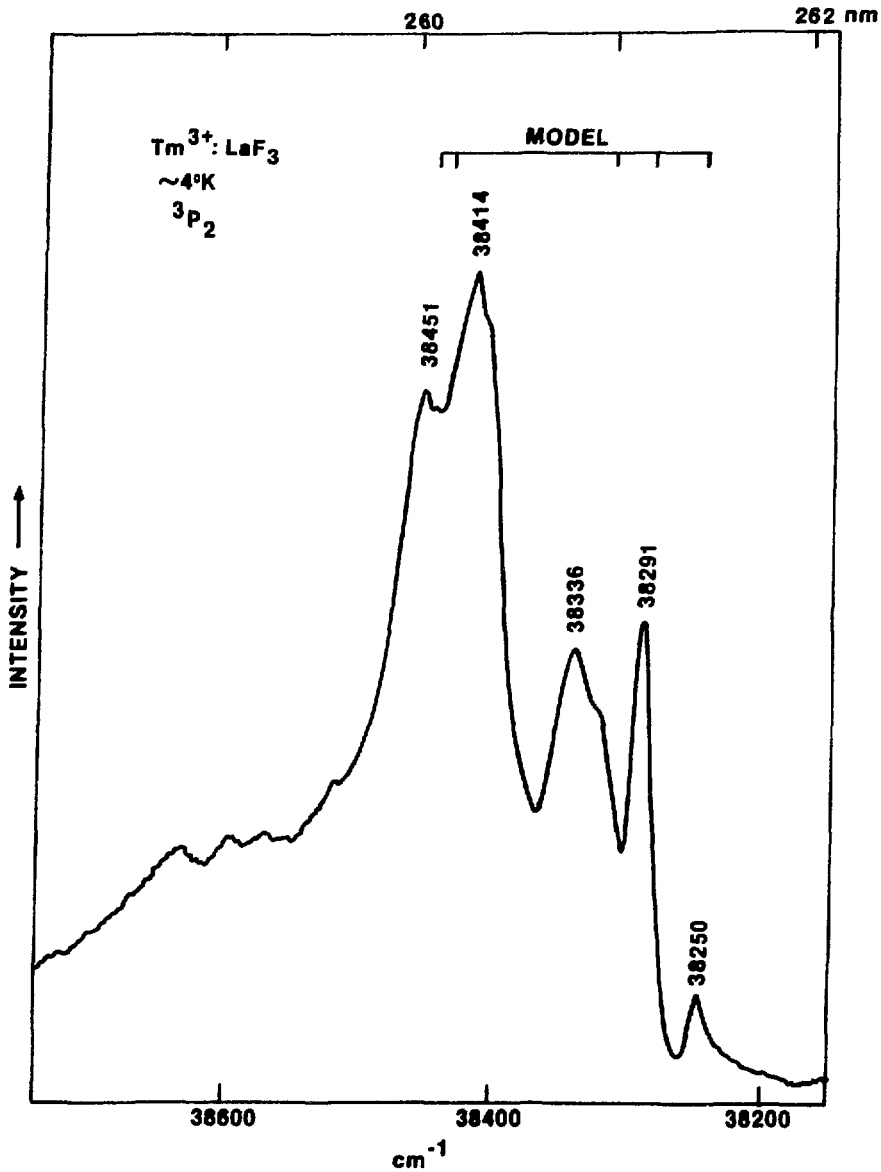

Fig. 12. Comparison of the Experimental Absorption Spectrum of $Tm^{3+}:LaF_3$ with the Model Energy Level Calculation in the Range 34500-37000 cm^{-1} (the $^1I_6$, $^3P_6$, and $^3P_1$ States) at ~ 4 K.

5.9. $Ho^{3+}:LaF_3$ ($4f^{10}$)

An extensive investigation of the absorption and fluorescence spectra of $Ho^{3+}:LaF_3$ has been reported by Caspers, Rast, and Fry (CRF).[62] Our additional experiments confirmed the published data, but only slightly extended the number of states that could be assigned,[14] Appendix VIII. In many cases, the number of observed components of atomic states was less than that allowed theoretically based on C_2 site symmetry, but the baricenters of these components appear to provide the basis for calculation of a consistent set of energy-level parameters. The experimental level energies shown in Appendix VIII are similar to those reported for $Ho^{3+}:LaCl_3$.[63]

Following the preliminary energy level calculation for the $Ho^{3+}:LaF_3$ system with approximate free-ion parameters and the crystal-field parameters derived for $Er^{3+}:LaF_3$ assuming C_{2v} site symmetry, there was obvious excellent correlation between the predicted pattern of crystal-field components in isolated groups and the measured spectra. In addition, there were numerous levels computed to be essentially degenerate in energy, thus predicting that the spectrum should appear somewhat less congested than might have been expected.

Interpretation of the absorption spectrum was complicated by the existence of a ground state crystal-field component at 4.5 cm^{-1}. This level appeared as a satellite on the majority of the bands we observed at 4 K. Most of our results correlated fully with the extensive data reported by CRF who did perform measurements at ~ 1.5 K, where the 4.5 cm^{-1} state was not significantly populated. In Appendix VIII we only report levels from the tabulation of Ref. 62 for which corresponding features could be found in our spectra,[14] or where there was some evidence that our observations might have been limited by resolution. However, the actual values cited are primarily those from Table 1 of Ref. 62. While the 4.5 cm^{-1} satellite in our spectra limited our resolution of structure in some cases, it also provided a check on the identification of electronic transitions.

We did not use the fluorescence-supplemented results given in Table III of Ref. 62 except for the ground state. An example of the problem in identifying crystal-field levels without the benefit of crystal-

field calculations is illustrated in comparing the results in Appendix VIII, and those tabulated in Table III of Ref. 62 for the $^5I_7$ state, Figs. 13 and 14. Comparison of the spectrum shown in Fig. 14 with the energies given in Appendix VIII suggests that not all the predicted bands are observed, but in part this may be ascribed to a number of nearly degenerate energy levels. There is, however, agreement between the structure observed in absorption and that computed in that the total splitting of the state is ~5307-5192 = 115 cm^{-1}. Thus, the extra levels (Y_{11}-Y_{15} in Table III of CRF), Fig. 13, observed only in fluorescence, are assumed to be incorrectly assigned to the $^5I_7$ state. CRF were suspicious of these levels, but had no basis for excluding them.

In contrast to the observation of fewer transitions than might have been expected to the $^5F_7$ state, CRF detected a number of levels, probably vibronic in origin, near 15610 cm^{-1} where the model calculation placed a single level for the $^5F_5$ state. One of the striking examples of excellent agreement between experiment and model calculation was obtained in the case of the $^3K_8$ state near 21400 cm^{-1} where all but one of the possible 2J + 1 = 17 components could be correlated with observed absorption features. This group in Ho^{3+}:$LaCl_3$ is experimentally complete, but assignments guided by polarization and Zeeman data led to large discrepancies between observed and computed level energies. In addition, the experimental energy span of the group was 121 cm^{-1} compared to a computed value of only 70 cm^{-1}.[63] No such discrepancies were noted in the present study. Although polarization and Zeeman affect data were not available for guidance, the model calculation based on Er^{3+}:LaF_3 did predict the observed pattern of electronic levels.

One of the characteristics of the Ho^{3+}:LaF_3 data that lends itself to the type of analysis discussed here is the relative isolation of so many states throughout the spectrum. The stronger general absorption observed at >39000 cm^{-1} was probably due to Ce^{3+} impurity in the LaF_3.

In the final analysis, 128 levels served to define the energy level parameters in Ho^{3+}:$LaCl_3$,[63] compared to 204 in the present case. There are clear differences in the values for γ and in some of the T^k in the two cases, but these parameters are not independent of the F^k which are also larger for Ho^{3+}:LaF_3. In the analysis of the Ho^{3+}:$LaCl_3$ spectrum, some

residual problems in the fit were attributed to the crystal-field part of the Hamiltonian. In $Ho^{3+}:LaF_3$ the preliminary and final crystal-field parameters, except for B_0^2, were similar, and resembled closely the values obtained via lattice sum calculation.[12] For reasons we could not discern, when allowed to vary freely, B_0^2 assumed a value of about half of that expected from trends in the series. Assignment of the value 240 cm^{-1} did

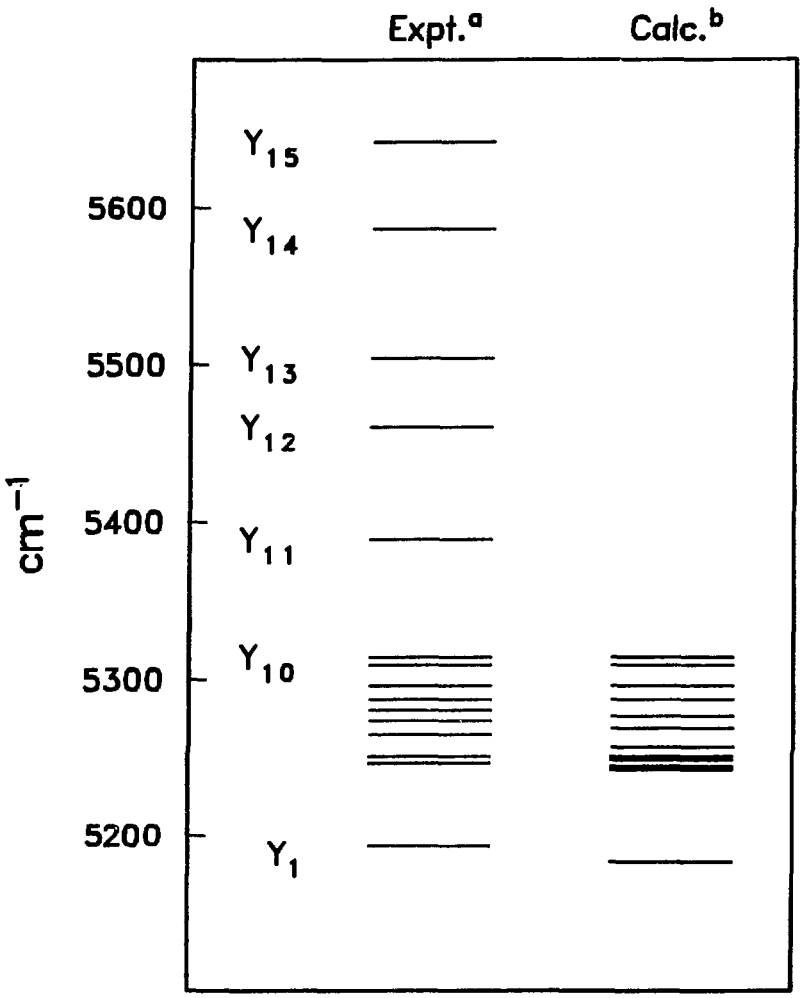

Fig. 13. Comparison of the Experimentally Observed and Model Computed Crystal-field Levels for the $^5I_7$ State of $Ho^{3+}:LaF_3$: (a) From Ref. 62, Table III, (b) Computed Levels from Appen. VIII.

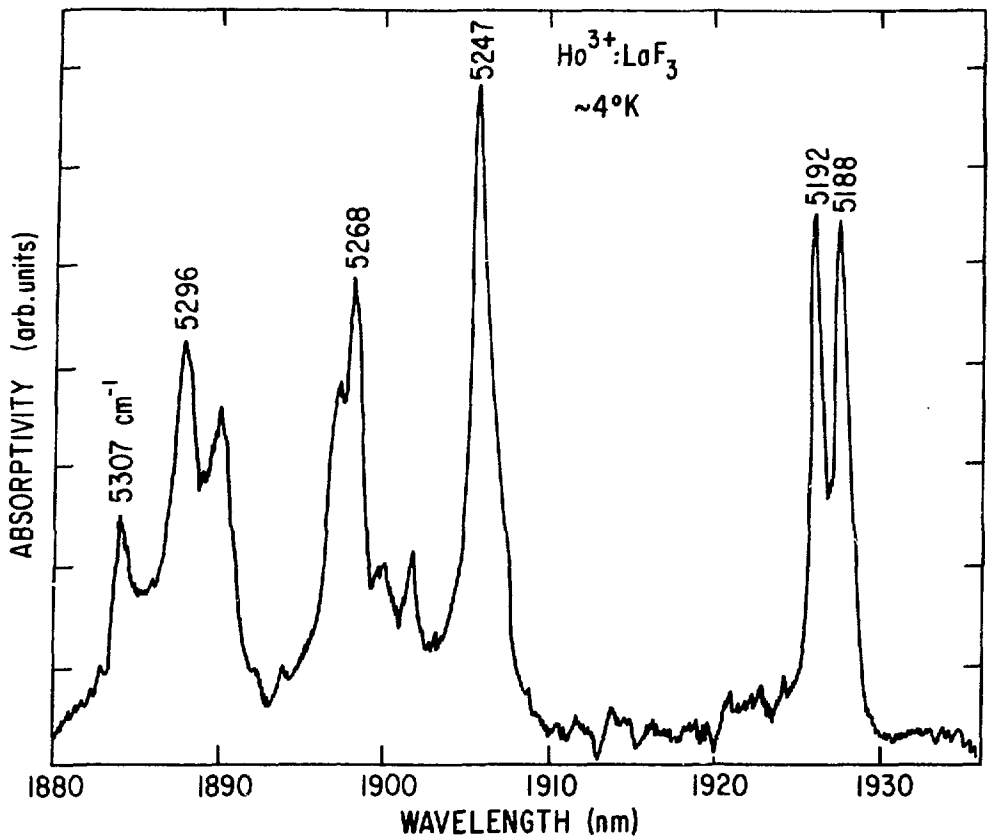

Fig. 14. Absorption Spectrum of $Ho^{3+}:LaF_3$ at ~ 4 K in the Range 1880-1930 nm

not appear to perturb any of the other parameters, Table 4. Similarly, series-inconsistent values of γ and T^2 were obtained when these parameters were free.

5.10. $Dy^{3+}:LaF_3$ ($4f^9$)

Absorption and fluorescence spectra of $Dy^{3+}:LaF_3$ including levels up to ~ 32000 cm^{-1} have been reported.[11,15,64] The results presented in Appendix IX at >5800 cm^{-1} represent for the most part observations made in the present investigation. They are nearly identical to those reported earlier[64] where the two sets overlap. In a few instances where weak bands were reported in the literature consistent with the computed structure but not observed in the present work, the entry was included in the line list.

The initial adjustment of atomic and crystal-field parameters was based on assignments made to isolated groups of levels, and final parameters are given in Table 4. Many of the assignments included all the expected crystal-field components of a particular state. Assignments to regions of extensive structure were only made after all parameter values were already well established.[15]

5.11. $Tb^{3+}:LaF_3$ ($4f^8$)

The spectrum of Tb^{3+} in single-crystal TbF_3 has been studied in absorption and fluorescence by Krupka and Guggenheim.[65] From this data the centers of gravity of the $^5D_4$ and the ground term ^7F multiplet components could be computed consistent with an earlier analysis of $Tb^{3+}:LaCl_3$.[1] However, the crystal symmetry is not that of $Tb^{3+}:LaF_3$. SmF_3 and heavier lanthanides crystallize in the orthorhombic YF_3 structure.[25] Experimental spectroscopic results for $Tb^{3+}:LaF_3$ do not appear to have been analysed previously. Considering the complexity of the spectrum this is understandable. The energies of the crystal-field levels assigned in the present investigation[16] are included in Appendix X together with a computed energy level scheme based on parameters given in Table 4.

The absorption spectrum of $Tb^{3+}:LaF_3$ represents a particularly challenging case for energy level structure analysis. Most of the band structure we observed was in the 26000-40000 cm^{-1} range. At higher energies the transitions in our ~ 1% doped crystals were too weak to be observed in absorption. Since the $^7F_6$-ground state is a very pure septet, and the amount of septet character in the higher energy states, (>6000 cm^{-1}), decreases rapidly, weaker transitions are expected at higher energies. Both the low intensity and high density of levels have been cited as problems in interpreting the spectrum of $Tb^{3+}:LaCl_3$ where "safe" crystal-field analysis[1] did not extend above ~26000 cm^{-1}. A summary of free-ion states of Tb^{3+} consistent with the present results has been reported.[66]

Since only a fraction of the $4f^6$-configuration is found at <40000 cm^{-1}, it is not surprising that the F^k parameters are not well established by the existing data. A number of constraints were adopted to

yield a parameter set that did provide an excellent correlation between observed and computed level energies, Table 4, and was consistent with systematic trends in parameter values.

5.12. $Gd^{3+}:LaF_3$ ($4f^7$)

The energy levels of the ^6P and ^6I groups in $Gd^{3+}:LaF_3$ have been reported by Caspers et al.[67] and by Schwiesow and Crosswhite.[68] These experimental results were subsequently extended to include the ^6D and ^6G crystal-field states in the 40000-50000 cm^{-1} range.[69] The data recorded in Appendix XI are a composite of the results published in Ref. 68 and 69.

A crystal-field analysis of the spectrum of $Gd^{3+}:LaF_3$ to ~37000 cm^{-1} demonstrated that good agreement with the optical measurements could be achieved by assuming a hexagonal site symmetry.[11,68] We have only recently attempted to analyze all of the available data via a complete free-ion and crystal-field matrix element diagonalization in C_{2v} symmetry.[16] An obvious problem in such an analysis lies in having experimental results for such a small fraction of the whole configuration. This was also encountered in $Tb^{3+}:LaF_3$, but is even more evident in the present case. The actual errors determined in the fitting procedure are deceptively low because they are established by the correlation between assigned and observed levels, not by what in principle should be included in the fit.

To begin the analysis, a preliminary set of crystal-field parameters for Tb^{3+} was combined with a previously established set of free-ion parameters for $Gd^{3+}:LaF_3$,[69] to provide the basis for a model calculation. In each free-ion group, all deviations of the model-computed levels from observed band energies were less than 12 cm^{-1}, for assignments in the range 32000-49250 cm^{-1}.[16] Further adjustment in parameters was therefore restricted to the free-ion set. Several of the latter were not well determined when they were freely varied, but fixing values consistent with systematic trends maintained an overall excellent agreement between observed transition and computed level energies. In the final parameter fitting, with additional experimental levels near 50000 cm^{-1} included, only seven free-ion parameters were freely varied as shown in Table 4.

Although the data set is even smaller for Eu^{3+}:LaF_3, comparison of its crystal-field parameters with those for Tb^{3+}:LaF_3 reveal distinct differences, particularly in the sixth degree terms, Table 4. However, when the crystal-field parameters of Eu^{3+}:LaF_3 were combined with the free-ion parameters of Gd^{3+}, the resulting fit to the observed crystal-field structure in Gd^{3+}:LaF_3 was also very good, with σ = 11 cm^{-1}. As was already revealed by the difference between our crystal-field parameter set for Gd^{3+}:LaF_3 in D_{3h} symmetry[11] and that of Schweisow and Crosswhite,[68] both quite adequately reproducing the available experimental data, more than one parameter set in D_{3h} symmetry can be found to yield a satisfactory correlation with experiment. This is clearly the case in C_{2v} symmetry too.

The difficulties posed for crystal-field theory, when dealing with the interpretation of ground-state splitting in ions having a half-filled shell, are well known. As a result of the special properties of the $4f^7$ configuration, first-order crystal-field matrix elements vanish and any explanation of observed splittings of the ground or excited states must involve at least second or higher order crystal-field interactions.[3] Wybourne's exposition of the situation and examination of possible mechanisms is still a valid statement of the problem.[70] For the lanthanides, the ordering of the crystal-field components in the ground state is dependent on the sign of B_0^2, and is $\pm 7/2$, $\pm 5/2$, $\pm 3/2$, $\pm 1/2$ with $\pm 7/2$ calculated lowest in energy for + B_0^2. A positive sign for B_0^2 appears to be consistent with EPR results for Gd^{3+} in LaF_3[71] and in fluorozirconate glass,[72] and also in agreement with the crystal-field analysis assuming D_{3h} site symmetry.[11] It has been pointed out that the crystal-field splitting of the ground state for Gd^{3+}-containing crystals is too small to have actually been observed by optical spectroscopy.[73]

Both the EPR results for Gd^{3+}:LaF_3 and lattice sum calculations for LaF_3,[12] emphasize that the sign of B_0^2 depends on the <u>details</u> of the site symmetry, as indicated in Table 2. In the present treatment of the optical spectra of Ln^{3+}:LaF_3, the crystal-field parameter sets that have provided a systematic correlation of the experimental data are based on an assumed approximate C_{2v} symmetry and have a negative B_0^2 term. However, as pointed out earlier, this choice had a practical basis. If, instead of the approximate C_{2v} symmetry we were to use C_2 symmetry, the results of Table 2 sug-

gest that alternate sets of crystal-field parameters, one with $+B_0^2$, the other with $-B_0^2$, depending on whether the z-axis is taken parallel or perpendicular to the crystal c axis, could be determined to give equally good representations of the actual data.

5.13. $Yb^{3+}:LaF_3$ ($4f^{13}$)

Classification and analysis of lines assigned to the fourth spectrum of atomic Yb, Yb IV, places the $^2F_{7/2}$ - $^2F_{5/2}$ ground term interval at 10214.0 cm^{-1}.[74] This yields a value of the spin-orbit coupling constant of 2918 cm^{-1}. Rast and co-workers[75] observed both the absorption and fluorescence spectra of $Yb^{3+}:LaF_3$, and interpreted their results, consistent with those for Yb IV, as indicating levels of $^2F_{5/2}$ at 10260, 10430, and 10660 cm^{-1}. Two excited levels belonging to the ground $^2F_{7/2}$ state were placed at 185 and 401 cm^{-1}, leaving one level unidentified. The electronic structure exhibited by Yb^{3+} in several different hosts has been summarized by Dieke,[1] with generally similar crystal-field splitting patterns to that reported for $Yb^{3+}:LaF_3$. The computed energy-level scheme, Table 7, using crystal-field parameters for $Tm^{3+}:LaF_3$, Table 4, provided the basis for interpretation of the experimental results. The correlation of computed energies for the ground $^2F_{7/2}$ state with the two reported states suggests that a low energy state near 50 cm^{-1} has not been observed. The fact that both absorption to and fluorescence from a level near 10260 cm^{-1} have been observed indicates that this is undoubtedly the lowest energy crystal-field component of the $^2F_{5/2}$ excited state. We have confirmed the existence of levels at 10260 and 10430 cm^{-1} by measuring the spectrum of 1% $Yb^{3+}:LaF_3$. Strong sharp bands were observed at both energies. However, no clear evidence was obtained for a band near 10660 cm^{-1}. As pointed out by Rast et al., there is a broad shoulder to the higher energy side of the 10430 cm^{-1} band. In the absence of clear evidence for an electronic transition superimposed on this shoulder, we have not made an assignment. However, the model calculation does place a level in the 10450-10750 cm^{-1} energy range. The limited data set precluded variation of the crystal-field parameters; only ζ was determined.

Table 7.

Experimental and Computed Energy Level Structure for $Yb^{3+}:LaF_3$

SLJ State	Obs.[a] (cm^{-1})	Calc.[b] (cm^{-1})	O-C
$^2F_{7/2}$	0	26	-26
	-	78	
	185	178	7
	401	382	19
$^2F_{5/2}$	10260	10301	-41
	430	389	41
	(660)[c]	571	

[a]Ref. 75 (cm^{-1} vac).

[b]Parameter values are given in Table 4.

[c]Not included in the parameter fitting.

6.0 SYSTEMATIC TRENDS

Developing a systematic set of atomic and crystal-field energy level parameters for the lanthanides doped into LaF_3 has been an evolutionary process. In the work reported here, each lanthanide was initially treated independently with as many of the parameters of the model varied as could be well established from the available data base before any intercomparison along the series was attempted. In all cases, the subsequent imposition of constraints to preserve what appeared to be systematic trends in parameter values, could be made without any significant change in the goodness of fit to the experimental levels. Thus to a large extent the constraints were imposed on parameters that turned out to be relatively insensitive to the available experimental data base.

The free-ion parameters in $Ln^{3+}:LaF_3$ were expected to approach those obtained in the few analyzed gaseous free-ion investigations. In fact, for $Pr^{3+}:LaF_3$ the F^k values are 96-97% of those for Pr IV, while the values of ζ for Ce^{3+}, Pr^{3+} and $Yb^{3+}:LaF_3$ are respectively 93, 98, and 100% of the corresponding gaseous free-ion values.[41] It was found that extremely good fits to experimental data could be obtained with nearly constant values over the series for some parameters, but trends in other parameters were evident.

6.1. Atomic (free-ion) Parametrization

The systematic variations of the F^k and ζ for $Ln^{3+}:LaF_3$ as a function of N are shown in Fig. 15. For comparison, we include a comparable set for $Ln^{3+}:LaCl_3$[10] using a scale which is offset from that for the $Ln^{3+}:LaF_3$. The actual values of the parameters in the two series are similar, and the parameter values plotted for $Ln^{3+}:LaCl_3$ are given in Table 8.

It has been pointed out that comparison of F^k and ζ calculated using ab initio methods with values of these integrals established by fitting experimental data, results in energy differences, i.e., E(HFR) - E (EXPT) = ΔE which tend to show a constancy over the series that can be useful for purposes of extrapolation.[10,41] Computations of the F^k and ζ with a Hartree-Fock program containing an approximate relativistic correction (HFR),[40,41] are given in Table 9. The differences, ΔE, for $Ln^{3+}:LaF_3$ are plotted in Fig. 16. Near the center of the series, when F^4 and/or F^6 were freely varied and assumed values that were clearly distorted compared to the trends established by other members of the series, we required that the ratios F^4/F^2 and/or F^6/F^2 remain fixed. This limited both the number of parameters varied and the range of values allowed.

Although the HFR ratios F^4/F^2 and F^6/F^2 are nearly constant across the series, 0.6275±0.0005 and 0.4515±0.0005, respectively, the values resulting from fitting the F^k parameters do show distinct but relatively uniform changes. For F^4/F^2 the ratio decreases from 0.731 for $Pr^{3+}:LaF_3$ to 0.695 for $Tm^{3+}:LaF_3$, whereas for F^6/F^2 the ratio increased from 0.478 for $Pr^{3+}:LaF_3$ to 0.559 for $Tm^{3+}:LaF_3$. Thus when requiring fixed ratios of

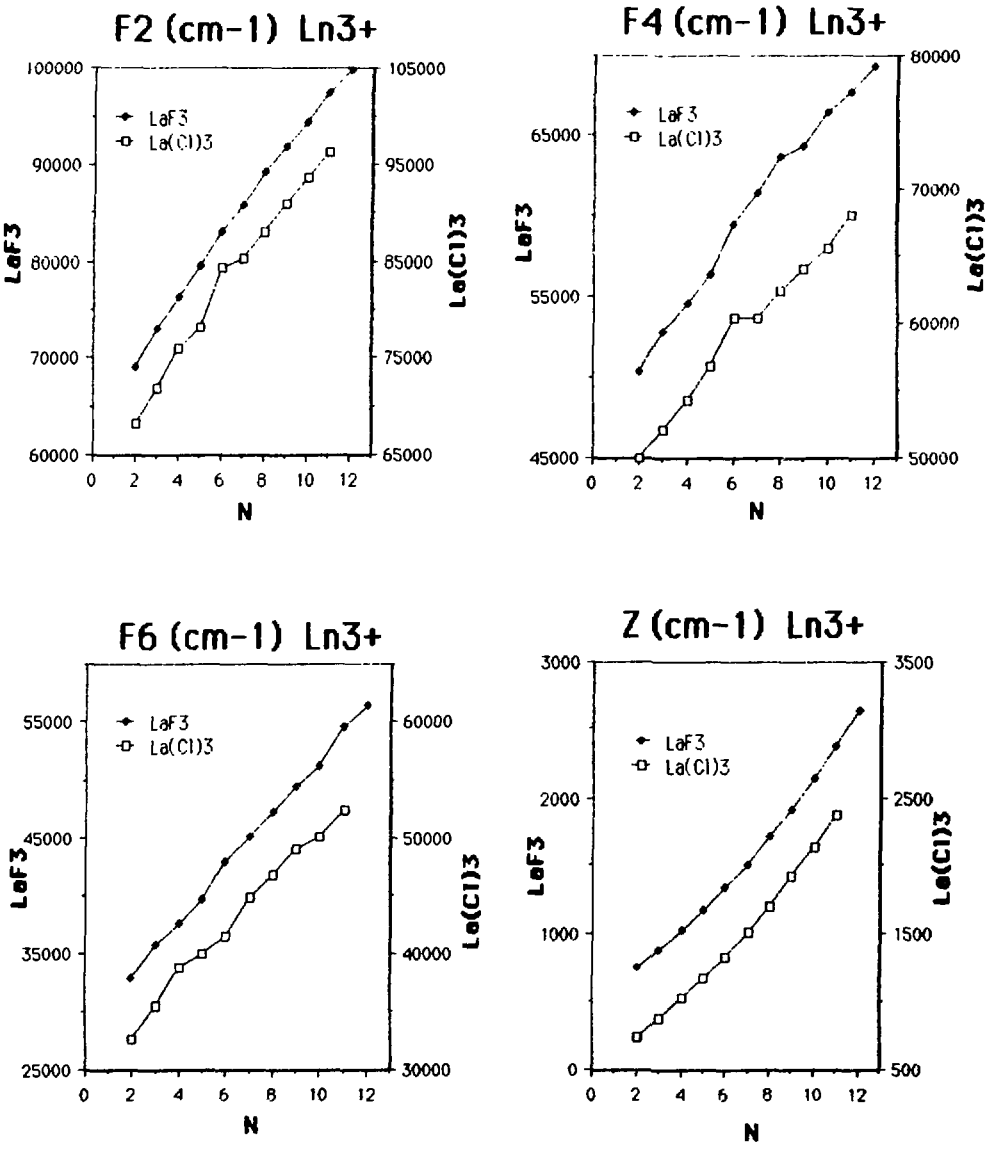

Fig. 15. Variation of the Parameters F^2, F^4, F^6, and Zeta (in cm^{-1}) for both $Ln^{3+}:LaF_3$ and $Ln^{3+}:LaCl_3$ as a Function of the Number of f-electrons (N).

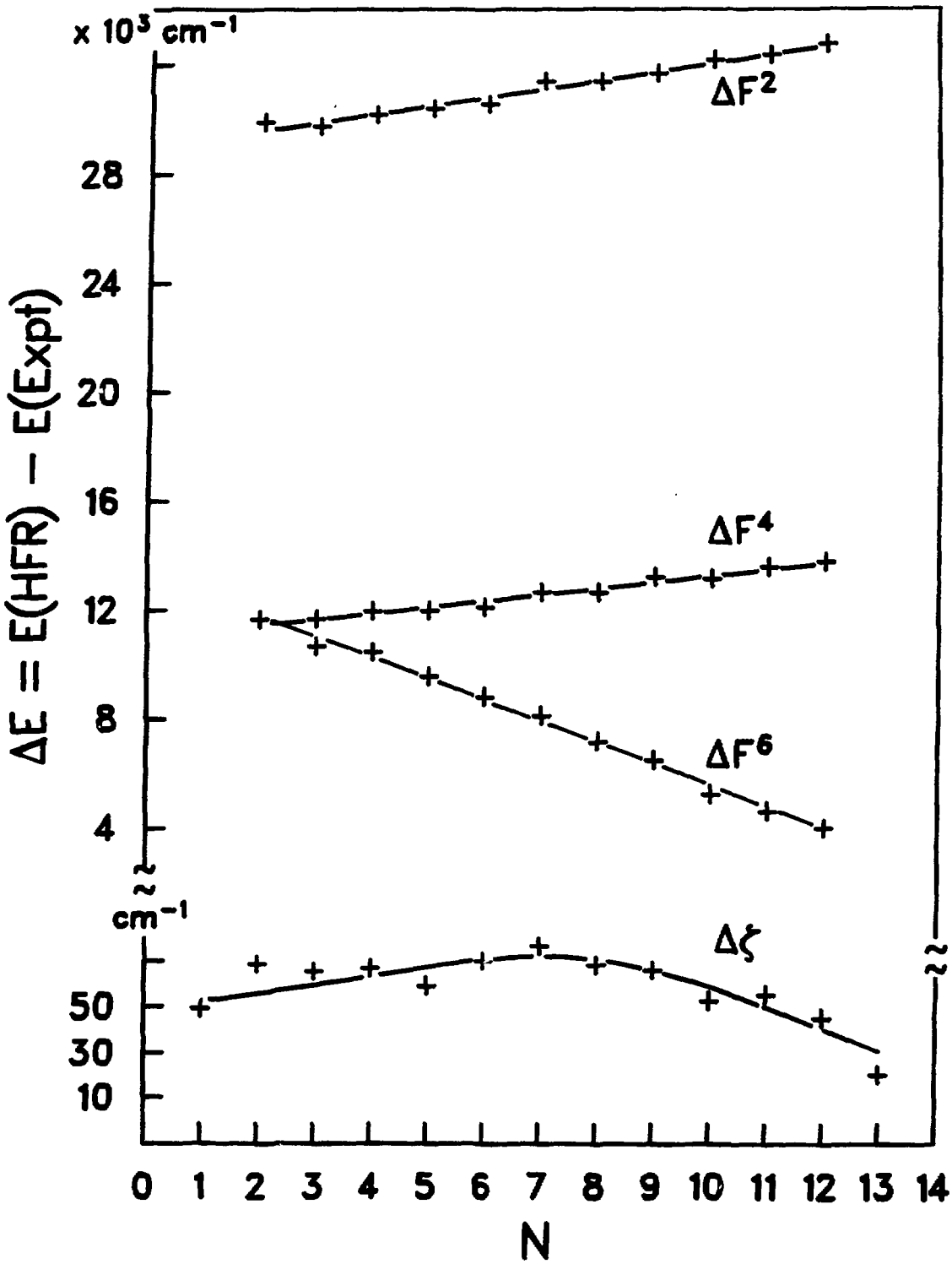

Fig. 16. Variation of the Energy Difference, ΔE=E(HFR)-E(EXPT), between the HFR Computed Energy and That Determined from Experimental Data as a Function of Number of f-electrons

TABLE 8.

Energy Level Parameters for $Ln^{3+}:LaCl_3$[a]

Ln	F^2	F^4	F^6	alpha	beta	gamma	T^2
Pr	68368.	50008.	32743.	22.90	-674.0	1453.	0.
Nd	71866.	52132.	35473.	22.10	-650.0	1586.	377.
Pm	75808.	54348.	38824.	21.00	-645.0	1425.	302
Sm	78125.	56809.	40091.	21.60	-724.0	1700.	291.
Eu	84399.	60343.	41600.	16.80	-640.0	1750.	370.
Gd	85200.	60399.	44874.	19.00	-643.0	1644.	315.
Tb	87988.	62384.	46782.	17.50	-630.0	1880.	340.
Dy	90899.	63922.	49053.	17.20	-622.0	1881.	311.
Ho	93680.	65523.	50104.	17.20	-621.0	2092.	300.
Er	96417.	67932.	52467.	15.90	-632.0	2017.	300.

[a]These parameters were adapted from Ref. 10. The values for N=2-7 were not modified, but those for N=8-11 were transformed following the normalization discussed in Ref. 63 to be consistent with the present results for $Ln^{3+}:LaF_3$.

F^4/F^2 or F^6/F^2, it is necessary to recognize the variation of the ratios across the series.

While the changes in ΔF^2 and ΔF^4 over the series are small enough to be treated as essentially constant over a limited range of N, this is a much less satisfactory assumption for ΔF^6. In addition, the slope of ΔF^6 is opposite to that of ΔF^2 and ΔF^4. There appears to be no basis to have expected the indicated behavior. When we reexamined the data for

Table 9.

HFR Integrals for Ln IV[a] (cm^{-1})

		F^2	F^4	F^6	ζ	M^0	M^2	M^4
Ce IV	$4f^1$	-	-	-	696.41	-	-	-
Pr IV	$4f^2$	98723	61937	44564	820.22	1.991	1.110	0.752
Nd IV	$4f^3$	102720	64462	46386	950.51	2.237	1.248	0.846
Pm IV	$4f^4$	106520	66856	48111	1091.46	2.492	1.391	0.943
Sm IV	$4f^5$	110157	69143	49758	1234.60	2.756	1.540	1.044
Eu IV	$4f^6$	113663	71373	51342	1407.71	3.031	1.694	1.149
Gd IV	$4f^7$	117058	73470	52873	1584.45	3.318	1.855	1.258
Tb IV	$4f^8$	120366	75541	54361	1774.46	3.615	2.022	1.372
Dy IV	$4f^9$	123592	77558	55810	1978.44	3.924	2.195	1.490
Ho IV	$4f^{10}$	126751	79530	57227	2197.06	4.246	2.376	1.612
Er IV	$4f^{11}$	129850	81462	58615	2431.00	4.580	2.563	1.739
Tm IV	$4f^{12}$	132897	83361	59978	2680.97	4.928	2.758	1.872
Yb IV	$4f^{13}$	-	-	-	2947.69	-	-	-

[a]These calculations were made using a version of a Hartree-Fock program written by Fischer[29] and adapted for use at Argonne by M. Wilson to contain an approximate correction for relativistic contraction of s-electron orbitals, Cowan and Griffin.[40] We designate this version as HFR, Crosswhite and Crosswhite.[41]

$Ln^{3+}:LaCl_3$,[10,11,14] we found perhaps less distinct but certainly similar evidence for a negative slope in ΔF^6. The greater magnitude of the slope for k=6 compared to k=2 or 4 places a much greater limit on the range over which ΔE values can be assumed to be constant.

It was possible to fit a cubic equation, $\zeta(cm^{-1}) = 528.606 + 104.116\ N + 4.2069\ N^2 + 0.1467\ N^3$, to the curve for $\zeta(Ln^{3+}:LaF_3)$ shown in Fig. 15. This equation yields $\zeta(cm^{-1}) = 637$ and 2915 for Ce^{3+} and Yb^{3+}, respectively, compared to experimental values of 647 and 2928 cm^{-1}. A similar plot of ζ(HFR) can also be fit by a cubic equation, but the mismatch in the two curves shown by the plot of $\Delta\zeta$ in Figure 16 results in a maximum near N=7, with decreasing mismatch at both N>7 and N<7. Predictions from the energy difference ζ(HFR) - ζ(EXPT) = $\Delta\zeta$ with $\Delta\zeta$ averaged over the series, 623 and 2892 cm^{-1} for Ce^{3+} and Yb^{3+}, respectively, are satisfactory as an approximation.

Some of the principal effects of configuration interaction were added to the Hamiltonian in the form of two- and three-body operators that operate wholly within the f^N configuration. The two-body electrostatic corrections α and β for $Ln^{3+}:LaF_3$ show relatively little variation over the series, but appear to decrease with increasing N, while γ appears to exhibit a slow increase, Fig. 17. As mentioned earlier in the discussion of experimental results for $Pr^{3+}:LaF_3$, the apparent systematic trends indicate that α should be >16. This would argue against our suggested interpretation of the energies of the $^1I_6$ group components.

The behavior of T^2 seems to parallel γ, but other T^i are essentially constant. Since these additional operators, in the form they were introduced, were not orthogonal to those associated with the F^k operators, their inclusion results in changes in the values taken by the original F^k appearing in Eqn. (3). Judd and coworkers have shown that these changes can be avoided if the problem is reformulated in terms of orthogonalized operators.[76,77] The transformation equations are those given in Eq. 9 of Ref. 76 for f^3 except that the expression for the orthogonalized Racah parameter E_0^3 becomes $E_0^3 - 2\alpha/5 + (N-2)\sqrt{2}\ T^2/140$.[78]

In the initial stages of the investigation, when we were attempting to define the two- and three-body operators, it would have been useful to

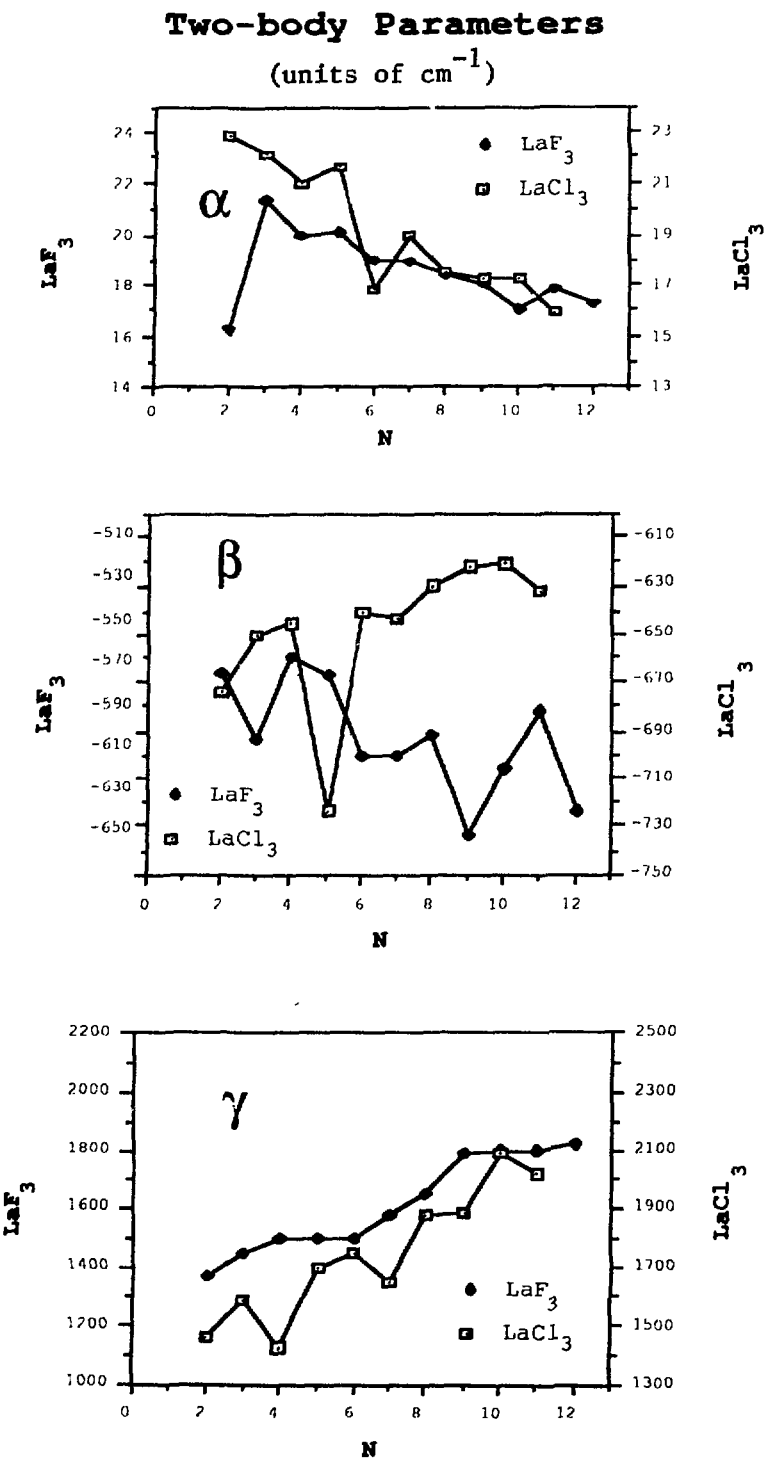

Fig. 17. Variation of the Parameters α, β, and γ (cm^{-1}) for Ln^{3+}:LaF$_3$ and Ln^{3+}:LaCl$_3$ as a Function of Number of f-electrons (N).

approach the problem via the orthogonal operators. However at this point we have satisfactorily defined all parameters. In Table 10, we give the orthogonalized parameters transformed from the values given in Table 4, and showing similar trends. Scatter in the parameter values appears to arise from the limited data available for some ions and some inadequacy of the Hamiltonian used rather than from the nonorthogonality of the operators.

Several different conventions have been suggested for introducing H_{ss} (spin-spin), H_{soo} (spin-other-orbit), and electrostatically correlated spin-orbit (EL-SO) interaction, into the analysis of f-electron systems. We adopted the use of the parameters M^0, M^2, and M^4, for H_{ss} and H_{soo} and found, as did Judd et al.,[37] that when freely varied the values tended to be poorly determined. Since there were significant shifts in the values of M^h depending upon the values of P^f, it appears to be useful to vary both sets simultaneously. Pasternak and Goldschmidt have stressed the necessity for including all spin-dependent parameters in the analysis of $3d^N$-configurations.[79] A reasonable course of action for the M^h is to use ratios for M^2/M^0 (= 0.56) and M^4/M^0 (= 0.38) that result from Hartree-Fock calculations, Table 9, allowing only M^0 to vary freely.[41] From the evidence we have assembled, this appears to be a better choice than either fixing M^h at actual Hartree-Fock calculated values, which are indeed approximated by the actual fit values, or setting the ratios noted above at unity.

The situation with respect to limiting the number of P^f parameters freely varied is more complicated than for the M^h. Since the mechanism of the EL-SO interaction involves a product of spin-orbit and electrostatic matrix elements, ratios of the p^f identical to the ratios of the F^k have been used for the lanthanides $F^4/F^2 \sim .7$ and $F^4/F^2 \sim .5$.[41] However, when Judd and coworkers used experimental results for Pr IV ($4f^2$) as the basis for determining values of the P^f, they found that when freely varied, P^2 and P^4 were indeterminate, and P^6 assumed a large negative value.[37] It was speculated that P^6 might, in fact, be reproducing effects such as the expansion of the 4f eigenfunction as the energy is increased, suggesting that large negative contributions to P^6 could arise if interactions with the continuum were considered.

TABLE 10.

Orthogonalized Energy Level Parameters for $Ln^{3+}:LaF_3$

Ln	F_o^2	F_o^4	F_o^6	alpha'	beta'	gamma'	T^2
Pr	68758.	50672.	34405.	12.98	29.5	98.	0.
Nd	72988.	53251.	37251.	17.07	13.5	110.	298.
Pr	76578.	55581.	38843.	16.40	11.3	113.	300.
Sm	80172.	58043.	41047.	16.13	13.8	114.	300.
Eu	83671.	60307.	43019.	16.13	13.8	114.	300.
Gd	86427.	62076.	44856.	15.14	24.3	116.	300.
Tb	90031.	64463.	46882.	14.72	24.9	122.	320.
Dy	93197.	66198.	48629.	14.42	33.5	130.	329.
Ho	96415.	68763.	50225.	13.72	32.7	131.	400.
Er	99565.	70504.	51812.	14.23	25.9	134.	400.
Tm	102461.	72439.	53287.	13.81	35.0	132.	400.

During the present investigation, when the P^f parameters were fit to data for $Er^{3+}:LaF_3$, we obtained a statistically determined positive value for P^2, an indeterminate value for P^4 and a determined negative value for P^6 that was equal in magnitude to that of P^2. For $Nd^{3+}:LaF_3$, when allowed to freely vary, the values of P^f were all statistically determined, but $P^2 \cong -P^6$. We found that in a fit of data for Pr III $(4f^3)^{80}$ as was the case for Pr IV, the value of P^6 was well determined but negative. We include the data for Pr III in Table 11 for reference.

When the P^f were varied freely and the M^h were varied in ratio or held constant, the values for P^6 became positive for $Ln^{3+}:LaF_3$ nearer the center of the series, but P^4 remained indeterminate and there was little change in the error whether the P^k were varied in ratio or varied freely. Since the M^h and P^f values do interact, we chose a modified convention. The parameter P^2 was varied freely while P^4 and P^6 were constrained by the ratios,

$P^4/P^2 = 0.5$ and $P^6/P^2 = 0.1$. Thus, we have deemphasized P^6 with the knowledge that it assumes negative values at the beginning and at the end of the series when it is allowed to vary freely. Using the indicated constraints, only in the fit of Pr^{3+}, Table 4, did P^2 assume a negative value. Over the series, the constraints adopted resulted in minor change in the value of M^0, and a reasonably uniform increase in P^2 with increasing atomic number in the light half of the series but less overall change in the heavier lanthanides.

It is clear that the relative values of the P^f require further investigation to find a mechanism which can account for the unusual behavior of P^6. That is beyond the scope of this work. However, it is unlikely that the ratios adopted here have caused a significant distortion of the overall results, although there may be individual groups of levels that would be better fit with a different convention than we have adopted.

6.2. Crystal-field Parametrization

While the practice of treating the effects of the crystalline field on a lanthanide ion by supplementing the free-ion Hamiltonian with a sum of single-electron operators, Eqn. (6), has generally yielded a very good correlation with experimental results, some exceptions, such as the $^3K_8$ group of $Ho^{3+}:LaCl_3$, and the $^1D_2$ state of $Pr^{3+}:LaCl_3$, have been recognized, and methods of improving the model have been explored.[81-84]

The effect of the crystalline environment is to reduce the magnitude of the free-ion parameters, but in the case of $4f^2$ we see that this reduction is relatively small as we compare values of F^k and ζ for Pr IV[41] and $Pr^{3+}:LaF_3$. The reduction is larger if we compare the $Pr^{3+}:LaCl_3$ case.[10] Some of the difficulties that arose in fitting crystal-field levels in $Ln^{3+}:LaCl_3$ (D_{3h}-symmetry) were not apparent in fitting the corresponding groups in the LaF_3 host. However, one must recognize that for LaF_3 we deal with a 9 parameter crystal-field model compared to 4 parameters for D_{3h}-symmetry, and thus there is considerably more flexibility in the lower symmetry parametrization. Given the fact that Zeeman or polarization data are *not normally useful in identifying crystal-field components in the*

TABLE 11.

Free-ion Energy Levels and Parameters for Pr III ($4f^3$)[a]

Largest[b] Eigen.	Component	obs. (cm^{-1})	calc. (cm^{-1})	Δ	Largest[b] Eigen.	Component	obs. (cm^{-1})	calc. (cm^{-1})	Δ
0.986	$^4I_{9/2}$	0.0	-11	11	-0.989	$^2D1_{5/2}$	19046.09	19045	16
0.995	$^4I_{11/2}$	1398.34	1390	8	0.721	$^2P_{3/2}$	20856.86	20842	-15
0.998	$^4I_{13/2}$	2893.14	2896	-3	0.910	$^4D_{3/2}$	23091.70	23105	-13
0.995	$^4I_{15/2}$	4453.76	4476	-22	0.889	$^4D_{5/2}$	23245.99	23253	-7
0.973	$^4F_{3/2}$	9370.66	9371	0	0.977	$^4D_{1/2}$	23465.43	23470	-5
-0.774	$^2H2_{9/2}$	10032.92	10022	11	-0.918	$^2I_{11/2}$	24357.98	24382	-24
0.989	$^4F_{5/2}$	10138.18	10138	0	0.992	$^4D_{7/2}$	24886.51	24864	22
-0.966	$^4F_{7/2}$	10859.06	10860	-1	0.984	$^2L_{15/2}$	25244.61	25258	-13
0.975	$^4S_{3/2}$	10950.24	10949	1	-0.996	$^2I_{13/2}$	25391.75	25392	0
-0.886	$^4F_{9/2}$	11761.69	11760	2	1.0	$^2L_{17/2}$	26477.88	26448	35
0.903	$^2H2_{9/2}$	12494.63	12520	-25	0.899	$^2D2_{3/2}$	26921.49	26930	-9
0.639	$^2G1_{7/2}$	13887.60	13890	-2	0.934	$^2H1_{9/2}$	27178.80	27163	16
-0.993	$^4G_{5/2}$	14187.35	14194	-7	-0.766	$^2D2_{5/2}$	27597.13	27598	-1
0.870	$^4G_{7/2}$	15443.48	15446	-3	-0.834	$^2H1_{11/2}$	28101.77	28134	-32
-0.721	$^4G_{9/2}$	15705.13	15696	9	-0.648	$^2F2_{5/2}$	-	30563	-
0.994	$^2K_{13/2}$	16089.14	16097	-8	0.779	$^2F2_{7/2}$	31787.93	31790	-2
-0.678	$^4G_{9/2}$	16763.98	16750	14	0.763	$^2G2_{9/2}$	39225.60	39216	10
0.699	$^2D1_{3/2}$	17095.63	17084	12	0.765	$^2G2_{7/2}$	39940.72	39947	-6
-0.973	$^4G_{11/2}$	17409.58	17408	2	-0.785	$^2F1_{7/2}$	53092.80	53095	-2
-0.979	$^2K_{15/2}$	17642.06	17628	14	-0.747	$^2F1_{5/2}$	54184.37	54180	4
0.977	$^2P_{1/2}$	18693.65	18691	3					

Parameters (cm^{-1})[c]

E(ave)	19718	T^2	449 (9)	M^0	0.19 (.35)
F^2	59960 (28)	T^3	34.9 (5)	M^2	0.11
F^4	39937 (112)	T^4	83.2 (7)	M^4	0.07
F^6	26429 (71)	T^6	-217 (11)	P^2	182 (51)
ζ_{4f}	664.9 (2)	T^7	314 (16)	P^4	-174 (131)
α	30.935 (.25)	T^8	284 (19)	P^6	-1158 (211)
β	-813.6 (15)				
γ	2203 (19)	σ = 17			

a. Experimental data from Sugar[80] modified by an analysis by Crosswhite et al.[3] where the value 27178.80 cm^{-1} was substituted for Sugar's original report of 26979.66 cm^{-1}, and levels at 53092.80 and 54184.37 cm^{-1} were added.

b. The largest eigenvector component is given with its phase.

c. Parameter errors are shown in parentheses; M^0 was freely varied, but M^2 and M^4 were constrained by the relations $M^2 = 0.56\ M^0$, $M^4 = 0.38\ M^0$.

fluorides, it is possible that, in making assignments for the best agreement with the calculated energies, some discrepanies may have been hidden. Thus, we cannot necessarily conclude on the basis of the fits to experimental data that the single-electron crystal-field model works better for the fluorides than the chlorides.

One of the critical aspects of crystal-field parametrization is the choice of initializing values. In the present investigation, initial values for D_{3h} site symmetry were taken from the work of Onopko,[9] and a consistent transformation to a C_2 symmetry was introduced by Morrison and Leavitt.[12] The superposition model of Newman[85,86] offers an alternative method for calculation of starting crystal-field parameters based on a knowledge of the crystal-structure. It can also be used to reduce the number of freely varied parameters by providing values for the ratios of selected parameters. However, both the lattice sum calculations[12] and the superposition model require detailed crystallographic data. The approach we have used yields sets of parameters that are in general of the same magnitude and sign as the real parts of the corresponding C_2 symmetry parameter sets, Table 2, but is not directly related to the crystal structure.

Trends in magnitude of the crystal-field parameters for $Ln^{3+}:LaF_3$ as a function of the number of f electrons are shown in Figs. 18-20. One would expect a decrease in magnitude of these parameters over the series due to the increased nuclear charge that the electrons experience. As the electron orbits are pulled in closer to the nucleus, the effect of the crystal-field should be reduced, even though the network of nearest neighbor F^- ions may to a certain extent collapse around the impurity ion as the latter radius decreases. One would also expect that the change would be greatest early in the series where ionic radii are exhibiting their greatest relative decrease. In the heavier members of the series the change in ionic radius from one ion to the next is much less pronounced. Interestingly, not all the parameters follow the expected trends.

B_0^2 appears to be essentially constant over the series, Fig. 18, as pointed out by Morrison and Leavitt.[12] B_2^2 was not well defined in a number of fits, and thus was frequently not varied. All of the other parameters

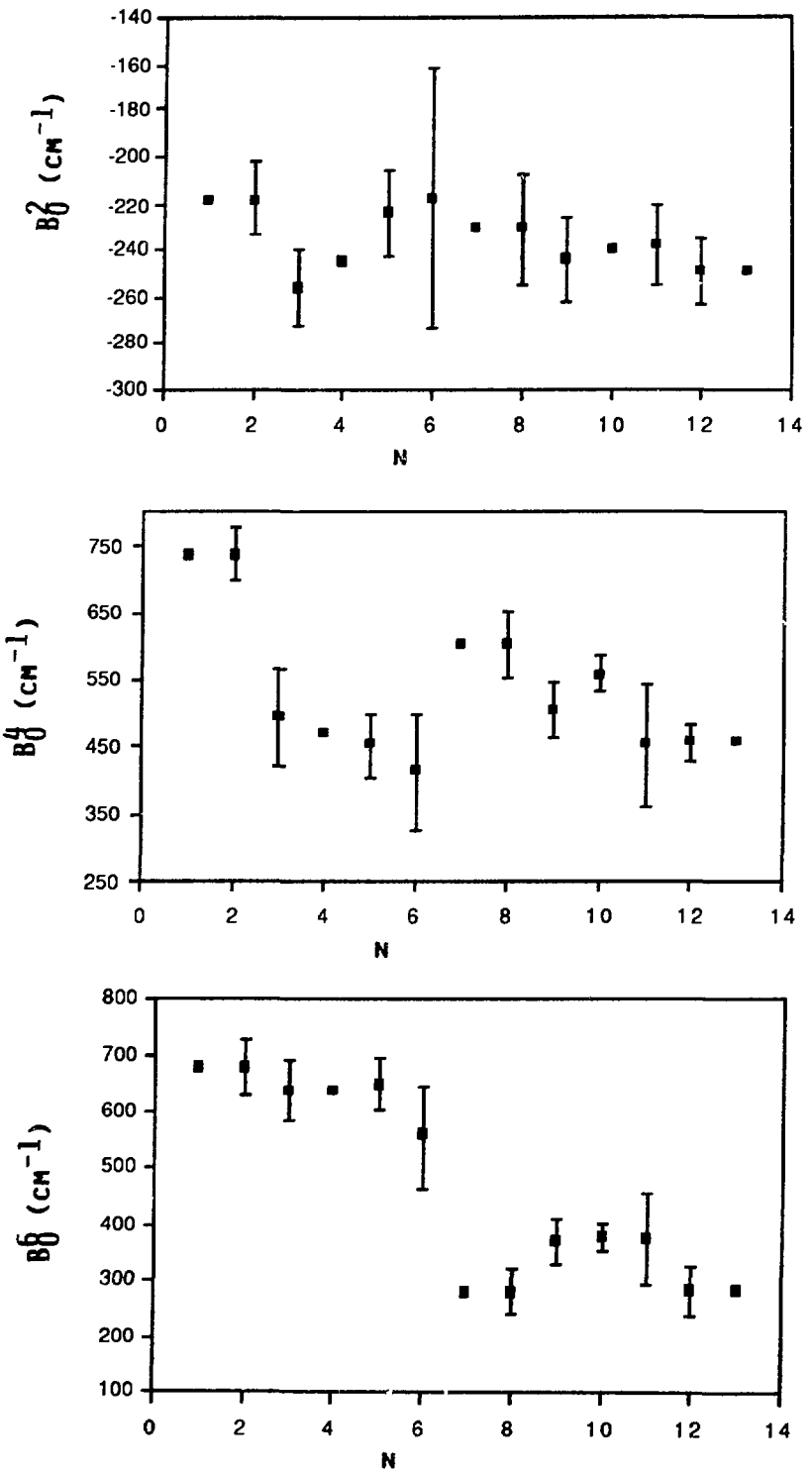

Fig. 18. Variation of the Crystal-field Parameters B_0^2, B_0^4, and B_0^6 (in cm^{-1}) for Ln^{3+}:LaF_3 as a Function of Number of f-electrons (N).

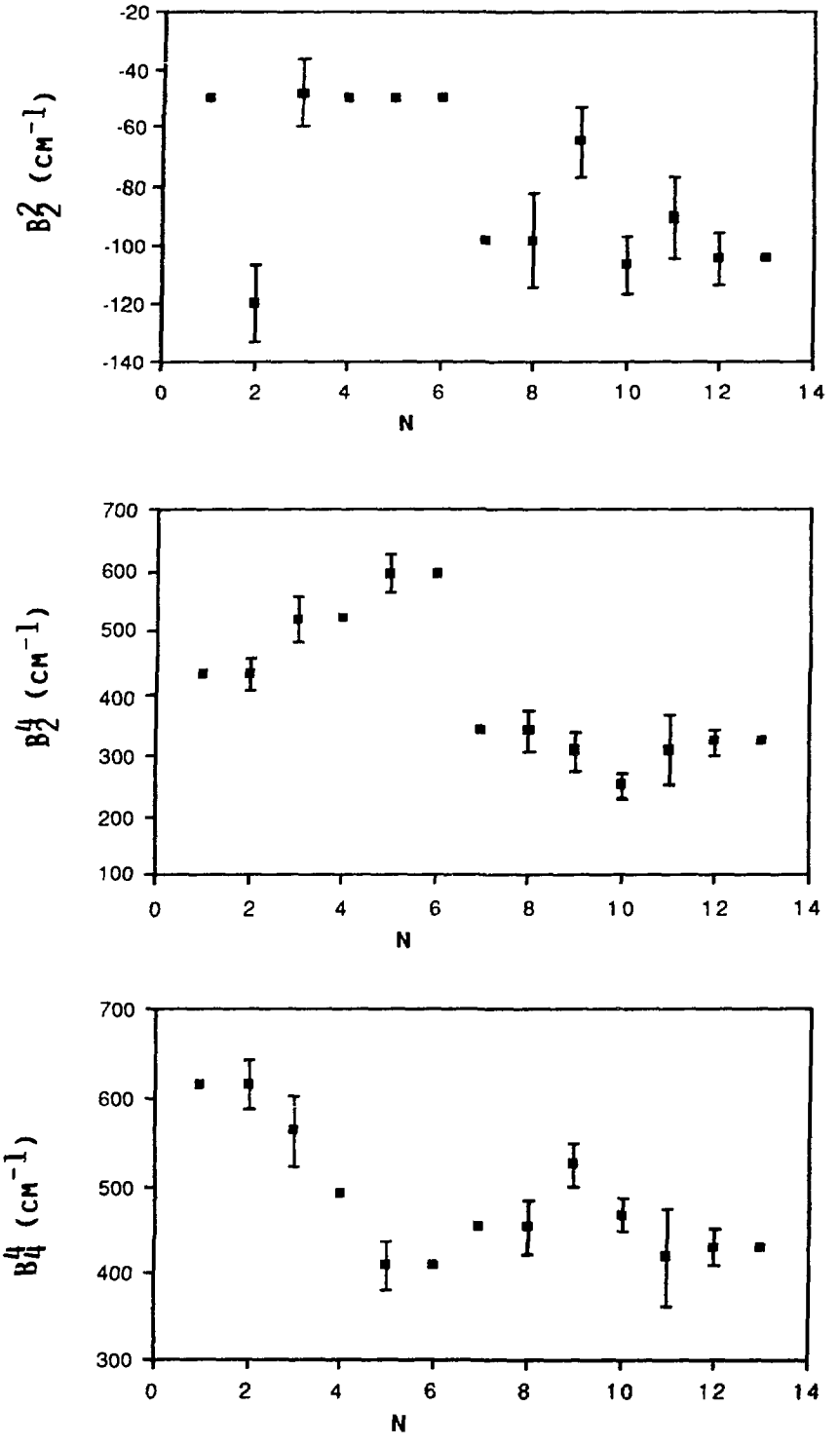

Fig. 19. Variation of the Crystal-field Parameters B_2^2, B_2^4, and B_4^4 (in cm^{-1}) for Ln^{3+}:LaF_3 as a Function of Number of f-electrons (N).

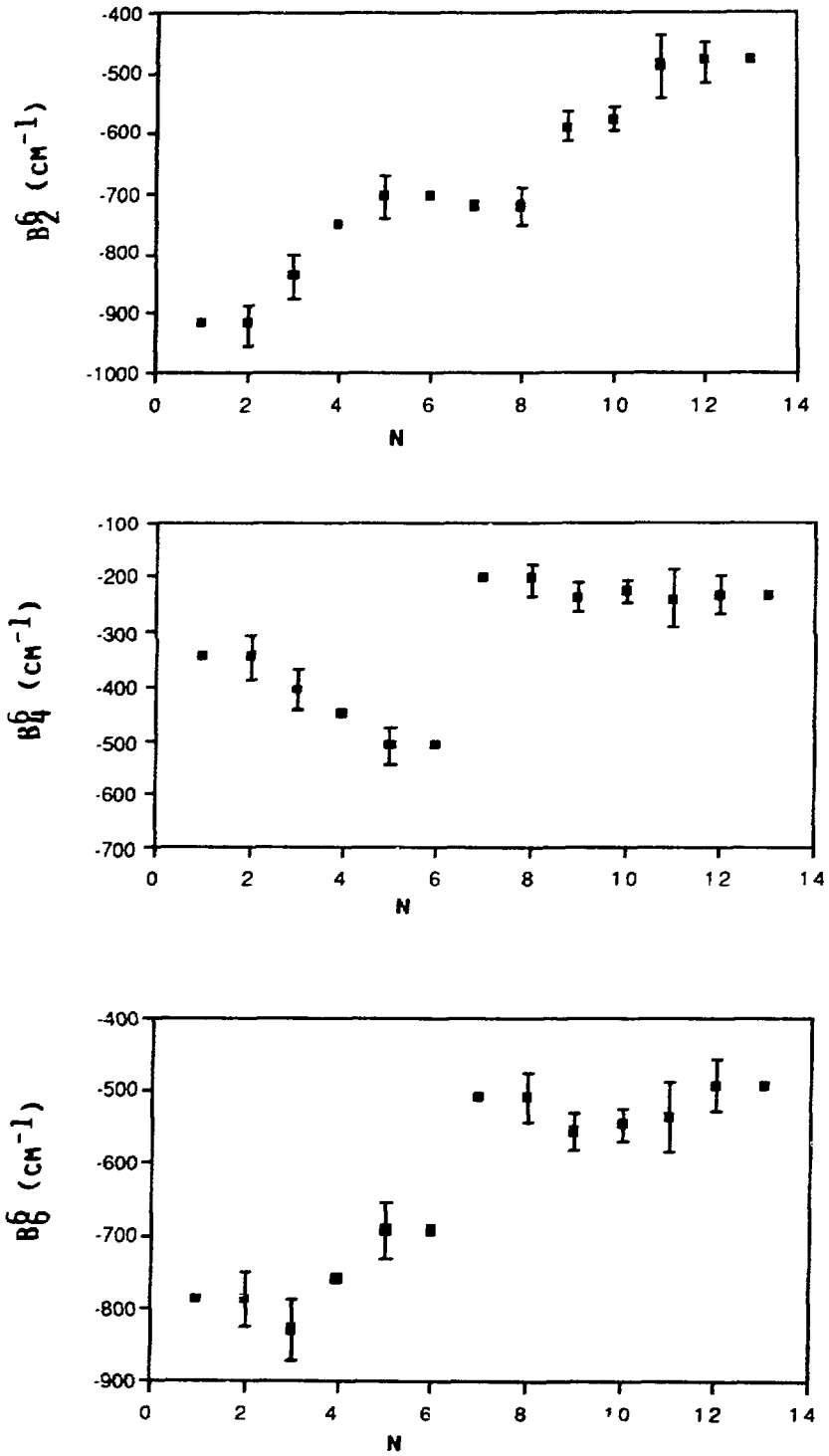

Fig. 20. Variation of the Crystal-field Parameters B_2^6, B_4^6, and B_6^6 (in cm^{-1}) for Ln^{3+}:LaF_3 as a Function of Number of f-electrons (N).

with the possible exception of B_2^6 are best represented by different lines for the light and heavy ends of the series, Figs. 18-20. All except B_0^4 and B_2^6 are essentially constant over the second half of the series.

For many of the parameters there is a marked discontinuity in magnitude between Eu^{3+} and Tb^{3+}; however, we found that the crystal-field parameters for both Eu^{3+} and Tb^{3+}:LaF_3 very adequately described the limited data for Gd^{3+}. For B_0^4 and possibly B_4^4 and B_4^6 there is an increase in the magnitude of the parameters for Tb^{3+} compared to Eu^{3+}, but for others there is a decrease. For comparison, parameters[10] for Ln^{3+}:$LaCl_3$ are plotted in Fig. 21. Only the k=6 terms show the discontinuity and the decrease in magnitude at the center of the series. Richardson and co-workers have carried out a related analysis of the spectra of Ln^{3+} in cubic $Cs_2NaLnCl_6$.[87] Their parameter values (which are normalized according to a convention different from that used elsewhere in this report) are plotted in Fig. 22. Again we see a marked decrease across the center of the series for k=6. The scatter is large for k=4 so that the existence of a break is not clear. However, if the values for Eu^{3+} and Tb^{3+} can be considered well established, there is also a decrease in B_0^4 in this case. While similar patterns can be recognized in previous systematic analyses of crystal-field parameters, the larger number of parameters involved in the present analysis in C_{2v} symmetry makes the trends over the series more striking. The common features already cited do not appear to be restricted to a particular symmetry or type of ligand.

Judd has interpreted the drop in the sixth-rank parameters in going from Eu^{3+} to Tb^{3+}:$LaCl_3$ as an indication of the need to include two-electron operators in the crystal-field Hamiltonian.[82] One-electron operators, U^k, change sign at the center of the series but the likely two-electron operators would not. Thus if contributions from two-electron operators are being absorbed by the crystal-field parameters, there would be a break when crossing the center of the series. If the two-electron terms were properly parametrized and not included in the one-electron crystal-field parameters, the latter would presumably vary smoothly across the series.

There are a number of possible two-electron operators which could be added to the crystal-field Hamiltonian,[88] but it has been pointed out that

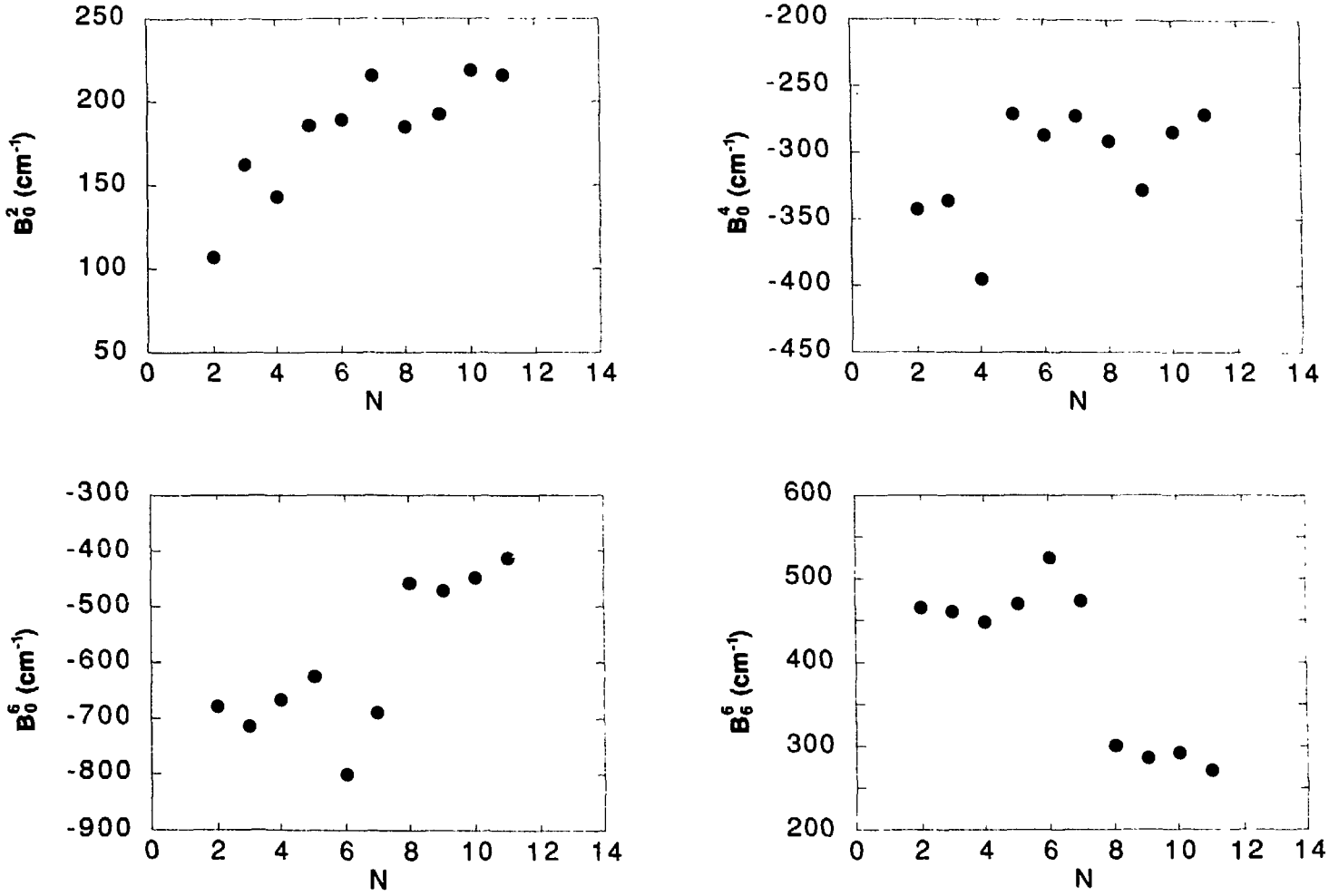

Fig. 21. Variation of the Crystal-field Parameters B_0^2, B_0^4, B_0^6, and B_6^6 (in cm^{-1}) for Ln^{3+}:$LaCl_3$ as a Function of Number of f-electrons (N).

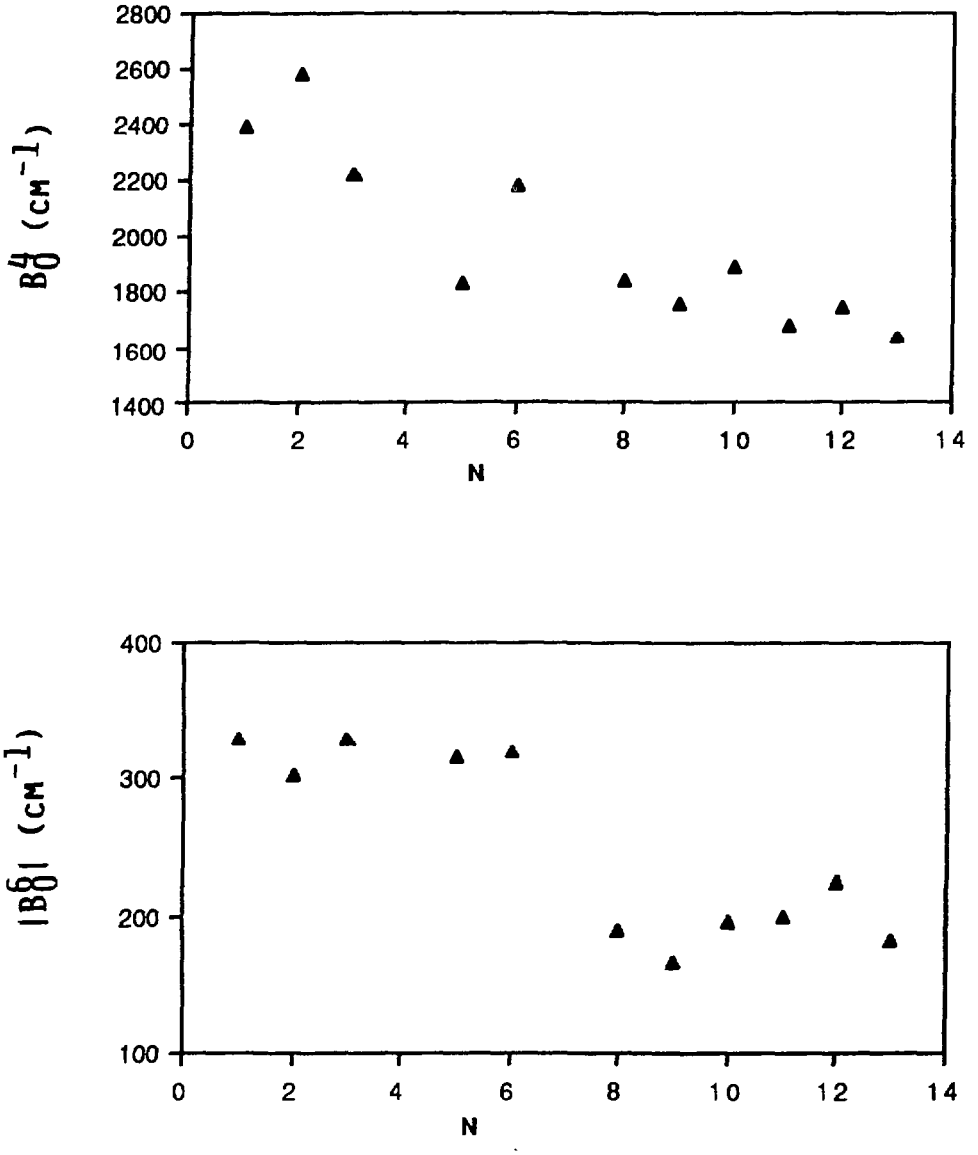

Fig. 22. Variation of the Crystal-field Parameters B_0^4, and B_0^6 (in cm^{-1}) for $Cs_2NaLnCl_6$ as a Function of Number of f-electrons (N).

a large part of the effect may be parametrized as a spin-correlated crystal-field, (SCCF), which requires only 3 additional parameters.[81,84] The one-electron crystal-field operator is supplemented by

$$H_{SCCF} = \sum_{k,q,i} b_q^k \, s_i \cdot S \, C_q^{(k)}$$

and the ratio $c_k = b_q^k / B_q^{(k)}$ is used as a measure of the importance of the 2-electron crystal-field. This has the advantage of being independent of the normalization used to define the crystal-field parameters. Values of c_k have been obtained for Gd^{3+} and Ho^{3+} in $LaCl_3$[89], for three lanthanide ions in Cs_2NaYCl_6,[90] and for Nd^{3+} in fluoride matrices.[91] However, the improvement in the fit in these investigtions was not enough to clearly establish the importance of this mechanism. In a recent paper, the role of orthogonal operators in representing the correlation crystal-field was examined.[92] Again, Gd^{3+} and Ho^{3+}:$LaCl_3$ data were chosen, but consistent results were limited to parameters related to the sixth rank SCCF. These results are of the correct sign to remove the drop in the center of the series. A positive c_k has been shown to result from a covalency (charge transfer) mechanism.[84]

One of the important applications of a systematic set of lanthanide energy level parameters is found in the calculation of intensity correlations using the Judd-Ofelt theory.[93,94] The matrix elements of the transition probability in absorption and luminescence are appropriately computed from a systematic set of atomic parameters. The intensity parameters can then be determined semi-empirically for any particular system from the observed variation in band intensities. We have already tabulated the matrix elements of $U^{(k)}$ based on an earlier more approximate assessment of the atomic parameters.[11] While the present results show clear deficiencies in some of the parameter trends originally deduced, the discrepancies are not sufficiently serious to warrant recalculation of the matrix elements.

The widely-circulated Dieke chart of energy level structure in the lanthanides[1] was limited by the extent of available analyses of the spectra of Ln^{3+}:$LaCl_3$. In the present case we extrapolated or interpolated to compute levels for Pm^{3+} and Eu^{3+}, but the remaining lanthanide spectra form the basis for a very consistent interpretation. We have prepared a new

chart, Fig. 23, based entirely on the computed energy level schemes. This more complete representation should provide a useful basis for comparison with spectra in other matrices.

7.0 CONCLUSIONS

Using a C_{2v} crystal-field to approximate the C_2 site symmetry, we have been able to correlate extensive spectroscopic data for $Ln^{3+}:LaF_3$ with a consistent set of free-ion and crystal-field parameters. The rms deviations are all ~10-15 cm^{-1}. These results provide the basis for the most complete analysis of rare earth ions that is available in any host. We have drawn a number of conclusions regarding systematic trends in parameter values which should prove useful in analyses of other rare earth and actinide spectra, and which point out directions where further work is needed. Considering the large experimental basis available for the LaF_3 matrix, the experimental similarities to the $LaCl_3$ case, and the inherent difficulty we experienced in defining the values of the free-ion parameters near the center of the series, it is evident that reservation must be exercised in evaluating published sets of atomic parameters derived by fits to severely limited data bases and without regard for systematics.

1. The variations of F^k across the series are well represented by linear equations while those of ζ are much better represented by a cubic equation.

2. The difference between HFR and empirical values for F^2 and F^4 (ΔF^2 and ΔF^4) increases slightly across the series while ΔF^6 decreases markedly. This is contrary to previous conclusions based on less complete data.

3. The P^f parameters do not appear to have the same ratios as the F^k parameters, and we have obtained additional evidence for P^6 assuming negative values at the ends of the series. Since the mechanism associated with the introduction of the P^f does not lead to negative values, this aspect of the parametrization requires further investigation.

4. Changes in magnitude of the crystal-field parameters across the series are in accord with previous indications of the importance of 2-electron operators in the crystal-field Hamiltonian. There is some indication

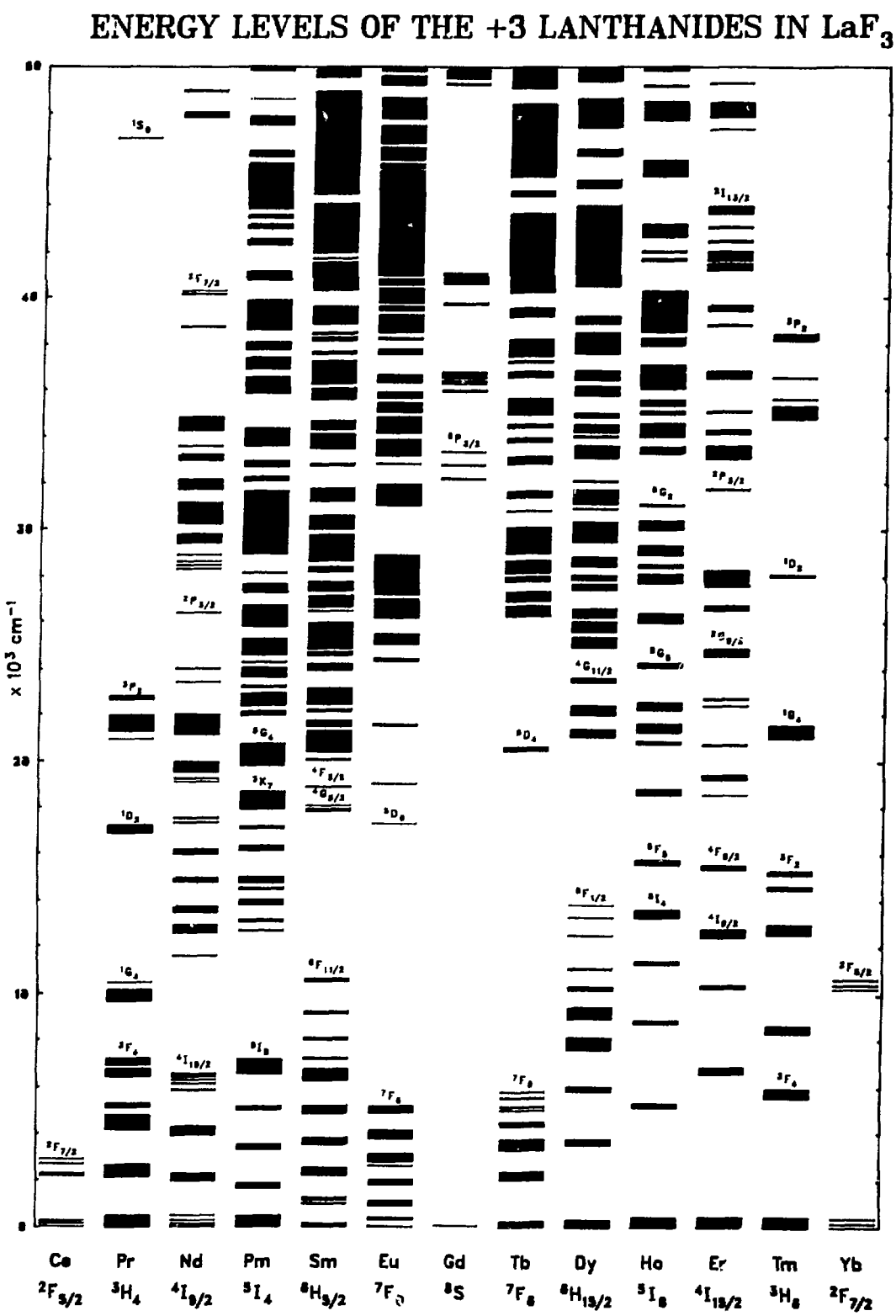

Fig. 23. Energy Level Structure of Ln^{3+}:LaF_3 Based on Computed Crystal-field Energies in the Range 0-50000 cm^{-1}.

of the need for such terms with ranks 4 and 6. The magnitudes of B_0^4 and B_4^4 increase at the center of the series whereas most other rank 4 and 6 parameters decrease. We conclude that variation of the crystal-field parameters is such that extrapolation from one half of the series to the other could lead to erroneous estimates of parameter values.

While the model used contains a large number of parameters associated with the atomic interactions, many of these do not show a significant variation over the series. Nevertheless, it is the inclusion of effective operators representing important classes of configuration interaction that has removed much of the distortion, particularly of the F^k parameters, found in early analyses. The two- and three-body effective operator parameters tabulated here can be used directly in the initial efforts to analyze spectra of lanthanides in other matrices.

8.0 ACKNOWLEDGEMENTS

This work was performed under the auspices of the Office of Basic Energy Sciences, Division of Chemical Sciences, U. S. Department of Energy, under contract number W-31-109-Eng-38. The contribution of Hannah Crosswhite in developing the computer programs is gratefully acknowledged.

9.0 REFERENCES

1. G. H. Dieke, "Spectra and Energy Levels of Rare Earth Ions in Crystals," H. M. Crosswhite and H. Crosswhite, Eds., Wiley, NY, 1968.
2. B. R. Judd, "Operator Techniques in Atomic Spectroscopy," McGraw-Hill, NY, 1963.
3. B. G. Wybourne, "Spectroscopic Properties of Rare Earths," Wiley, NY, 1965.
4. S. Hüfner, "Optical Spectra of Transparent Rare Earth Compounds," Academic Press, NY, 1978.
5. C. A. Morrison and R. P. Leavitt, in "Handbook of the Physics and Chemistry of Rare Earths," Ed. K.A. Gschneidner and L. Eyring, North-Holland Publishing Co., NY, 1982, Vol. 5, pp. 461.
6. E. Y. Wong, O. M. Stafsudd, D. R. Johnston, Phys. Rev. 131, 990 (1963).
7. U. V. Kumar, D. R. Rao, P. Venkateswarlu, J. Chem. Phys. 66, 2019 (1977).
8. A. Zalkin, D. H. Templeton, and T. E. Hopkins, Inorg. Chem. 5, 1466 (1966).
9. D. E. Onopko, Opt. Spectrosc. (U.S.S.R.) 24, 301 (1968); Opt. Spectrosc. (U.S.S.R.), Suppl. 4, 11-12 (1968).
10. H. M. Crosswhite, "Spectroscopie des elements de transition et des elements lourds dans les solides," Colloq. Int. CNRS 255, 65 (1977).
11. W. T. Carnall, H. M. Crosswhite, and H. Crosswhite, Special Rep. 1977 (Chemistry Division, Argonne National Laboratory, Argonne, IL). (Quoted incorrectly in Ref. 5 as ANL-78-xx-95).
12. C. A. Morrison and R. P. Leavitt, J. Chem. Phys. 71, 2366 (1979).
13. W. T. Carnall and H. Crosswhite, J. Less-Commmon Metals 93, 127 (1983).
14. W. T. Carnall, G. L. Goodman, R. S. Rana, P. Vandevelde, L. Fluyt, and C. Görller-Walrand, J. Less-Common Metals 116, 17 (1986).
15. G. L. Goodman, W. T. Carnall, R. S. Rana, P. Vandevelde, L. Fluyt, and C. Görller-Walrand, J. Less-Common Metals 126, 283 (1986).

16. W. T. Carnall, G. L. Goodman, G. M. Jursich, R. S. Rana, P. Vandevelde, L. Fluyt, and C. Görller-Walrand, Inorg. Chim. Acta 139, 275 (1987).
17. Optovac Inc., North Brookfield, MA, 01535.
18. W. S. Heaps, L. R. Elias, W. M. Yen, Phys. Rev. B13, 94 (1976).
19. M. J. Weber, in "Optical Properties of Ions in Crystals," H. M. Crosswhite and H. W. Moos, Eds., Wiley Interscience, NY, 1967, p. 467.
20. I. Oftedal, Z. Physik. Chem. B5, 272 (1929); B13, 190 (1931).
21. K. Schlyter, Arkiv Kemi 5, 73 (1953).
22. M. Mansmann, Z. Anorg. Allgem. Chemie 331, 98 (1964); Z. Krist. 122, 375 (1965).
23. R. P. Lowndes, J. F. Parrish, C. H. Perry, Phys. Rev. 182, 913 (1969).
24. A. K. Cheetham, B. E. F. Fender, H. Fuess, A. F. Wright, Acta Cryst. B32, 94 (1976).
25. A. Zalkin and D. H. Templeton, J. Am. Chem. Soc. 75, 2453 (1953).
26. E. V. Sayre and S. Freed, J. Chem. Phys. 23, 2066 (1955).
27. R. P. Bauman and S. P. S. Porto, Phys. Rev. 161, 842 (1967).
28. V. V. Azarov, P. V. Zinovev, B. I. Minkov, B. S. Skorobogatov, and E. V. Shcherbina, Optics Spectrosc. 30, 491 (1971).
29. C. Froese Fischer, "The Hartree-Fock Method for Atoms; a numerical approach," Wiley, NY, 1977.
30. K. Rajnak and B. G. Wybourne, Phys. Rev. 132, 280 (1963).
31. J. C. Morrison and K. Rajnak, Phys. Rev. A4, 536 (1971).
32. Jan P. Hessler and W. T. Carnall, ACS Symposium Series No. 131, 349 (1980).
33. J. C. Morrison, Phys. Rev. A6, 643 (1972).
34. B. R. Judd, Phys. Rev. 141, 4 (1966).
35. H. Crosswhite, H. M. Crosswhite, and B. R. Judd, Phys. Rev. 174, 89 (1968).
36. G. Balasubramanian, M. M. Islam, and D. J. Newman, J. Phys. B8, 2601 (1975).
37. B. R. Judd, H. M. Crosswhite, and H. Crosswhite, Phys. Rev. 169, 130 (1968).

38. H. H. Marvin, Phys. Rev. 71, 102 (1947).
39. G. M. Copland, D. J. Newman, and C. D. Taylor, J. Phys. B4, 1388 (1971).
40. R. D. Cowan and D. C. Griffin, J. Opt. Soc. Am. 66, 1010 (1976).
41. H. M. Crosswhite and H. Crosswhite, J. Opt. Soc. Am. B1, 246 (1984).
42. P. Caro, J. Derouet, L. Beaury, G. Teste de Sagey, J. P. Chaminade, J. Aride, M. Pouchard, J. Chem. Phys. 74, 2698 (1981).
43. R. A. Buchanan, H. E. Rast, H. H. Caspers, J. Chem. Phys. 44, 4063 (1966).
44. H. Gerlinger and G. Schaak, Phys. Rev. B33, 7438 (1986).
45. W. T. Carnall, P. R. Fields, R. Sarup, J. Chem. Phys. 51, 2587 (1969).
46. E. Y. Wong, O. M. Stafsudd, D. R. Johnston, J. Chem. Phys. 39, 786 (1963).
47. W. M. Yen, W. C. Scott, and A. L. Schawlow, Phys. Rev. 136, A271 (1964).
48. H. H. Caspers, H. E. Rast, and R. A. Buchanan, J. Chem. Phys. 43, 2124 (1965).
49. L. R. Elias, W. S. Heaps, W. M. Yen, Phys. Rev. B8, 4989 (1973).
50. C. D. Cordero-Montalvo and N. Bloembergen, Phys. Rev. B30, 438 (1984); Erratum, Phys. Rev. B31, 613 (1985).
51. C. G. Levy, T. J. Glynn, W. M. Yen, J. Lumin. 31/32, 245 (1984).
52. H. H. Caspers, H. E. Rast, and R. A. Buchanan, J. Chem. Phys. 42, 3214 (1965).
53. U. V. Kumar, H. Jagannath, D. R. Rao, P. Venkateswarlu, Indian J. Phys. 50, 90 (1976).
54. Y. K. Voron'ko, V. V. Osiko, N. V. Savost'yanova, V. S. Fedorov, I. A. Shcherbakov, Soviet Physics-Solid State 14, 2294 (1973).
55. H. M. Crosswhite, H. Crosswhite, F. W. Kaseta, and R. Sarup, J. Chem. Phys. 64, 1981 (1976).
56. W. T. Carnall, H. Crosswhite, H. M. Crosswhite, and J. G. Conway, J. Chem. Phys. 64, 3582 (1976).
57. H. E. Rast, J. L. Fry, and H. H. Caspers, J. Chem. Phys. 46, 1460 (1967).

58. W. F. Krupke and J. B. Gruber, J. Chem. Phys. 39, 1024 (1963); 41, 1225 (1964); Erratum, J. Chem. Phys. 42, 1134 (1965).

59. W. T. Carnall, P. R. Fields, and R. Sarup, J. Chem. Phys. 57, 43 (1972).

60. M. J. Weber, Phys. Rev. 157, 262 (1967).

61. W. T. Carnall, P. R. Fields, J. Morrison, and R. Sarup, J. Chem. Phys. 52, 4054 (1970).

62. H. H. Caspers, H. E. Rast, and J. L. Fry, J. Chem. Phys. 53, 3208 (1970).

63. H. M. Crosswhite, H. Crosswhite, N. Edelstein, and K. Rajnak, J. Chem. Phys. 67, 3002 (1977).

64. J. L. Fry, H. H. Caspers, H. E. Rast, and S. A. Miller, J. Chem. Phys. 48, 2342 (1968).

65. D. C. Krupka and H. J. Guggenheim, J. Chem. Phys. 51, 4006 (1969).

66. J. A. Caird, W. T. Carnall, and J. P. Hessler, J. Chem. Phys. 74, 3225 (1981).

67. H. H. Caspers, S. A. Miller, H. E. Rast, J. L. Fry, Phys. Rev. 180, 329 (1969).

68. R. L. Schwiesow and H. M. Crosswhite, J. Opt. Soc. Am. 59, 602 (1969).

69. W. T. Carnall, P. R. Fields, R. Sarup, J. Chem. Phys. 54, 1476 (1971).

70. B. G. Wybourne, Phys. Rev. 148, 317 (1966).

71. V. K. Sharma, J. Chem. Phys. 54, 496 (1971).

72. D. Furniss, E. A. Harris, D. B. Hollis, J. Phys. C20, L147 (1987).

73. R. L. Schwiesow and H. M. Crosswhite, J. Opt. Soc. Am. 59, 592 (1969).

74. J. Sugar, V. Kaufman, and N. Spector, J. Res. Natl. Bur. Stan. 83, 233 (1978).

75. H. E. Rast, H. H. Caspers, S. A. Miller, J. Chem. Phys. 47, 3874 (1967).

76. B. R. Judd and H. Crosswhite, J. Opt. Soc. Am. B1, 255 (1984).

77. B. R. Judd and M. A. Suskin, J. Opt. Soc. Am. B1, 261 (1984).

78. B. R. Judd, Private communication, April 1987.

79. A. Pasternak and Z. B. Goldschmidt, Phys. Rev. A6, 55 (1972).

80. J. Sugar, J. Opt. Soc. Am. 53, 831 (1963).
81. B. R. Judd, Phys. Rev. Lett. 39, 242 (1977).
82. B. R. Judd, J. Lumin. 18/19, 604, (1979).
83. B. R. Judd, J. Phys. C13, 2695, (1980).
84. D. J. Newman, G. G. Siu, W. Y. P. Fung, J. Phys. C15, 3113 (1982).
85. D. J. Newman, Adv. Phys. 20, 197 (1971).
86. Y. Y. Yeung and D. J. Newman, J. Chem. Phys. 82, 3747 (1985).
87. F. S. Richardson, M. F. Reid, J. J. Dallara, and R. D. Smith, J. Chem. Phys. 83, 3813 (1985).
88. S. S. Bishton and D. J. Newman, J. Phys. C3, 1753 (1970).
89. H. Crosswhite and D. J. Newman, J. Chem. Phys. 81, 4959 (1984).
90. M. F. Reid and F. S. Richardson, J. Chem. Phys. 83, 3831 (1985).
91. C. K. Jayasankar, F. S. Richardson, M. F. Reid, P. Porcher, and P. Caro, Inorg. Chim. Acta 139, 287 (1987)
92. M. F. Reid, J. Chem. Phys. 87, 2875 (1987).
93. B. R. Judd, Phys. Rev. 127, 750 (1962).
94. G. S. Ofelt, J. Chem. Phys. 37, 511 (1962).

Appendix I.

Experimental and Computed Energy Level Structure for $Pr^{3+}:LaF_3$

SLJ State	Model[a] (cm^{-1})	Expt.[b] (cm^{-1})	Calc.[c] (cm^{-1})	O-C	SLJ State	Model[a] (cm^{-1})	Expt.[b] (cm^{-1})	Calc.[c] (cm^{-1})	O-C
$^3H_4$	0	0	0.2	0	$^3H_5$	2281	2272	2284	-12
	90	57	71	-14		2289	2299	2290	9
	95	71	95	-24		2294	2304	2295	9
	124	136	138	-2		2327	2354	2318	36
	144	195	183	12		2363	2412	2399	13
	226	204[d]	221	-17		2441	2431	2412	19
	305	322[d]	333	-11		2442	2457	2438	19
	386	-	444			2538	2567	2540	27
	479	(508)[e]	463						
					$^3H_6$	4220	-	4179	
$^3H_5$	2160	-	2126			4230	4223	4200	23
	2184	-	2158			4319	4268	4283	-15
	2188	2179	2191	-12		4381	4305	4321	-16

Appendix I. (Cont.)

SLJ State	Model[a] (cm^{-1})	Expt.[b] (cm^{-1})	Calc.[c] (cm^{-1})	O-C	SLJ State	Model[a] (cm^{-1})	Expt.[b] (cm^{-1})	Calc.[c] (cm^{-1})	O-C
$^3H_6$	4414	4388	4384	4	$^3F_2$	5263	5280[d]	5276	4
	4473	4440[d]	4467	-27					
	4494	-	4478		$^3F_3$	6420	6453	6456	-3
	4507	4508	4496	12		6481	6495	6490	5
	4545	4529	4508	21		6489	6499	6508	-9
	4621	4581	4590	-9		6562	6587	6579	8
	4713	4673	4693	-20		6576	6602	6600	2
	4715	-	4712			6602	6622	6628	-6
	4821	4785	4814	-29		6701	6722	6740	-18
$^3F_2$	5130	5137	5145	-8	$^3F_4$	6907	6927	6918	9
	5153	5182	5182	0		6920	-	6936	
	5180	5201	5185	16		6944	6946	6950	-4
	5245	5275	5270	5		6956	-	6952	

Appendix I (Cont.)

SLJ State	Model[a] (cm^{-1})	Expt.[b] (cm^{-1})	Calc.[c] (cm^{-1})	O-C	SLJ State	Model[a] (cm^{-1})	Expt.[b] (cm^{-1})	Calc.[c] (cm^{-1})	O-C
$^3F_4$	6958	6946	6953	-7	$^1G_4$	10477	10499	10516	-17
	6996	6980	6983	-3					
	7000	7029	7034	-5	$^1D_2$	16879	16873	16887	-14
	7084	7104	7096	8		925	893	895	-2
	7129	7165	7152	13		17072	17083	17082	1
						095	-	117	
$^1G_4$	9720	9716	9721	-5		149	183	170	13
	9761	9751	9762	-11					
	9840	9876	9860	16	$^3P_0$	20942	20927	20911	16
	9936	9912	9927	-15					
	9937	-	9958		$^1I_6$	21276	21279	21284	-5
	9979	10005	9996	9		313	-	304	
	10031	042	10030	12		320	331	340	-9
	10154	10163	10150	13		398	404	390	14

Appendix I (Cont.)

SLJ State	Model[a] (cm^{-1})	Expt.[b] (cm^{-1})	Calc.[c] (cm^{-1})	O-C	SLJ State	Model[a] (cm^{-1})	Expt.[b] (cm^{-1})	Calc.[c] (cm^{-1})	O-C
$^1I_6$	21440	21418	21406	12	$^1I_6$	21852	21897	21889	8
	447	-	481			905	942	958	-16
$^3P_1$	472	475	487	-12					
	532	522	519	3	$^3P_2$	22607	22691	22668	23
$^1I_6$	541	-	570			664	714	704	10
$^3P_1$	556	567	592	-25		673	734	738	-4
$^1I_6$	598	585	588	-3		725	772	787	-15
	619	-	637			767	819	817	2
	650	668	666	2					
	738	-	804		$^1S_0$	46961	46965[f]	46965	0

[a]Ref. 13. Values for the $^1I_6$ components (but not the $^3P_1$) were reduced by 100 cm^{-1} to correspond to present assignments.
[b]Ref. 45 and 48 except as indicated; cm^{-1} vac.
[c]Energy level parameters are given in Table 4.
[d]Ref. 47.
[e]Not used in fitting parameters.
[f]Ref. 51.

Appendix II.

Experimental and Computed Energy Level Structure of $Nd^{3+}:LaF_3$

SLJ[a] State	Obsd.[b] (cm^{-1})	Calc.[c] (cm^{-1})	O-C	Caspers et al.[d] (cm^{-1})	Wong et al.[e] (cm^{-1})	Voron'ko et al.[f] (cm^{-1})
$^4I_{9/2}$	0	5	-5	0		0
	45	48	-3	45		44
	136	153	-17	136		140
	296	304	-8	296		297
	500	513	-13	500		502
$^4I_{11/2}$	1978	1965	13	1978		1980
	2037	2027	10	2037		2039
	2068	2070	-2	2068		2069
	2091	2089	2	2091		2093
	2187	2193	-6	2187		2190
	2223	2226	-3	2223		2225
$^4I_{13/2}$	3918	3902	16	3919		3919
	3978	3970	8	3979		3973
	4038	4033	5	4039		4039
	4076	4087	-11	4078		4077
	4118	4115	3	4120		4119
	4208	4205	3	4213		4213
	4278	4267	11	4278		4277
$^4I_{15/2}$	5816	5804	12	5815		5817
	5874	5871	3	5877		5876
	5986	5999	-13	5988		5989
	6141	6163	-22			6142
	6167	6185	-18			6173

Appendix II. (cont.)

SLJ[a] State	Obsd.[b] (cm^{-1})	Calc.[c] (cm^{-1})	O-C	Caspers et al.[d] (cm^{-1})	Wong et al.[e] (cm^{-1})	Voron'ko et al.[f] (cm^{-1})
$^4I_{15/2}$	6323	6113	10			6320
	6454	6445	9			6448
	6556	6538	18			6551
$^4F_{3/2}$	11592	11596	-4	11592	11591.6	11594
	634	638	-4	634	633.6	637
$^2H_{9/2}$,	12596	12576	20	12596	12595.6	
$^4F_{5/2}$	614	595	19	613	612.9	
	622	633	-11	621	620.7	
	676	680	-4	675	674.6	
	694	704	-10	693	692.6	
	754	761	-7	755	755.3	
	843	847	-4	-	-	
	902	874	27	-	-	
$^4F_{7/2}$	13514	13521	-7	13515	13514.8	
	590	591	-1	591	590.8	
$^4S_{3/2}$	671	670	1	671	670.9	
	676	678	-2	677	676.7	
$^4F_{7/2}$	711	690	21	710	710.1	
	715	725	-10	714	714.2	
$^4F_{9/2}$	14834	14840	-6	14835	14834.7	
	861	860	1	860	861.8	
	892	891	1	891	890.6	

Appendix II. (cont.)

SLJ[a] State	Obsd.[b] (cm^{-1})	Calc.[c] (cm^{-1})	O-C	Caspers et al.[d] (cm^{-1})	Wong et al.[e] (cm^{-1})
$^4F_{9/2}$	14926	14925	1	14927	
	959	955	4	958	14959.4
$^2H_{11/2}$	15997	16025	-28	15998	15998.1
	16033	043	-10	16033	-
	046	049	-3	045	16046.4
	060	067	-7	059	-
	100	093	7	103	-
	165	136	29	-	-
$^4G_{5/2}$,	17306	17301	5	17304	17304.6
$^4G_{7/2}$	316	318	-2	315	316.0
	363	360	3	364	362.9
	511	492	19	512	509.2
	518	512	6	520	520.3
	571	567	4	570	
	605	607	-2	601	603.2
$^4G_{7/2}$	19147	19134	13	19147	19147.4
	235	243	-8	235	236.2
	252	266	-14	251	252.1
	324	322	2	323	325.4
$^2K_{13/2}$,	19567	19570	-3	19568	19568.2
$^4G_{9/2}$	615	622	-7	617	
	651	638	13	651	650.9
	686	681	5	685	686.2

Appendix II. (cont.)

SLJ[a] State	Obsd.[b] (cm^{-1})	Calc.[c] (cm^{-1})	O-C	Caspers et al.[d] (cm^{-1})	Wong et al.[e] (cm^{-1})
$^2K_{13/2}$,	19704	19696	8	19702	19704.0
$^4G_{9/2}$	-	727		-	-
	741	741	0	739	739.4
	799	786	13	801	
	835	834	1	839	
	-	892		-	
	-	946		-	
	960	970	-10	-	
$^2G_{9/2}$	21155	21151	4	21158	
	176	180	-4	176	
	198	202	-4	201	
	232	242	-10	234	
	252	271	-19	254	
$^2D_{3/2}$	21338	21337	1	21339	
	353	355	-2	351	
$^4G_{11/2}$,	21542	21535	7		
$^2K_{15/2}$	-	618			
	633	630	3		
	718	704	14		
	-	754			
	768	767	1		
	-	783			
	807	810	-3		
	-	821			
	846	861	-15		
	-	884			

Appendix II. (cont.)

SLJ[a] State	Obsd.[b] (cm^{-1})	Calc.[c] (cm^{-1})	O-C	Caspers et al.[d] (cm^{-1})
$^4G_{11/2}$,	-	21929		
$^2K_{15/2}$	-	957		
	21992	989	3	
$^2P_{1/2}$	23473	23463	10	23468
$^2D_{5/2}$	23991	23985	6	23991
	24033	24035	-2	
	080	075	5	
$^2P_{3/2}$	26378	26389	-11	
	426	424	2	
$^4D_{3/2}$	28341	28342	-1	
	374	371	3	
$^4D_{5/2}$	28501	28500	1	
	525	526	-1	
	676	672	4	
$^4D_{1/2}$	28962	28943	19	
$^2I_{11/2}$	29463	29467	-4	
	489	476	13	
	568	558	10	
	644	646	-2	
	-	648		
	773	777	-4	

Appendix II. (cont.)

SLJ[a] State	Obsd.[b] (cm^{-1})	Calc.[c] (cm^{-1})	O-C
$^2L_{15/2}$,	30275	30270	5
$^4D_{7/2}$	318	317	1
	-	363	
	-	471	
	517	523	-6
	-	536	
	576	593	-17
	-	600	
	631	644	-13
	682	691	-9
	719	722	-3
	807	796	11
$^2I_{13/2}$	-	30860	
	30893	898	-5
	933	948	-15
	994	31010	-16
	31030	31029	1
	068	054	14
	-	118	
$^2L_{17/2}$	31781	31768	13
	-	817	
	859	851	8
	-	983	

SLJ[a]	Obsd.[b] (vac cm^{-1})	Calc.[c] (cm^{-1})	O-C
$^2L_{17/2}$	-	31987	
	-	32008	
	-	030	
	-	074	
	-	172	
$^2H_{9/2}$	33030	33036	-6
	107	117	-10
	181	178	3
	228	226	2
	255	255	0
$^2D_{3/2}$	33619	33616	3
	649	647	2
$^2H_{11/2}$,	34292	34264	28
$^2D_{5/2}$	380	368	12
	419	443	-24
	-	501	
	521	534	-13
	-	578	
	678	659	19
	706	723	-17
	-	811	

Appendix II. (cont.)

SLJ[a] State	Obsd.[b] (cm^{-1})	Calc.[c] (cm^{-1})	O-C	SLJ[a]	Obsd.[b] (vac cm^{-1})	Calc.[c] (cm^{-1})	O-C
$^2F_{5/2}$	38690	38708	-18	$^2G_{7/2}$	48839	48852	-13
	735	764	-29		908	868	40
	841	811	30		977	979	-2
					49088	49071	17
$^2F_{7/2}$	40103	40104	-1				
	-	120		$^2F_{7/2}$	-	66565	
	155	176	-21		-	716	
	288	247	41		-	772	
					-	916	
$^2G_{9/2}$	-	47867					
	47894	887	7	$^2F_{5/2}$	-	67856	
	937	954	-17		-	900	
	999	48021	-22		-	68126	
	48043	056	-13				

[a]The principal component of the eigenvector is given.

[b](cm^{-1} vac). Components of $^4I_{9/2}$ and $^4I_{11/2}$ taken from ref. 52.

[c]Energy level parameters are given in Table 4.

[d]Ref. 52.

[e]Ref. 6.

[f]Ref. 54.

Appendix III.

Computed Energy Level Structure for $Pr^{3+}:LaF_3$

SLJ[a] State	Calc.[b] (cm^{-1})	SLJ[a] State	Calc.[b] (cm^{-1})	SLJ[a] State	Calc.[b] (cm^{-1})	SLJ[a] State	Calc.[b] (cm^{-1})
$^5I_4$	0	$^5I_6$	3376	$^5I_8$	6556	$^5F_2$	13156
	135		3389		6605		170
	189		3392		6621		
	233		3413		6653	$^5F_3$	13853
	266		3413		6672		900
	294		3416		6746		918
	332		3439		6763		952
	437		3462		6824		965
	474		3470		6827		998
					6857		14020
$^5I_5$	1667	$^5I_7$	5042		6959		
	1710		5045		6977	$^5S_2$	14525
	1717		5059		7060		529
	1769		5060		7063		529
	1769		5066		7129		529
	1810		5074		7131		530
	1812		5078		7152		
	1821		5084			$^5F_4$	14804
	1828		5086	$^5F_1$	12650		837
	1829		5090		671		892
	1845		5110		684		894
			5114				895
$^5I_6$	3285		5116	$^5F_2$	13031		898
	3322		5143		076		926
	3326		5149		091		965
	3369						998

Appendix III. (cont.)

SLJ[a] State	Calc.[b] (cm^{-1})	SLJ[a] State	Calc.[b] (cm^{-1})	SLJ[a] State	Calc.[b] (cm^{-1})	SLJ[a] State	Calc.[b] (cm^{-1})
$^5F_5$	16145	$^5G_4$,	18045	$^5G_3$	18679	$^5G_5$,	20471
	148	$^5G_3$,	066	$^3K_7$	689	$^5G_4$	492
	149	$^3K_7$	068				532
	151		076	$^3K_8$	19854		541
	212		079		859		579
	226		104		870		592
	249		104		872		611
	250		126		885		664
	273		147		890		700
	307		252		928		713
	322		316		951		
			364		973	$^3G_3$	21968
$^3K_6$	17071		381		974		974
	088		408		20005		22020
	088				012		040
	091	$^5G_3$,	18426		035		062
	092	$^3K_7$	426		036		070
	093		444		107		117
	104		461		111		
	106		500		136	$^5G_5$,	22424
	109		508			$^5G_6$	429
	115		510	$^5G_5$,	20243		433
	123		535	$^5G_4$	260		461
	123		536		294		469
	137		545		303		480
			557		20361		500
$^5G_2$	17904		559		365		503
	932		611		366		512
	949		657		387		539
	18007		665		445		563
	017				463		575

Appendix III. (cont.)

SLJ[a] State	Calc.[b] (cm^{-1})	SLJ[a] State	Calc.[b] (cm^{-1})	SLJ[a] State	Calc.[b] (cm^{-1})
$^5G_5$, $^5G_6$	22663	$^3L_7$	24028	$^3H_6$, $^3G_4$, $^3L_8$	24992
	683		043		25014
	696		046		018
	696				023
	754	$^3P_1$	24289		038
	769		299		068
	779		306		071
	827				073
	831	$^3H_6$, $^3G_4$, $^3L_8$	24635		122
	895		661		136
	909		664		156
	942		678		157
			695		171
$^3D_2$	23189		708		172
	253		762		224
	288		772		263
	327		780		
	327		785		(25816-50000[c])
			810		
$^3L_7$	23699		817		
	701		834		
	828		849		
	840		869		
	841		874		
	887		893		
	889		24905		
	954		917		
	956		918		
	965		924		
	968		945		
	24022		950		

Appendix III. (cont.)

---

[a]The leading component of the state eigenvector is indicated.

[b]The energy level parameters (interpolated) used to compute these level energies are given in Table 4.

[c]Since there are no experimental data available, the tabulation has been arbitrarily stopped at 25263 cm^{-1}. At higher energies, starting with the next level at 25816 cm^{-1}, the computed density of states is relatively high. Some additional results are given for $Pm^{3+}:LaCl_3$ in Ref. 56. Figure 21 indicates the larger gaps in energy where no crystal-field components are computed to occur.

Appendix IV.

Experimental and Computed Energy Level Structure of $Sm^{3+}:LaF_3$

SLJ[a] State	Expt.[b] (cm^{-1})	Calc.[c] (cm^{-1})	O-C	Rast[d] et al. (cm^{-1})	Dieke[e] (cm^{-1})
$^6H_{5/2}$	0	-6	6	0	0
	44	53	-9	48	44
	159	135	24	115	159
$^6H_{7/2}$	1000	990	10	1000	1003
	1044	1027	17	044	046
	1185	1205	-20	185	100
	1280	1262	18	280	187
$^6H_{9/2}$	2209	2193	16	2209	2213
	244	233	11	244	247
	342	332	10	342	344
	409	408	1	409	404
	473	468	5	473	493
$^6H_{11/2}$	3520	3510	10	3517	
	568	553	15	567	
	651	628	23	647	
	671	667	4	670	
	727	739	-12	726	
	791[d]	793	-2	791	
$^6H_{13/2}$	4972	4947	25	4971	4969
	982	975	7	982	
	5007	5004	3	5007	5005
	046	042	4	047	044
	057	059	-2	057	
	122	114	8	122	
	160	170	-10	160	

Appendix IV. (cont.)

SLJ[a] State	Expt.[b] (cm^{-1})	Calc.[c] (cm^{-1})	O-C	Rast[d] et al. (cm^{-1})	Dieke[e] (cm^{-1})
$^6H_{15/2}$,	6309	6300	9	-	
$^6F_{1/2}$	341	334	7	6346	
	406	417	-11	408	6404
	460	465	-5	454	
	-	472		462	
	-	553		492	
	568	578	-10	538	
	609	605	4	571	
	-	666			
$^6F_{3/2}$	6707	6724	-17	6707	
	-	738		-	
$^6F_{5/2}$	7177	7177	0	7174	7173
	184	190	-6	184	180
	223	239	-16	225	
$^6F_{7/2}$	7992	8008	-16	7993	7987
	8041	026	15	8042	8034
	060	059	1	059	054
	092	108	-16	092	086
$^6F_{9/2}$	9170	9173	-3	9170	9162
	178	189	-11	180	173
	228	223	5	231	222
	252	243	9	254	247
	268	281	-13	270	262
$^6F_{11/2}$	10561	10567	-6	10559	
	584	583	1	581	
	592	590	2	590	
	603	621	-18	602	
	613	633	-20		
	644	656	-12		

Appendix IV. (cont.)

SLJ[a] State	Expt.[b] (cm^{-1})	Calc.[c] (cm^{-1})	O-C	Rast[d] et al. (cm^{-1})	Dieke[e] (cm^{-1})
$^4G_{5/2}$	17858	17863	-5		17858
	949	960	-11		949
	(18045)	18087			18046
$^4F_{3/2}$	18924	18933	-9		18924
	942	951	-9		942
$^4G_{7/2}$	20037	20041	-4		20037
	093	094	-1		093
	112	123	-11		111
	164	168	-4		
$^4I_{9/2}$	20416	20406	10		20417
	472	472	0		471
	499	505	-6		497
	522	531	-9		523
	570	551	19		
$^4M_{15/2}$, $^4I_{11/2}$	-	20685			
	-	770			
	-	808			
	-	858			
	-	892			
	-	904			
	-	922			20944
	-	974			
	-	21004			
	-	071			
	-	164			
	-	179			
	-	248			
	-	265			

SLJ[a] State	Obsd.[b] (cm^{-1})	Calc.[c] (cm^{-1})	O-C	Dieke[e] (cm^{-1})
$^4I_{13/2}$	21520	21541	-21	21520
	602	602	0	
	636	616	20	637
	665	649	16	647
	-	652		
	674	666	8	
	706	684	22	709
$^4F_{3/2}$	22164	22178	-14	22164
	207	213	-6	207
	240	254	-14	241
$^4M_{17/2}$, $^4G_{9/2}$, $^4I_{15/2}$	22501	22500	1	22501
	531	539	-8	532
	542	552	-10	
	-	573		
	579	581	-2	
	628	630	-2	
	695	693	2	
	-	738		
	-	770		
	808	801	7	
	829	834	-5	
	-	867		
	-	912		
	942	943	-1	
	-	982		
	-	23020		
	-	023		
	-	036		
	-	054		
	-	083		
$^4M_{17/2}$, $^4G_{9/2}$, $^4I_{15/2}$	-	23116		
	-	158		
$^4M_{19/2}$, $^6P_{5/2}$	23988	23989	-1	
	24022	24035	-13	
	031	068	-37	
	064	080	-16	
	084	101	-17	24084
	119	126	-7	119
	135	134	1	
	153	162	-9	153
	-	169		
	-	181		
	-	186		
	-	207		
	-	218		
$^4L_{13/2}$	24608	24616	-8	24607
	629	632	-3	628
	631	642	-11	631
	644	658	-14	643
	679	689	-10	678
	683	695	-12	683
	710	720	-10	709
$^4F_{7/2}$	24911	24900	11	24911
	993	987	6	993
	25007	25002	5	25007
	064	071	-7	064
$^6P_{3/2}$	081	088	-7	
	-	106		

Appendix IV. (cont.)

SLJ[a] State	Obsd.[b] (cm^{-1})	Calc.[c] (cm^{-1})	O-C	Dieke[e] (cm^{-1})
$^4G_{11/2}$,	25166	25169	-3	
$^4M_{21/2}$,	182	177	5	
$^4M_{15/2}$,	204	203	1	
$^4H_{11/2}$	216	217	-1	
	-	220		
	-	243		
	248	259	-11	
	282	285	-3	
	-	308		
	-	343		
	-	398		
	-	439		
	-	476		
	-	543		
	-	565		
	611	603	8	25614
	636	621	15	632
	650	645	5	649
	672	654	18	666
	684	682	2	681
	-	698		
	711	708	3	
	718	713	5	
	771	762	9	767
	789	782	7	787
	801	795	6	798
	826	823	3	
	832	845	-13	
	866	866	0	
	904	882	22	
	-	921		
$^4D_{1/2}$	26495	26472	23	26495
$^4L_{17/2}$,	26702	26694	8	26699
$^6P_{7/2}$	712	705	7	709
	717	718	-1	712
	743	751	-8	758
	776	763	13	776
	792	777	15	791
	797	800	-3	796
	-	803		
	812	812	0	810
	822	826	-4	822
	859	849	10	857
	-	862		
	874	868	6	
$^4K_{13/2}$	26942	26931	11	
	962	955	7	
	27003	991	12	
	018	27014	4	
	031	026	5	
	061	073	-12	
	120	109	11	
$^4F_{9/2}$	27417	27381	36	27419
	432	443	-11	434
	448	467	-19	448
	508	510	-2	
	-	552		
$^4D_{3/2}$	27648	27646	2	27649
	658	654	4	659

SLJ[a] State	Obsd.[b] (cm^{-1})	Calc.[c] (cm^{-1})	O-C	Dieke[e] (cm^{-1})
$^4P_{5/2}$	27691	27714	-23	27692
	734	763	-29	735
	758	787	-29	759
$^4H_{7/2}$	28247	28242	5	28247
	261	252	9	262
	344	359	-15	
	409	393	16	410
$^4K_{15/2}$	28722	28735	-13	
	732	743	-11	28732
	760	757	3	
	-	770		
	784	783	1	
	797	793	4	
	-	804		
	817	823	-6	
$^4H_{9/2}$	28938	28925	13	28938
	-	929		
	981	989	-8	980
	29035	29045	-10	036
	055	070	-15	052
$^4D_{7/2}$	29086	29098	-12	29083
	094	108	-14	092
	112	115	-3	111
	-	122		
$(^4K,^4L)_{17/2}$		137		
	-	140		
	29154	154	0	29154
	-	156		
$(^4K,^4L)_{17/2}$	29166	29169	-3	
	-	183		
	195	191	4	
	-	219		
	-	238		
$^4L_{19/2}$,	29268	29270	-2	
$^4H_{11/2}$,	304	298	6	
$^4H_{13/2}$	-	315		
	-	325		
	-	335		
	-	347		
	-	356		
	-	363		
	-	397		
	-	416		
	-	457		
	-	478		
	-	505		
	-	514		
	-	555		
	-	558		
	-	562		
	-	607		
	-	615		
	-	650		
	709	681	28	
	723	693	30	
	738	738	0	
$^4G_{7/2}$,	30027	30031	-4	30028
$^4G_{9/2}$	120	118	2	120
	136	159	-23	136

SLJ[a] State	Obsd.[b] (cm^{-1})	Calc.[c] (cm^{-1})	O-C	Dieke[e] (cm^{-1})	SLJ[a] State	Obsd.[b] (cm^{-1})	Calc.[c] (cm^{-1})	O-C	Dieke[e] (cm^{-1})
$^4G_{7/2}$,	-	30193			$^4P_{5/2}$	32800	32797	3	32799
$^4G_{9/2}$	30216	210	6	213		823	824	-1	823
	235	212	23			857	856	1	858
	-	260							
	293	289	4		$^2F_{5/2}$,	-	33548		
	332	347	-15		$^2K_{13/2}$,	33615	642	-27	
					$^4F_{9/2}$	-	708		
$^4G_{5/2}$	-	30438				777	787	-10	
	-	508				-	813		
	-	549				-	865		
						-	900		
$^4P_{1/2}$	-	31226				-	955		
						-	962		
$^2L_{15/2}$,	-	31337				-	977		
$^4G_{11/2}$,	-	352				-	34007		
$^4P_{3/2}$	31410	394	16	31412		-	028		
	433	445	-12	435		-	049		
	463	476	-13	465		-	081		
	488	495	-7	489		-	095		
	511	504	7	511					
	523	513	10	524	$^2L_{17/2}$,	-	34341		
	532	530	2	533	$^4I_{9/2}$	-	358		
	543	558	-15	538		-	386		
	583	604	-21	582		-	426		
	624	623	1	627		-	434		
	-	630				34454	467	-13	
	-	682				468	468	0	
	-	707				481	488	-7	34484
	759	734	25			497	495	2	499
						519	536	-17	
						-	552		
						-	590		

SLJ[a] State	Obsd.[b] (cm^{-1})	Calc.[c] (cm^{-1})	O-C
$^2L_{17/2}$, $^4I_{9/2}$	-	34612	
	-	654	
$^4F_{7/2}$, $^2N_{19/2}$	(35612-35823)[f]		
$^2P_{1/2}$	-	35846	
$^4I_{11/2}$	35890	35892	-2
	905	905	0
	-	932	
	954	945	9
	996	987	9
	36007	999	8
	055	36054	1
	(36315-37273)[f] (39 levels)		
$^4H_{9/2}$	37623	37607	16
	-	618	
	634	638	-4
	657	654	3
	679	667	12
$^2F_{7/2}$, $^2P_{3/2}$	-	38175	
	-	219	
	-	300	
	38467	461	6
	492	485	7
	-	512	
	(38906-41774)[f] 46 levels		
$^2G_{9/2}$	-	42039	
	42066	072	-6
	124	104	20
	135	137	-2
	176	183	-7
$^2O_{23/2}$, $^4G_{5/2}$, $^4G_{7/2}$	42227	42215	12
	378	400	-22
	-	456	
	462	472	-10
	486	480	6
	-	506	
	-	514	
	-	546	
	-	574	
	-	594	
	-	612	
	616	614	2
	-	642	
	-	643	
	658	661	-3
	-	668	
	-	699	
	711	720	-9
	-	744	
$^2O_{21/2}$, $^4K_{15/2}$	-	809	
	-	914	
	-	951	
	959	963	-4

SLJ[a] State	Obsd.[b] (cm^{-1})	Calc.[c] (cm^{-1})	O-C
$^2O_{21/2}$, $^4K_{15/2}$	-	42976	
	42990	996	-6
	-	43022	
	43040	041	-1
	-	056	
	074	080	-6
		(43088-43658)[f]	
		27 levels	
$^2H_{11/2}$	43769	43760	9
	-	762	
	-	808	
	844	855	-11
	-	869	
	-	921	
$^2G_{7/2}$	43991	43975	16
	-	44005	
	-	033	
	-	041	

SLJ[a] State	Obsd.[b] (cm^{-1})	Calc.[c] (cm^{-1})	O-C
		(44491-47029)[f]	
		54 levels	
$^2H_{11/2}$	47336	47306	30
	374	363	11
	-	430	
	-	523	
	-	536	
	-	675	
		(47812-48909)[f]	
		45 levels	
$^4P_{1/2}$, $^2H_{9/2}$, $^2F_{5/2}$		(49581-49865)[f]	

Appendix IV. (cont.)

[a]Largest or two largest eigenvector components are indicated.
[b]Experimental results for the $^6H_{5/2}$ state taken from Ref. 1 based on correlation with model calculation. Observed data for the $^6H_{9/12}$ and $^6H_{9/2}$ states in the ground multiplet from Ref. 57. Values in parentheses were not included in the parameter fitting process. All entries in cm^{-1} vac.
[c]Energy level parameters are given in Table 4.
[d]Ref. 57.
[e]Ref. 1.
[f]In certain regions of the spectrum where no structure was observed and computations indicated a high density of levels, only the initial and final energies of the group are indicated. In some cases one or two very weak bands were observed consistent with calculation, but not included.

Appendix V.

Experimental and Computed Energy Level Structure for $Eu^{3+}:LaF_3$

SLJ[a] State	Obsd.[b] (cm^{-1})	Species[c]	Model[d] Calc. (cm^{-1})	Fit[e] Calc. (cm^{-1})
$^7F_0$	0	A_1	-10	-13
$^7F_1$	313	A_2	318	318
	375	B_1 (2)	375	372
	415	B_2 (1)	414	412
$^7F_2$	964	A_1	940	943
	-	$B_{(1)}$	975	974
	997	A_1	1011	1012
	-	$A_{(2)}$	1109	1110
	1098	B_2	1118	1118
$^7F_3$	-	$B_{(2)}$	1834	1839
	1843	B_1	1852	1855
	1867	A_1 (2)	1861	1866
	1884	A_2 (1)	1888	1893
	1889	B_1 (2)	1892	1894
	1908	A_2	1923	1919
	1996	B_2 (1)	2007	2010
$^7F_4$	2614	B_1 (2)	2582	2593
	2788	A_1 (2)	2769	2768
	2852	A_2 (1)	2816	2822

Appendix V. (cont.)

SLJ[a] State	Obsd.[b] (cm^{-1})	Species[c]	Model[d] Calc. (cm^{-1})	Fit[e] Calc. (cm^{-1})
$^7F_4$	2873	$B_{2\ (1)}$	2880	2896
	2926	B_2	2890	2900
	(2894)	A_1	2966	2972
	-	$A_{(2)}$	2988	2987
	3047	B_1	3060	3065
	3068	$A_{2\ (1)}$	3077	3075
$^7F_5$	-	$B_{(2)}$	3775	3787
	-	$B_{(1)}$	3800	3809
	-	$A_{(1)}$	3864	3873
	-	$A_{(2)}$	3921	3931
	-	$A_{(2)}$	3991	3995
	-	$B_{(2)}$	3994	4005
	-	$B_{(2)}$	4035	4036
	-	$A_{(1)}$	4050	4056
	-	$B_{(1)}$	4052	4061
	-	$A_{(2)}$	4098	4096
	-	$B_{(1)}$	4102	4109
$^7F_6$	-	$A_{(1)}$	4919	4934
	-	$A_{(2)}$	4935	4950
	-	$B_{(2)}$	5000	5012
	-	$B_{(1)}$	5027	5039
	-	$A_{(1)}$	5035	5046
	-	$B_{(1)}$	5036	5046
	-	$A_{(1)}$	5112	5124
	-	$B_{(2)}$	5120	5129
	-	$A_{(2)}$	5123	5130

Appendix V. (cont.)

SLJ[a] State	Obsd.[b] (cm^{-1})	Species[c]	Model[d] Calc. (cm^{-1})	Fit[e] Calc. (cm^{-1})
$^7F_6$	-	$B_{(2)}$	5140	5151
	-	$A_{(2)}$	5159	5168
	-	$A_{(1)}$	5167	5176
	-	$B_{(1)}$	5174	5182
$^5D_0$	17293	A_1	17296	17294
$^5D_1$	19043	A_2	19037	19034
	056	B_2	055	052
	063	B_1	066	064
$^5D_2$	21507	B_1 (2)	21512	21512
	512	A_1 (2)	525	525
	532	B_2 (1)	538	539
$^5D_2$	21541	A_1	21532	21532
	565	A_2 (1)	561	562
$^5D_3$	-	$B_{(2)}$		24398
	-	$A_{(2)}$		415
	-	$B_{(2)}$		422
	-	$B_{(1)}$		429
	-	$B_{(1)}$		439
	-	$A_{(1)}$		445
	-	$A_{(2)}$		449
$^5L_6$	-	$A_{(2)}$		25067
	-	$A_{(1)}$		095
	-	$B_{(1)}$		098

Appendix V. (cont.)

SLJ[a] State	Obsd.[b] (cm^{-1})	Species[c]	Model[d] Calc. (cm^{-1})	Fit[e] Calc. (cm^{-1})	SLJ[a] State	Obsd.[b] (cm^{-1})	Species[c]	Model[d] Calc. (cm^{-1})	Fit[e] Calc. (cm^{-1})
$^5L_6$	-	$B_{(2)}$		25144	$^5L_6$	-	$A_{(1)}$		25375
	-	$A_{(1)}$		188		-	$B_{(2)}$		390
	-	$B_{(1)}$		238		-	$B_{(1)}$		394
	-	$A_{(2)}$		245		-	$A_{(2)}$		408
	-	$B_{(2)}$		256		-	$A_{(1)}$		464

Gaps in the Energy Level Structure at 25464-35000 cm^{-1} [f]

Energy Range (cm^{-1})	Energy Gap (cm^{-1})
25465 - 26158	693
28826 - 30910	2084
31838 - 33136[g]	1298

Appendix V. (cont.)

[a]The leading eigenvector component is shown.

[b]Values in cm^{-1} vacuo from Ref. 7. The level at 2894 cm^{-1} was not included in the parameter fitting process, and a reported level at 2847 cm^{-1} was excluded.

[c]Symmetry species from Ref. 7. In cases where the sub species A_1, A_2, B_1 or B_2 was not identified by experiment, or the calculated symmetry was different than that assigned in Ref. 7, the subscript is shown in parenthesis.

[d]Computed level structure based on approximate free-ion parameters estimated for Eu^{3+} from apparent systematic trends together with the crystal-field parameters of $Sm^{3+}:LaF_3$.

[e]The energy level parameters used to compute these levels are given in Table 4.

[f]In most of the energy range from 25465-50000 cm^{-1} the density of computed crystal-field components is high. Since the fit parameters are approximate, and no experimental results are available for this region, we have indicated the few gaps of at least 650 cm^{-1} where no levels are computed to occur in the 25465-35000 cm^{-1}.

[g]A single J=0 level ($^3P_0$) is computed to occur in this range at 32958 cm^{-1}.

Appendix VI.

Experimental and Computed Energy Level Structure for $Er^{3+}:LaF_3$

SLJ[a] State	Obsd.[b] (cm^{-1})	Calc.[c] (cm^{-1})	O-C	SLJ[a] State	Obsd.[b] (cm^{-1})	Calc.[c] (cm^{-1})	O-C
$^4I_{15/2}$	0	-22	22	$^4F_{9/2}$	15391	15406	-15
	51.2	27	24		432	443	-11
	121.2	92	30		443	462	-19
	199.7	176	24		474	488	-14
	219.4	193	26		527	538	-11
	313.8	289	25				
	400.3	375	25	$^4S_{3/2}$	18557	18577	-20
	442.9	420	23		588	610	-22
$^4I_{13/2}$	6604	6612	-8	$^2H_{11/2}$	19266	19299	-33
	630	637	-7		307	324	-17
	670	686	-16		314	344	-30
	700	699	1		363	371	-8
	723	732	-9		367	379	-12
	754	771	-17		419	430	-11
	823	830	-7				
				$^4F_{7/2}$	20656	20654	2
$^4I_{11/2}$	10301	10300	1		703	697	6
	311	314	-3		734	735	-1
	330	336	-6		786	790	-4
	344	351	-7				
	358	364	-6	$^4F_{5/2}$	22370	22380	-10
	395	405	-10		374	389	-15
					407	414	-7
$^4I_{9/2}$	12419	12392	27				
	518	512	6	$^4F_{3/2}$	22684	22692	-8
	615	596	19		751	748	3
	701	681	20				
	730	720	10				

Appendix VI. (cont.)

SLJ[a] State	Obsd.[b] (cm^{-1})	Calc.[c] (cm^{-1})	O-C
$^2G_{9/2}$	24602	24587	15
	680	698	-18
	754	755	-1
	840	831	9
	862	864	-2
$^4G_{11/2}$	26526	26534	-8
	554	559	-5
	582	586	-4
	(621)[d]	637	
	647	640	7
	707	700	7
$^4G_{9/2}$	27602	27608	-6
	616	615	1
	628	625	3
	641	637	4
	668	660	8
$^2K_{15/2}$	27817	27826	-9
	827	838	-11
	872	877	-5
	898	893	5
	933	932	1
	-	978	
	-	28014	
	28125	132	-7
$^2G_{7/2}$	28239	28233	16
	255	237	18
	-	246	
	264	250	14
$^2P_{3/2}$	31695	31723	-28
	752	786	-34
$^2K_{13/2}$	33107	33086	21
	116	106	10
	141	154	-13
	163	161	2
	186	196	-10
	-	228	
$^2P_{1/2}$	33346	33350	-4
$^2K_{13/2}$	397	405	-8
$^4G_{5/2}$	-	33510	
	-	522	
	-	628	
$^4G_{7/2}$	34159	34154	5
	197	182	15
	222	215	7
	280	271	9

Appendix VI. (cont.)

SLJ[a] State	Obsd.[b] (cm^{-1})	Calc.[c] (cm^{-1})	O-C
$^2D_{5/2}$	35026	35043	-17
	052	052	0
	085	091	-6
$^2H_{9/2}$	36520	36526	-6
	556	549	7
	623	637	-14
	720	729	-9
	804	796	8
$^4D_{5/2}$	38807	38815	-8
	837	858	-21
	844	863	-19
$^4F_{7/2}$	39454	39460	-6
	537	540	-3
	603	605	-2
	634	630	4
$^2I_{11/2}$	41237	41211	26
	294	269	25
	313	304	9
	380	352	28
	395	375	20
	493	466	27
$^2L_{17/2}$	41680	41720	-40
	-	801	
	783	822	-39
$^2L_{17/2}$	41802	41832	-30
	-	861	
	-	922	
	934	957	-23
	42002	42045	-43
	-	054	
$^4D_{3/2}$	42499	42484	15
	529	517	12
$^2D_{3/2}$	43090	43108	-18
	127	138	-11
$^2I_{13/2}$	43686	43672	14
	742	725	17
	759	750	9
	770	769	1
	833	815	18
	914	898	16
	-	956	
$^4D_{1/2}$	-	47347	
$^2L_{15/2}$	47891	47891	0
	951	922	29
	-	990	
	-	48007	
	48071	066	5
		083	

Appendix VI. (cont.)

SLJ[a] State	Obsd.[b] (cm^{-1})	Calc.[c] (cm^{-1})	O-C
$^2L_{15/2}$	-	48168	
	-	199	
$^2H_{9/2}$	-	48306	
	-	349	
	-	394	
	-	438	
	-	461	
$^2D_{5/2}$	49223	49178	45
	272	248	24
	357	321	36

[a]The principal SLJ-component of the state is indicated.

[b]All energies are corrected to vacuum cm^{-1}. The energies of the ground $^4I_{15/2}$ state are taken from Ref. 58.

[c]Energy level parameters are given in Table 4.

[d]Not included in the energy level parameter fitting.

Appendix VII.

Experimental and Computed Energy Level Structure for $Tm^{3+}:LaF_3$

SLJ State	Model[a] (cm^{-1})	Expt.[b] (cm^{-1})	Calc.[c] (cm^{-1})	O-C
$^3H_6$	0	0	-4	4
	67	67	66	1
	74	-	76	
	156	118	131	-13
	204	-	197	
	235	-	193	
	272	-	254	
	274	-	273	
	349	-	339	
	354	-	346	
	400	-	386	
	418	-	399	
	441	-	420	
$^3F_4$	5585	5615	5613	2
	5689	5706	5703	3
	5790	5814	5820	-6
	5813	5826	5838	-12
	5836	5859	5857	2
	5851	5866	5863	3
	5903	-	5905	
	5916	5918	5924	-6
	5929	5958	5941	17
$^3H_5$	8306	8305	8293	12
	8354	8332	8331	1

Appendix VII. (cont.)

SLJ State	Model[a] (cm^{-1})	Expt.[b] (cm^{-1})	Calc.[c] (cm^{-1})	O-C
$^3H_5$	8365	8338	8337	1
	8395	8366	8368	-2
	8451	8400	8415	-15
	8460	-	8442	
	8470	-	8446	
	8481	-	8464	
	8522	-	8499	
	8581	8550	8562	-12
	8589	-	8568	
$^3H_4$	12547	12561	12553	8
	597	570	578	-8
	678	700	690	10
	734	727	719	8
$^3H_4$	12784	-	12770	
	826	12825	819	6
	832	-	824	
	880	868	863	5
	909	-	890	
$^3F_3$	14514	14508	14522	-14
	530	-	537	
	534	539	538	1
	550	554	556	-2
	582	588	588	0
	590	596	593	3
	622	-	627	

Appendix VII. (cont.)

SLJ State	Model[a] (cm^{-1})	Expt.[b] (cm^{-1})	Calc.[c] (cm^{-1})	O-C
$^3F_2$	15153	15138	15144	-6
	180	169	171	-2
	200	207	193	14
	254	240	240	0
	266	-	264	
$^1G_4$	21016	21037	21041	-4
	193	196	198	-2
	300	309	319	-10
	335	349	339	10
	362	366	372	-6
	364	380	382	-2
	425	-	406	
	508	-	511	

SLJ State	Model[a] (cm^{-1})	Expt.[b] (cm^{-1})	Calc.[c] (cm^{-1})	O-C
$^1G_4$	21511	21519	21512	7
$^1D_2$	28022	28021	28024	-3
	023	034	024	10
	041	057	049	8
	074	088	088	0
	100	106	114	-8
$^1I_6$	34781	34769	34772	-3
	808	-	795	
	906	896	906	-10
	35000	-	997	
	022	-	35015	
	078	-	106	

Appendix VII. (cont.)

SLJ State	Model[a] (cm^{-1})	Expt.[b] (cm^{-1})	Calc.[c] (cm^{-1})	O-C
$^1I_6$	35079	35107	35109	-2
	149	160	143	17
	201	-	184	
	216	-	226	
	217	-	234	
	257	-	253	
	272	-	270	
$^3P_0$	35588	35604	35624	-20
$^3P_1$	36502	36531	36525	6
$^3P_1$	36549	36587	36575	12
	588	-	624	
$^3P_2$	38225	38250	38244	6
	266	291	290	1
	296	336	326	10
	415	414	427	-13
	426	451	464	-13
$^1S_0$	75158	-	75025	

[a]Ref. 13.

[b]Ref. 61 (cm^{-1} vac).

[c]Energy level parameters are given in Table 4.

Appendix VIII.

Experimental and Computed Energy Level Structure for $Ho^{3+}:LaF_3$

SLJ[a] State	Obsd.[b] (cm^{-1})	Calc.[c] (cm^{-1})	O-C	SLJ[a] State	Obsd.[b] (cm^{-1})	Calc.[c] (cm^{-1})	O-C
$^5I_8$	0	-2	2	$^5I_7$	5287	5291	-4
	4.5	3	1		296	293	3
	42	29	13		309	300	9
	50	54	-4		314	303	11
	69	67	2				
	122	130	-8	$^5I_6$	8726	8722	4
	145	151	-6		730	723	7
	201	221	-20		733	732	1
	215	222	-7		735	735	0
	227	232	-5		747	740	7
	(261)[d]	298			753	754	-1
	307	307	-0		761	767	-6
	322	324	-2		773	776	-3
	349	339	10		783	778	5
	387	388	-1		786	791	-5
	398	391	7		814	812	2
	409	410	-1		-	817	
					834	839	-5
$^5I_7$	-	5182					
	5192	182	10	$^5I_5$	11304	11298	6
	-	242			306	303	3
	-	243			308	303	5
	-	244			311	314	-3
	246	248	-2		-	315	
	250	250	0		321	319	2
	-	256			332	333	-1
	264	268	-4		-	338	
	273	276	-3		363	360	3
	280	276	4				

Appendix VIII. (cont.)

SLJ[a] State	Obsd.[b] (cm^{-1})	Calc.[c] (cm^{-1})	O-C
$^5I_5$	-	11369	
	11386	392	-6
$^5I_4$	-	13260	
	13286	285	1
	362	382	-20
	380	388	-8
	-	394	
	-	419	
	-	455	
	-	477	
	-	607	
$^5F_5$	15576	15587	-11
	593	603	-10
	608	615	-7
	625	629	-4
	641	637	4
	659	661	-2
	-	681	
	-	712	
	-	714	
	708	717	-9
	730	734	-4
$^5S_2$	18590	18597	-7
	600	598	2
	603	601	2
$^5S_2$	18603	18602	1
	620	620	0
$^5F_4$	18677	18677	0
	688	683	5
	709	719	-10
	720	728	-8
	737	749	-12
	753	760	-7
	-	767	
	776	793	-17
	814	812	2
$^5F_3$	20744	20725	19
	754	750	4
	796	789	7
	799	791	8
	826	821	5
	832	823	9
	866	861	5
$^5F_2$	21238	21228	10
	249	232	17
	265	260	5
	275	281	-6
	286	287	-1
$^3K_8$	21411	21405	6
	419	424	-5

Appendix VIII. (cont.)

SLJ[a] State	Obsd.[b] (cm^{-1})	Calc.[c] (cm^{-1})	O-C
$^3K_8$	21423	21427	-4
	432	426	6
	440	449	-9
	451	457	-6
	461	458	3
	-	468	
	481	479	2
	495	480	15
	514	507	7
	527	514	13
	532	546	-14
	550	552	-2
	566	564	2
	-	573	
	579	574	5
$^5G_6$	22220	22238	-18
	235	250	-15
	263	260	3
	283	303	-20
	328	331	-3
	346	342	4
	361	348	13
	374	360	14
	389	380	9
	407	395	12
	424	423	1
	438	429	9
	454	479	-25
$^5F_1$	-	22504	
	22508	504	4
	-	535	
$^5G_5$	24112	24123	-11
	116	130	-14
	125	136	-11
	146	165	-19
	-	167	
	170	173	-3
	182	180	2
	-	185	
	196	194	2
	-	222	
	247	222	25
$^5G_4$	25985	25982	3
	26008	980	28
	037	26051	-14
	054	057	-3
	-	058	
	084	059	25
	096	096	0
	-	155	
	161	169	-8
$^3K_7$	26255	26261	-6
	-	262	
	-	266	

Appendix VIII. (cont.)

SLJ[a] State	Obsd.[b] (cm^{-1})	Calc.[c] (cm^{-1})	O-C
$^3K_7$	26266	26267	-1
	277	282	-5
	-	287	
	288	287	1
	293	298	-5
	-	299	
	298	299	-1
	312	312	0
	320	314	6
	-	324	
	328	331	-3
	328	332	-4
$^5G_5, ^3H_6$	27749	27746	3
	758	751	7
	804	788	16
	-	814	
	815	814	1
	-	819	
	-	820	
	825	826	-1
	839	840	-1
	-	846	
	854	851	3
	869	859	10
	879	882	-3
	-	926	
	-	927	
	932	928	4

SLJ[a] State	Obsd.[b] (cm^{-1})	Calc.[c] (cm^{-1})	O-C
$^5G_5, ^3H_6$	27945	27948	-3
	-	973	
	-	984	
	-	991	
	997	28000	-3
	-	020	
	-	076	
	28092	077	15
$^5F_2$	28426	28433	-7
	-	450	
	-	479	
	-	492	
	-	506	
$^5G_3, ^3L_9$	-	28956	
	28981	996	-15
	29011	29017	-6
	020	019	1
	032	020	12
	035	028	7
	039	036	3
	-	049	
	-	051	
	068	052	16
	-	094	
	-	094	4
	-	095	
	102	100	2

Appendix VIII. (cont.)

SLJ[a] State	Obsd.[b] (cm^{-1})	Calc.[c] (cm^{-1})	O-C
$^5G_3, ^3L_9$	29122	29125	-3
	-	127	
	-	128	
	-	146	
	161	160	1
	-	164	
	-	166	
	187	174	13
	-	220	
	230	220	10
	-	303	
	292	303	-11
$^3F_4, ^3K_6$	-	30023	
	-	027	
	30058	058	0
	078	072	6
	094	101	-7
	101	105	-4
	-	114	
	116	122	-6
	-	140	
	157	155	2
	186	187	-1
	-	197	
	197	198	-1
	213	218	-5
	-	228	
	234	231	3
$^3F_4, ^3K_6$	-	30267	
	-	288	
	30292	306	-14
	-	322	
	-	325	
	330	331	-1
$^5G_2$	-	30997	
	31002	31006	-4
	020	008	12
	-	026	
	062	072	-10
$^3D_3$	-	33313	
	-	330	
	-	346	
	-	360	
	-	382	
	-	412	
	-	437	
$^3P_1$	-	33554	
	-	560	
	-	564	
$^3M_{10}, ^3L_8$	34022	34033	-11
	-	040	
	-	048	
	061	057	4

Appendix VIII. (cont.)

SLJ[a] State	Obsd.[b] (cm^{-1})	Calc.[c] (cm^{-1})	O-C
$^3M_{10}, ^3L_8$	-	34105	
	34116	122	-6
	-	138	
	-	166	
	-	191	
	205	205	0
	-	212	
	-	221	
		(34234-34542)[e]	
$^5G_4$	-	34967	
	-	978	
	-	978	
	34994	984	10
	-	998	
	35003	35002	1
	023	024	-1
	-	024	
	049	032	17
$^3F_3$	35335	35327	8
	-	343	
	369	368	1
	424	415	9
	-	435	
	489	491	-2
	-	530	
$^5D_4$	36058	36040	18
	070	071	-1
	086	085	1
	100	090	10
	111	140	-29
	-	221	
	-	251	
	244	252	-8
	-	270	
$^3P_0$	-	36318	
		(36450-36703)[f]	
$^3H_5$	36852	36868	-16
	869	875	-6
	894	909	-15
	-	935	
	-	965	
	37001	990	11
	-	37021	
	034	032	2
	-	032	
	-	045	
	-	066	
		(37975-38237)[g]	

Appendix VIII. (cont.)

SLJ[a] State	Obsd.[b] (cm^{-1})	Calc.[c] (cm^{-1})	O-C
$^3I_7$	-	38560	
	-	568	
	38570	571	-1
	-	585	
	-	590	
	-	590	
	599	597	2
	-	612	
	-	614	
	-	620	
	-	621	
	-	624	
	38638[h]	646	
	-	647	
	-	652	

[a]The principal SLJ-component of the state is given.

[b]The energies quoted as observed are primarily from ref. 62 as confirmed in the present study. In some instances the band energies reported are those found in the present work where no corresponding observations were quoted in (62); there were also cases in which more crystal-field components than would be allowed for a given J-value were quoted in (62). The present model crystal-field calculations were used as the basis for excluding the extra levels. Units of cm^{-1} vac.

[c]Energy level parameters are given in Table 4.

[d]Not included in the energy level parameter fitting.

Appendix VIII. (cont.)

[e]There are 24 crystal-field components belonging principally to the $^3M_{10}$ and $^3L_8$ states computed in the energy range between 34234 and 34542 cm^{-1}. No structure was observed in this range.

[f]There are 22 crystal-field components belonging principally to the $^3F_2$ and $^1L_8$ states computed in the energy range 36450-36703 cm^{-1}. No structure was observed.

[g]There are 20 crystal-field components belonging principally to the $^3P_2$ and $^3L_7$ states computed in the energy range 37975-38237 cm^{-1}. No structure was observed.

[h]No structure attributable to f→f transitions was observed at energies >36638 cm^{-1}.

Appendix IX.

Experimental and Computed Energy Level Structure of $Dy^{3+}:LaF_4$

SLJ[a] State	Obsd.[b] (cm^{-1})	Calc.[c] (cm^{-1})	O-C	Fry et al.[d] Obs. (cm^{-1})
$^6H_{15/2}$	0	0	0	0
	17	28	-11	17
	69	76	-7	69
	124	126	-2	124
	184	188	-4	184
	208	209	-1	208
	-	296		
	307	316	-9	307
$^6H_{13/2}$	3503	3502	1	3502
	575	568	7	576
	621	602	19	618
	628	624	4	630
$^6H_{13/2}$	3645	3639	6	3645
	-	678		-
	701	681	20	695
$^6H_{11/2}$	5883	5875	8	5882
	908	912	-4	909
	924	918	6	925
	945	934	11	945
	976	973	3	977
	6021	6024	-3	6024
$^6H_{9/2}$,	7632	7630	2	7633
$^6F_{11/2}$	664	673	-9	665

Appendix IX. (cont.)

SLJ[a] State	Obsd.[b] (cm^{-1})	Calc.[c] (cm^{-1})	O-C	Fry et al.[d] Obs. (cm^{-1})
$^6H_{9/2}$,	7726	7728	-2	7727
$^6F_{11/2}$	756	776	-20	758
	812	828	-16	803
	837	832	5	813
	840	841	-1	842
	854	862	-8	887
	930	927	3	933
	996	998	-2	8019
	8075	8065	10	075
$^6H_{7/2}$,	8992	8996	-4	8990
$^6F_{9/2}$	9074	9085	-11	9071
	087	091	-4	085
	144	139	5	141
$^6H_{7/2}$,	9181	9185	-4	9179
$^6F_{9/2}$	234	238	-4	235
	282	265	17	279
	343	330	13	343
	435	435	0	438
$^6H_{5/2}$	10222	10220	2	10222
	285	284	1	284
	345	346	-1	344
$^6F_{7/2}$	11037	11038	-1	11044
	108	099	9	116
	138	138	0	159
	152	142	10	206

Appendix IX. (cont.)

SLJ[a] State	Obsd.[b] (cm^{-1})	Calc.[c] (cm^{-1})	O-C	Fry et al.[d] Obs. (cm^{-1})
$^6F_{5/2}$	12456	12466	-10	12456
	502	501	1	501
	514	517	-3	520
$^6F_{3/2}$	13271	13288	-17	13271
	285	296	-11	284
$^6F_{1/2}$	-	13839		-
$^4F_{9/2}$	21057	21058	-1	21059
	142	131	11	141
	159	147	12	159
	205	190	15	175
	-	358		218

SLJ[a] State	Obsd.[b] (cm^{-1})	Calc.[c] (cm^{-1})	O-C	Fry et al.[d] Obs. (cm^{-1})
$^4I_{15/2}$	22022	21996	26	22020
	132	121	11	126
	175	168	7	169
	189	185	4	190
	213	211	2	214
	292	297	-5	290
	342	328	14	342
	379	352	27	380
$^4G_{11/2}$	23468	23460	8	23468
	497	504	-7	501
	513	525	-12	513
	537	542	-5	534
	551	555	-4	550

Appendix IX. (cont.)

SLJ[a] State	Obsd.[b] (cm^{-1})	Calc.[c] (cm^{-1})	O-C
$^4G_{11/2}$	-	23611	
$^4M_{21/2}$	24984	24971	13
	25001	998	3
	067	25070	-3
	090	092	-2
	-	172	
	187	185	2
	-	186	
	226	223	3
	-	273	
	303	307	-4
	341	333	8

SLJ[a] State	Obsd.[b] (cm^{-1})	Calc.[c] (cm^{-1})	O-C
$^4I_{13/2}$,	-	25626	
$^4F_{7/2}$,	25661	674	-13
$^4K_{17/2}$	691	722	-31
	740	742	-2
	748	759	-11
	778	814	-36
	-	829	
	824	837	-13
	-	845	
	849	861	-12
	867	892	-25
	-	894	
	-	912	
	903	919	-16

Appendix IX. (cont.)

SLJ[a] State	Obsd.[b] (cm^{-1})	Calc.[c] (cm^{-1})	O-C
$^4I_{13/2}$,	25918	25929	-11
$^4F_{7/2}$,	-	935	
$^4K_{17/2}$	940	952	-12
	953	962	-9
	-	981	
	990	982	8
$^4M_{19/2}$	-	26242	
	-	251	
	26260	257	3
	-	291	
	-	397	
	448	445	3
	-	475	
$^4M_{19/2}$	26509	26528	-19
	571	552	19
	583	563	20
$^6P_{3/2}$	27476	27493	-17
	529	545	-16
$^6P_{5/2}$	27574	27580	-6
	616	611	5
	658	660	-2
$^4I_{11/2}$	27912	27903	9
	-	984	
	982	991	-9

Appendix IX. (cont.)

SLJ[a] State	Obsd.[b] (cm^{-1})	Calc.[c] (cm^{-1})	O-C
$^4I_{11/2}$	-	28036	
	28030	046	-16
	068	072	-4
$^4M_{15/2}$,	-	28492	
$^6P_{7/2}$	536	523	13
	572	575	-3
	605	607	-2
	630	634	-4
	651	641	10
	666	673	-7
	-	676	
	703	698	5
	726	727	-1
$^4M_{15/2}$,	28819	28808	11
$^6P_{7/2}$	834	835	-1
$^4F_{5/2}$,	29527	29517	10
$^4I_{9/2}$	630	614	16
	660	658	2
	676	683	-7
	746	725	21
	780	783	-3
	851	842	9
	884	883	1
$^4G_{9/2}$,	-	29960	
$^4M_{17/2}$	29980	986	-6

Appendix IX. (cont.)

SLJ[a] State	Obsd.[b] (cm^{-1})	Calc.[c] (cm^{-1})	O-C
$^4G_{9/2}$,	-	29997	
$^4M_{17/2}$	-	30020	
	-	025	
	-	041	
	30073	081	-8
	-	092	
	-	106	
	139	151	-12
	-	194	
	241	224	17
	-	263	
	301	296	5

SLJ[a] State	Obsd.[b] (cm^{-1})	Calc.[c] (cm^{-1})	O-C
$^6P_{3/2}$	30879	30862	17
	914	898	16
$^4K_{15/2}$,	31119	31105	14
$^4L_{19/2}$	134	148	-14
	170	169	1
	195	190	5
	214	218	-4
	226	245	-19
	262	266	-4
	282	285	-3
	294	298	-4
	-	316	
	-	350	

Appendix IX. (cont.)

SLJ[a] State	Obsd.[b] (cm^{-1})	Calc.[c] (cm^{-1})	O-C
$^4K_{15/2}$,	-	31356	
$^4L_{19/2}$	31369	370	-1
	-	375	
	-	389	
	-	415	
	443	456	-13
	-	462	
$^4G_{7/2}$	31571	31565	6
	651	648	3
	-	698	
	707	710	-3
$^4D_{5/2}$	-	32062	
$^4D_{5/2}$	-	32087	
$^4D_{1/2}$	-	152	
$^4D_{5/2}$	-	168	
$^4K_{13/2}$	-	33148	
	-	180	
	33185	185	0
	-	197	
	205	203	2
	221	206	15
	239	219	20
$^4H_{13/2}$	-	33485	

Appendix IX. (cont.)

SLJ[a] State	Obsd.[b] (cm^{-1})	Calc.[c] (cm^{-1})	O-C
$^4H_{13/2}$	-	33497	
	33500	500	0
	508	506	2
	537	518	19
	552	553	-1
	600	566	34
$^4F_{3/2}$	33628	33632	-4
	642	639	3
$^4D_{7/2}$	34009	34021	-12
	020	030	-10
	031	041	-10
	070	069	1

SLJ[a] State	Obsd.[b] (cm^{-1})	Calc.[c] (cm^{-1})	O-C
$^4H_{11/2}$,	34227	34237	-10
$^4L_{17/2}$,	240	241	-1
$^4F_{5/2}$,	-	260	
$^4H_{9/2}$	278	274	4
	293	285	8
	-	292	
	-	298	
	-	324	
	-	338	
	346	348	-2
	-	355	
	-	358	
	-	370	
	373	381	-8

Appendix IX. (cont.)

SLJ[a] State	Obsd.[b] (cm^{-1})	Calc.[c] (cm^{-1})	O-C
$^4H_{11/2}$,	34398	34383	15
$^4L_{17/2}$,	406	400	6
$^4F_{5/2}$,	-	420	
$^4H_{9/2}$	430	436	-6
	445	448	-3
	-	457	
	-	470	
	-	472	
	505	493	12
$^4H_{11/2}$	34847	34846	1
	869	874	-5
	902	891	11
	910	910	0

SLJ[a] State	Obsd.[b] (cm^{-1})	Calc.[c] (cm^{-1})	O-C
$^4H_{11/2}$	34933	34934	-1
	969	990	-21
$^4K_{11/2}$,	-	35776	
$^4G_{7/2}$	-	818	
	-	902	
	35936	948	-12
	961	971	-10
	36002	36005	-3
	022	014	8
	051	056	-5
	077	100	-23
	-	153	

Appendix IX. (cont.)

SLJ[a] State	Obsd.[b] (cm^{-1})	Calc.[c] (cm^{-1})	O-C
$^4L_{13/2}$,	36484	36480	4
$^4G_{5/2}$,	498	500	-2
$^4L_{15/2}$	-	505	
	522	533	-11
	-	553	
	-	558	
	-	574	
	-	579	
	590	588	2
	-	597	
	-	606	
	614	611	3
	-	624	
	633	627	6

SLJ[a] State	Obsd.[b] (cm^{-1})	Calc.[c] (cm^{-1})	O-C
$^4L_{13/2}$,	-	36645	
$^4G_{5/2}$,	36653	660	-7
$^4L_{15/2}$	672	664	8
	686	692	-6
$^4G_{9/2}$	36752	36746	6
	780	781	-1
	-	803	
	-	833	
	-	846	
$^4G_{7/2}$	-	37649	
$^4P_{1/2}$	-	674	
$^4G_{7/2}$	-	682	

Appendix IX. (cont.)

SLJ[a] State	Obsd.[b] (cm^{-1})	Calc.[c] (cm^{-1})	O-C
$^4G_{7/2}$	-	37 75	
	-	789	
$^4F_{3/2}$	37933	37921	12
	962	952	10
$^2L_{15/2}$	-	38047	
	-	084	
	-	170	
	-	264	
	-	274	
$^2L_{15/2}$	-	38366	
	-	451	
	-	502	
$^4P_{5/2}$	38926	38911	15
	997	989	8
	39085	39077	8
$^4P_{3/2}$	39159	39163	-4
	182	185	3
		(39185-50000)[e]	

[a]The leading component of the eigenvector is given.
[b]The components of the ground state are from Ref. 64. All values in cm^{-1} vac.
[c]Energy level parameters are given in Table 4.
[d]Ref. 64.
[e]At >39185 cm^{-1}, a large number of crystal-field components is computed over the energy range to 50000 cm^{-1}; however, there are five intervals of ≥ 650 cm^{-1} in whic no energy levels are computed. These are 39185-40531 (Δ = 1346) cm^{-1}, 43977-44798 (Δ = 821) cm^{-1}, 45073-46225 (Δ = 1152) cm^{-1}, 46471-47462 (Δ = 991) cm^{-1}, and 48618-49406 (Δ = 788) cm^{-1}.

Appendix X.

Experimental and Computed Energy Level Structure of $Tb^{3+}:LaF_3$

SLJ[a] State	Obsd.[b] (cm^{-1})	Calc.[c] (cm^{-1})	O-C	SLJ[a] State	Obsd.[b] (cm^{-1})	Calc.[c] (cm^{-1})	O-C
$^7F_6$	0	-6	6	$^7F_4$	-	3281	
	6	0	-6		-	293	
	-	13			-	383	
	-	20			-	396	
	44	26	18		-	397	
	49	58	-9		-	441	
	80	86	-6		-	446	
	-	88			-	506	
	-	108			-	506	
	-	119			-	685	
	-	162					
	-	233		$^7F_3$	4329	4331	-2
	-	244			413	407	6
					421	415	6
$^7F_5$	-	2035			429	425	4
	-	043			440	442	-2
	-	063			461	448	13
	-	076			487	473	14
	-	082					
	-	131		$^7F_2$	5016	5041	-25
	-	133			038	045	-7
	-	167			-	161	
	-	261			166	164	2
	-	263			197	200	-3
	-	313					
				$^7F_1$	5502	5522	-20
					568	586	-18
					617	632	-15

Appendix X. (cont.)

SLJ[a] State	Obsd.[b] (cm^{-1})	Calc.[c] (cm^{-1})	O-C
$^7F_0$	5819	5806	13
$^5D_4$	-	20504	
	20507	506	1
	534	533	1
	534	534	0
	-	539	
	-	548	
	555	560	-5
	569	568	1
	580	588	-8
$^5D_3$	26270	26263	7
	274	266	8
	-	281	
	-	285	
	296	302	-6
	325	318	7
	346	344	2
$^5G_6$	26405	26410	-5
	415	423	-8
	454	462	-8
	482	494	-12
	493	503	-10
	-	536	
	532	537	-5
	549	556	-7
	-	564	
$^5G_6$	-	26578	
	-	609	
	26631	634	-3
	-	680	
$^5L_{10}$	-	26946	
	26962	949	13
	-	966	
	-	966	
	981	972	9
	994	981	13
	-	27012	
	27029	015	14
	048	041	7
	078	075	3
	142	152	-10
	161	154	7
	183	166	17
	-	201	
	225	215	10
	-	234	
	251	249	2
	-	274	
	-	278	
	-	286	
	322	306	16
$^5G_5$	-	27829	
	-	833	

Appendix X. (cont.)

SLJ[a] State	Obsd.[b] (cm^{-1})	Calc.[c] (cm^{-1})	O-C
$^5G_5$	27833	27833	0
	839	837	2
	856	872	-16
	882	883	-1
	-	891	
	903	905	-2
	910	916	-6
	930	926	4
	989	972	17
$^5D_2$	28197	28215	-18
	206	222	-16
	-	240	
	233	241	-8
	262	260	2
$^5G_4$, $^5L_9$	-	28316	
	28336	344	-8
	-	345	
	-	350	
	348	351	-3
	364	367	-3
	-	375	
	378	376	2
	392	392	0
	428	411	17
	-	459	
	460	460	0
	-	479	
$^5G_4$, $^5L_9$	28480	28483	-3
	491	496	-5
	514	510	4
	540	542	-2
	-	552	
	-	563	
	-	581	
	604	598	6
	618	614	4
	-	626	
	-	633	
	-	663	
	-	665	
	-	671	
	-	678	
$^5G_3$	29030	29019	11
	032	029	3
	037	038	-1
	045	039	6
	-	050	
	068	051	17
	090	087	3
$^5L_8$,	-	29183	
$^5L_7$,	29216	220	-4
$^5G_2$,	234	230	4
$^5L_6$	-	246	
	-	249	

Appendix X. (cont.)

SLJ[a] State	Obsd.[b] (cm^{-1})	Calc.[c] (cm^{-1})	O-C
$^5L_8$,	29274	29279	-5
$^5L_7$,	-	284	
$^5G_2$,	-	291	
$^5L_6$	295	295	0
	336	329	7
	-	348	
	360	354	6
	-	370	
	392	399	-7
	-	406	
	-	412	
	-	413	
	430	426	4
	-	434	
	465	447	18
	-	481	
	503	502	1
	-	504	
	520	521	-1
	552	542	10
	-	565	
	-	572	
	-	592	
	(29598-30057)[d]		
$^5D_1$	30765	30755	10
	774	770	4
	800	788	12

SLJ[a] State	Obsd.[b] (cm^{-1})	Calc.[c] (cm^{-1})	O-C
$^5D_0$	-	31391	
$^5H_7$	-	31399	
	31402	402	0
	-	408	
	-	452	
	-	459	
	494	496	-2
	-	506	
	509	506	3
	-	522	
	-	528	
	533	535	-2
	-	545	
	-	592	
	613	608	5
	637	628	9
$^5H_6$	32889	32894	-5
	918	929	-11
	941	942	-1
	982	992	-10
	-	998	
	999	999	0
	-	33025	
	33027	028	-1
	-	031	
	047	038	9
	-	102	

Appendix X. (cont.)

SLJ[a] State	Obsd.[b] (cm^{-1})	Calc.[c] (cm^{-1})	O-C	SLJ[a] State	Obsd.[b] (cm^{-1})	Calc.[c] (cm^{-1})	O-C
$^5H_5$	33114	33104	10	$^5F_5$,	35021	35030	-9
	146	119	27	$^5H_3$,	044	053	-9
	-	817		$^5I_8$	-	060	
	-	838			072	062	10
	-	850			-	068	
	-	878			-	085	
	-	882			-	090	
	887	885	2		-	094	
	909	919	-10		-	102	
	-	923			-	117	
	-	924			139	137	2
	-	927			167	168	-1
	939	937	2		-	176	
					179	178	1
$^5H_4$	-	34435			-	183	
	-	442			203	214	-11
	-	452			211	228	-17
	34452	455	-3		-	229	
	-	461			237	235	2
	-	462			-	243	
	-	482			-	246	
	-	485			256	250	6
	488	489	-1		274	261	13
					-	309	
$^5F_5$,	-	34958			-	313	
$^5H_3$,	-	960			-	315	
$^5I_8$	-	986			316	316	0
	34980	987	-7		-	323	
	35005	990	15		-	327	
					348	330	18

Appendix X (cont.)

SLJ[a] State	Obsd.[b] (cm^{-1})	Calc.[c] (cm^{-1})	O-C
$^5F_4$	35479	35474	5
	-	505	
	-	510	
	-	510	
	-	523	
	-	533	
	555	546	9
	-	581	
	588	588	0
$^5F_3$,	-	36587	
$^5I_7$	-	588	
	36619	599	20
	-	635	
	-	663	
	-	670	
	679	682	-3
	-	723	
	-	729	
	731	735	-4
	731	736	-5
	348	330	18
$^5F_3$,	-	36737	
$^5I_7$	-	739	
	36741	748	-7
	-	750	
	-	764	
	-	766	
	-	766	
	773	774	-1
	-	783	
	786	787	-1
	-	796	
$^5F_2$	-	37226	
	-	230	
	-	256	
	-	278	
	-	280	
$^5F_1$	-	37527	
	-	555	
	-	579	
		(37652-38193)[e]	

Appendix X (cont.)

SLJ[a] State	Obsd.[b] (cm^{-1})	Calc.[c] (cm^{-1})	O-C	SLJ[a] State	Obsd.[b] (cm^{-1})	Calc.[c] (cm^{-1})	O-C
$^5K_9$,	39210	39221	-11		-	410	
$^5D_2$	-	224			-	450	
	-	226	11		-	454	
	-	233			-	475	
	-	246			-	480	
	-	269			-	489	
	265	280	-15		-	502	
	-	303			-	503	
	-	305			-	513	
	356	374	-18		-	521	
	-	378			-	521	
	383	399	-16				
	-	405				(39522-50000)[f]	

[a]The leading component of the eigenvector is given.

[b]Units of cm^{-1} vac.

[c]The energy level parameters are given in Table 4.

[d]There are 22 levels belonging principally to the $^5L_7$, $^5D_2$, and $^5L_6$ states in the interval 29598-30059 cm^{-1}.

[e]There are 33 levels belonging principally to the $^5I_6$, $^5I_4$, and $^5I_5$ states in the interval 37657-38193 cm^{-1}. No structure was observed.

[f]At >39521 cm^{-1} the density of computed levels is high. Energy gaps in the range 39522-50000 cm^{-1}, i.e., regions of >650 cm^{-1} where no crystal-field components are computed, are as follows: 39522-40253 (Δ=731) cm^{-1}, 43645-44415 (Δ=770) cm^{-1}, 44568-45281 (Δ=713) cm^{-1}, and 48392-49112 (Δ=720) cm^{-1}.

Appendix XI.

Experimental and Computed Energy Level Structure for $Gd^{3+}:LaF_3$

SLJ State	Expt.[a] (cm^{-1})	Calc.[b] (cm^{-1})	O-C	SLJ State	Expt.[a] (cm^{-1})	Calc.[b] (cm^{-1})	O-C
$^8S_{7/2}$	0	19.6	-20	$^6I_{17/2}$	36340	36351	-11
		19.7			342	351	-9
		19.8			346	352	-6
		19.9			351	354	-3
					354	355	-1
$^6P_{7/2}$	32176	32169	7		363	357	6
	185	177	8		370	360	10
	199	194	5		377	362	15
	226	224	2		384	364	20
$^6P_{5/2}$	32771	32774	-3	$^6I_{11/2}$	36549	36554	-5
	791	780	11		561	563	-2
	808	802	6		571	572	-1
					584	585	-1
$^6P_{3/2}$	33352	33368	-16		592	590	2
	370	386	-16		611	606	5
$^6I_{7/2}$	35923	35934	-11	$^6I_{15/2}$,	36659	36671	-12
	945	945	0	$^6I_{13/2}$	668	680	-12
	968	964	4		677	683	-6
	996	979	17		687	696	-9
					698	699	-1
$^6I_{9/2}$	36274	36277	-3		701	707	-6
	285	286	-1		710	713	-3
	305	303	2		712	714	-2
	313	311	2		717	715	2
	332	323	9		722	724	-2

Appendix XI. (cont.)

SLJ State	Expt.[a] (cm^{-1})	Calc.[b] (cm^{-1})	O-C
$^6I_{15/2}$,	36731	36725	6
$^6I_{13/2}$	736	729	7
	749	747	2
	760	753	7
	769	760	9
$^6D_{9/2}$	39667	39647	20
	686	681	5
	719	709	10
	742	731	11
	758	747	11
$^6D_{1/2}$	-	40620	
$^6D_{7/2}$	40734	40734	0
	740	737	3
	744	741	3
	751	753	-2
$^6D_{3/2}$	-	40876	
	-	905	
$^6D_{5/2}$	-	41003	
	-	045	
	-	059	
$^6G_{7/2}$	49170	49160	10
	49221	49225	-4
$^6G_{7/2}$	240	243	3
	298	284	14
$^6G_{11/2}$,	49533	49545	-12
$^6G_{9/2}$,	560	556	4
$^6G_{5/2}$	604	623	-19
	638	654	-16
	651	661	-10
	680	688	-8
	-	696	
	-	711	
	-	731	
	740	741	-1
	-	757	
	-	810	
	824	823	1
	-	860	
$^6G_{3/2}$	-	50486	
	-	568	
$^6G_{13/2}$	-	51310	
	-	357	
	-	382	
	-	402	
	-	414	
	-	436	
	-	483	

[a]Experimental results from Refs. 68 and 69, cm^{-1} vac.
[b]The parameter values used in this calculation are given in Table 4.

Distribution for ANL-88-8

Internal:

J. V. Beitz
F. A. Cafasso
W. T. Carnall (40)
G. L. Goodman (4)
J. P. Hessler
D. J. Lam
L. R. Morss
L. C. Soderholm
L. M. Stock
C. W. Williams
ANL Patent Dept.
ANL Contract File
ANL Libraries (2)
TIS Files (3)

External:

DOE-OSTI, for distribution per (UC-411) (40)
Manager, Chicago Operations Office, DOE
L. Brewer, U. California, Berkeley
J. L. Burnett, DOE, Washington
R. D. Cowan, Los Alamos National Lab.
B. R. Judd, Johns Hopkins U.
V. Kaufman, National Bureau of Standards, Washington
W. F. Krupke, Lawrence Livermore National Lab.
W. C. Martin, National Bureau of Standards, Washington
C. A. Morrison, Harry Diamond Labs.
K. Rajnak, Kalamazoo College (4)
R. Rana, College of the Holy Cross (4)
F. S. Richardson, U. Virginia
J. S. Sugar, National Bureau of Standards, Washington
W. Wadt, Los Alamos National Lab.
M. J. Weber, Lawrence Livermore National Lab.
J. C. Wright, U. Wisconsin
W. M. Yen, U. Georgia
J. P. Young, Oak Ridge National Lab.
J. Blaise, Laboratoire Aime Cotton, Orsay, France
J. Fuger, U. Liege, Liege, Belgium

J. Genet, Inst. Physique Nucleaire, Orsay, France

C. K. Jorgensen, U. Geneva, Switzerland

B. Kanellakopulos, Kernforschungscentrum, Karlsruhe, Germany

C. Keller, Kernforschungscentrum, Karlsruhe, Germany

J. C. Krupa, Inst. Physique Nucleaire, Orsay, France

D. J. Newman, U. Hong Kong, Hong Kong

M. F. Reid, U. Hong Kong, Hong Kong